

**EXPERIMENTAL EVALUATION OF FLEXURAL STRENGTHENING
METHODS FOR EXISTING REINFORCED CONCRETE MEMBERS
USING FIBER REINFORCED POLYMER (FRP) SYSTEMS**

by

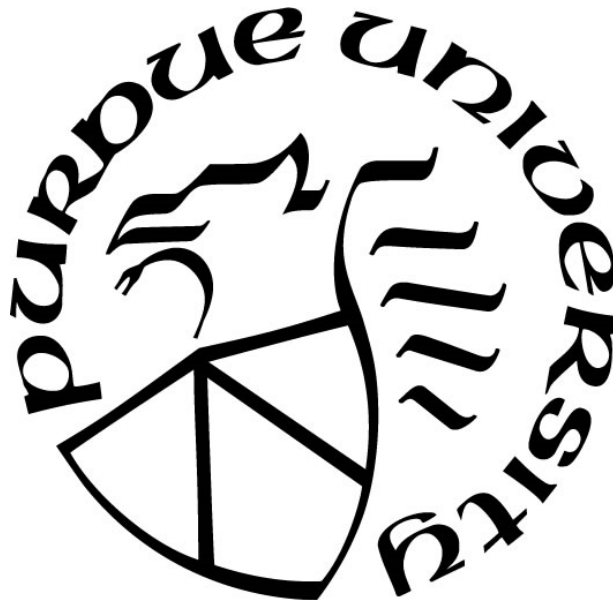
Robert R. Jacobs

A Thesis

Submitted to the Faculty of Purdue University

In Partial Fulfillment of the Requirements for the degree of

Master of Science in Civil Engineering



Lyles School of Civil Engineering

West Lafayette, Indiana

December 2020

**THE PURDUE UNIVERSITY GRADUATE SCHOOL
STATEMENT OF COMMITTEE APPROVAL**

Dr. Christopher S. Williams, Chair

Lyles School of Civil Engineering

Dr. Robert J. Frosch

Lyles School of Civil Engineering

Dr. Mark D. Bowman

Lyles School of Civil Engineering

Approved by:

Dr. Dulcy Abraham

*Dedicated to my family,
for all of their love and support*

ACKNOWLEDGMENTS

I will be forever grateful for the experience I was afforded by the Lyles School of Civil Engineering at Purdue University. My time at Purdue would not have been the same if not for my advisor, Dr. Christopher Williams, who gave me the chance to work as a research assistant on this project. I want to thank Dr. Williams for his interest in not only my engineering development, but also my personal development. I am incredibly fortunate to have had the opportunity to study under his guidance and I will leave Purdue a better person because of it.

I want to thank Dr. Robert Frosch for his assistance in the development and oversight of this project. It was invaluable to have access to his vast knowledge of structural engineering and it was truly a pleasure to work with him. I would also like to thank Dr. Mark Bowman for taking the time to serve on my committee as well as his gracious efforts in assisting with my job search.

It was a privilege to work at Bowen Laboratory around some of the most talented engineers in the world. The chance to work with the other students at the lab not only elevated the project but also pushed me to want to become a better engineer. I want to thank all of my friends at the lab who volunteered their time on the lab floor to help move the project forward.

A special thank you is in order for Jon Pevey. Simply, the experimental program detailed in this document would not have been the same without his assistance. Jon was instrumental in helping to develop the research study and, in many ways, played a large role in my overall success at Purdue. Also directly contributing to the research, Will Rich is owed my full appreciation. Will went above and beyond to assist on the lab floor and do everything necessary to ensure the project was successful.

This project was supported by the Federal Highway Administration and the Indiana Department of Transportation through the Joint Transportation Research Program. An acknowledgment is owed for this support, without which this project would not have been possible.

TABLE OF CONTENTS

LIST OF FIGURES	8
LIST OF TABLES	11
ABSTRACT	12
CHAPTER 1. INTRODUCTION	13
1.1 Background and Motivation	13
1.2 Project Scope and Objectives	15
1.3 Organization	16
CHAPTER 2. INTRODUCTION TO FRP FLEXURAL STRENGTHENING SYSTEMS	17
2.1 Introduction	17
2.2 Overview	17
2.2.1 Common FRP Materials	17
2.2.2 Common FRP Systems for Flexural Strengthening	18
2.2.3 Behavior of FRP Composites and FRP Flexurally-Strengthened Elements	19
2.3 Externally Bonded Sheets	19
2.3.1 Anchorage Systems	20
2.4 Near Surface Mounted Strips	24
2.5 Calculation of Nominal Flexural Strength	25
2.6 Research Need	34
CHAPTER 3. EXPERIMENTAL PROGRAM	35
3.1 Introduction	35
3.2 Specimen Design	35
3.3 FRP Strengthening System Details	40
3.3.1 Externally Bonded (EB) Sheet Details	41
3.3.2 Near-Surface-Mounted (NSM) Strip Details	46
3.4 Material Properties	48
3.4.1 Concrete	48
3.4.2 Steel Reinforcement	49

3.4.3 Fiber Reinforced Polymer (FRP) Systems	50
3.5 Specimen Construction	52
3.6 FRP Strengthening System Application Procedures	54
3.6.1 Externally Bonded Sheets.....	54
3.6.2 Near-Surface-Mounted Strips: Surface Preparation and FRP Application	62
3.7 Test Setup and Procedure	64
3.8 Summary	67
CHAPTER 4. EXPERIMENTAL RESULTS AND DISCUSSION	68
4.1 Introduction	68
4.2 Overview of Experimental Results	68
4.3 Load-Deflection Behavior from Analysis	72
4.3.1 Input Values.....	72
4.3.2 Analysis	76
4.3.3 Results	78
4.4 Pilot Specimen Test Results.....	80
4.5 Test Results By Specimen Type.....	85
4.5.1 Introduction	85
4.5.2 Control (C) Specimens	85
4.5.3 Artificially Deteriorated (D) Specimens.....	87
4.5.4 Externally Bonded (EB) FRP Sheet Specimens	92
4.5.5 Near-Surface-Mounted (NSM) FRP Strip Specimens.....	106
4.6 Test Results By Group	111
4.6.1 Group 1	111
4.6.2 Group 2	113
4.6.3 Group 3	115
4.7 Summary	117
CHAPTER 5. SUMMARY AND CONCLUSIONS	120
5.1 Summary	120
5.2 Observations and Conclusions	121
5.3 Concluding Remarks	123

APPENDIX A. LOAD-DEFLECTION PLOTS.....	124
APPENDIX B. INDOT 1961 STANDARD DRAWING.....	136
APPENDIX C. GROUP 3 MIDSPAN DEFLECTION MEASUREMENTS	137
APPENDIX D. CONCRETE COMPRESSION TESTS	138
REFERENCES	146

LIST OF FIGURES

Figure 1.1: Process of Deterioration at Bottom Corners of Box Beams.....	13
Figure 1.2: Elkhart, Indiana, Bridge No. 102 CR 35 over Little Elkhart River.....	14
Figure 1.3: Dimensions of Geometric Constraints	15
Figure 2.1: FRP Flexural Strengthening Systems Investigated During Experimental Program...	19
Figure 2.2: U-Wrap Anchor.....	21
Figure 2.3: FRP Anchors	22
Figure 2.4: FRP Anchor Force Transfer (adapted from Pham 2009)	23
Figure 2.5: Near-Surface-Mounted (NSM) Strengthening System	24
Figure 2.6: Minimum Dimension of Grooves (adapted from ACI 440.2R-17).....	25
Figure 2.7: Internal Strain and Stress Distribution for FRP-Strengthened Reinforced Concrete Section at Nominal Moment Capacity (adapted from ACI 440.2R-17).....	27
Figure 3.1: WS-42 Box Beam Cross Section (INDOT 1961 Standard Set).....	36
Figure 3.2: General Specimen Dimensions	37
Figure 3.3: Simulated Field Conditions.....	38
Figure 3.4: Specimen Identification Label.....	40
Figure 3.5: EB.1 Strengthening System.....	42
Figure 3.6: EB.2 Strengthening System.....	44
Figure 3.7: EB.3 Strengthening System.....	45
Figure 3.8: NSM Strengthening System	47
Figure 3.9: Typical Concrete Strength Gain over 28 Days.....	49
Figure 3.10: Stress-Strain Response of Longitudinal Reinforcement Samples	50
Figure 3.11: Formwork for Casting a Typical Group of Specimens	52
Figure 3.12: Reinforcing Cage in Forms	53
Figure 3.13: Casting Process.....	53
Figure 3.14: Curing Process.....	54
Figure 3.15: Surface Preparation for Externally Bonded Strengthening System	55
Figure 3.16: Application of Externally Bonded Sheets	57
Figure 3.17: Installation of FRP Anchors for Externally Bonded Strengthening System.....	59

Figure 3.18: Application of Patches over FRP Anchors.....	60
Figure 3.19: Additional Surface Preparation for U-Wrap Anchors.....	61
Figure 3.20: Application of FRP on Specimen with U-Wrap Anchors.....	61
Figure 3.21: Cutting NSM Grooves.....	62
Figure 3.22: Installation of NSM Strips.....	63
Figure 3.23: NSM Overhead Application.....	64
Figure 3.24: Loading Configuration.....	65
Figure 3.25: Elevation View of Test Setup.....	65
Figure 3.26: Photograph of Test Setup.....	66
Figure 3.27: High-Speed Camera.....	67
Figure 4.1: Applied Load, P , and Midspan Deflection, Δ	71
Figure 4.2: Stress-Strain Model for Concrete.....	73
Figure 4.3: Stress-Strain Model for Steel Reinforcement.....	74
Figure 4.4: Stress-Strain Model for FRP.....	75
Figure 4.5: Example Moment-Curvature Plot.....	76
Figure 4.6: Example Plot of Curvature over Member Length.....	78
Figure 4.7: Example of Comparison of Theoretical and Experimental Responses.....	80
Figure 4.8: Applied Load vs. Midspan Deflection for Group 0 (Pilot) Specimens.....	81
Figure 4.9: U-Wrap Anchor After Failure.....	83
Figure 4.10: Partially Debonded FRP Sheet Between Anchor Points.....	84
Figure 4.11: Applied Load vs. Midspan Deflection for Control Specimens.....	86
Figure 4.12: Comparison of Theoretical and Experimental Responses for Control Specimens ..	87
Figure 4.13: Applied Load vs. Midspan Deflection for Artificially Deteriorated Specimens.....	88
Figure 4.14: Artificially Deteriorated Specimens after Failure.....	90
Figure 4.15: Comparison of Theoretical and Experimental Responses for Artificially Deteriorated Specimens.....	91
Figure 4.16: Applied Load vs. Midspan Deflection for EB.1 Specimens.....	93
Figure 4.17: EB.1 Specimens After Failure.....	95
Figure 4.18: Typical FRP Sheet Rupture at Anchor Point – EB.1 Specimens.....	96
Figure 4.19: Applied Load vs. Midspan Deflection for EB.2 Specimens.....	97

Figure 4.20: Specimen 0-EB.2 After Failure	99
Figure 4.21: Specimen 1-EB.2 After Failure	100
Figure 4.22: Specimen 2-EB.2 After Failure	101
Figure 4.23: Specimen 3-EB.2 After Failure	102
Figure 4.24: FRP Sheet Rupture at Anchor Point (Specimen 1-EB.2).....	103
Figure 4.25: Applied Load vs. Midspan Deflection for EB.1 and EB.2 Specimens	104
Figure 4.26: Comparison of Theoretical and Experimental Responses for Externally Bonded Specimens	105
Figure 4.27: Applied Load vs. Midspan Deflection for NSM.1 Specimens.....	107
Figure 4.28: Applied Load vs. Midspan Deflection for Group 3 NSM Specimens.....	107
Figure 4.29: FRP Strips of Specimen 1-NSM.1a.....	109
Figure 4.30: Comparison of Theoretical and Experimental Responses for Near-Surface-Mounted Specimens	111
Figure 4.31: Applied Load vs. Midspan Deflection for Group 1 Specimens	112
Figure 4.32: Applied Load vs. Midspan Deflection for Group 2 Specimens	114
Figure 4.33: Applied Load vs. Midspan Deflection for Group 3 Specimens	116

LIST OF TABLES

Table 2.1: FRP Material Properties (adapted from ACI Committee 440 2017).....	18
Table 2.2: Environmental Reduction Factor for Various FRP Systems and Exposure Conditions (from ACI 440.2R-17)	31
Table 3.1: Test Matrix.....	38
Table 3.2: Concrete Mixture Design.....	48
Table 3.3: FRP Strengthening System Components and Design Values.....	51
Table 4.1: Test Results.....	70
Table 4.2: Group 0 (Pilot) Test Results	81
Table 4.3: Control Specimen Test Results.....	85
Table 4.4: Artificially Deteriorated Specimen Test Results	88
Table 4.5: EB.1 Specimen Test Results.....	92
Table 4.6: EB.2 Specimen Test Results.....	97
Table 4.7: Test Results for All EB Specimens	103
Table 4.8: NSM Specimen Test Results	106
Table 4.9: Group 1 Test Results	112
Table 4.10: Group 2 Test Results	114
Table 4.11: Group 3 Test Results	116

ABSTRACT

Research has shown that many adjacent box beam bridges in Indiana experience premature deterioration. Primarily caused by leaking joints between beams, this deterioration leads to corrosion and/or fracturing of prestressing strands, ultimately resulting in flexural deficiency of the bridge. A testing program was designed to simulate this observed deterioration by constructing test specimens and implementing various strengthening techniques using fiber reinforced polymer (FRP) systems. The objective of this testing program is to investigate the effectiveness of FRP strengthening systems to increase or even regain the full capacity of beams that have effectively lost tension reinforcing steel due to corrosion. The FRP-strengthened beam specimens incorporate the use of near-surface-mounted and externally bonded systems. Reinforcing bars in the beams are excluded or cut to simulate deterioration. Furthermore, two different methods of end anchorage for the externally bonded sheets, FRP fan anchorage and U-wrap anchorage, are investigated. Results and conclusions from the testing program are described in order to help advise best practices in implementing the aforementioned strengthening systems.

CHAPTER 1. INTRODUCTION

1.1 Background and Motivation

Many of the box beam bridges that are currently in service in Indiana were built or reconstructed in the 1960s and 1970s, as described in Frosch et al. (2020a). Box beam bridges from this era are coming to the end of their services lives as determined by noticeable deterioration. This deterioration is leading to flexural deficiencies and the possibility of structural collapse (Frosch et al. 2020a, 2020b). As detailed in Frosch et al. (2020a, 2020b), researchers from Purdue University have inspected box beam bridges in Indiana to identify common types of deterioration and potential causes of the poor performance of box beams. During the study of box beam bridges, deterioration of the bottom flanges of the girders were commonly observed. Failed shear keys between adjacent box beams allow chloride-laden water to penetrate between the members. When the water reaches the bottom flange, it curls along the bottom surface of the member, initiating corrosion. This process is illustrated in Figure 1.1. Along the bottom corners of the beams, spalled concrete and exposed, deteriorated prestressing strands were commonly observed. Moreover, water was found to collect in the voids of the beams, eventually leading to corrosion of the prestressing strands in the bottom flange (Frosch et al. 2020a, 2020b). Examples of common deterioration patterns are shown in Figure 1.2.

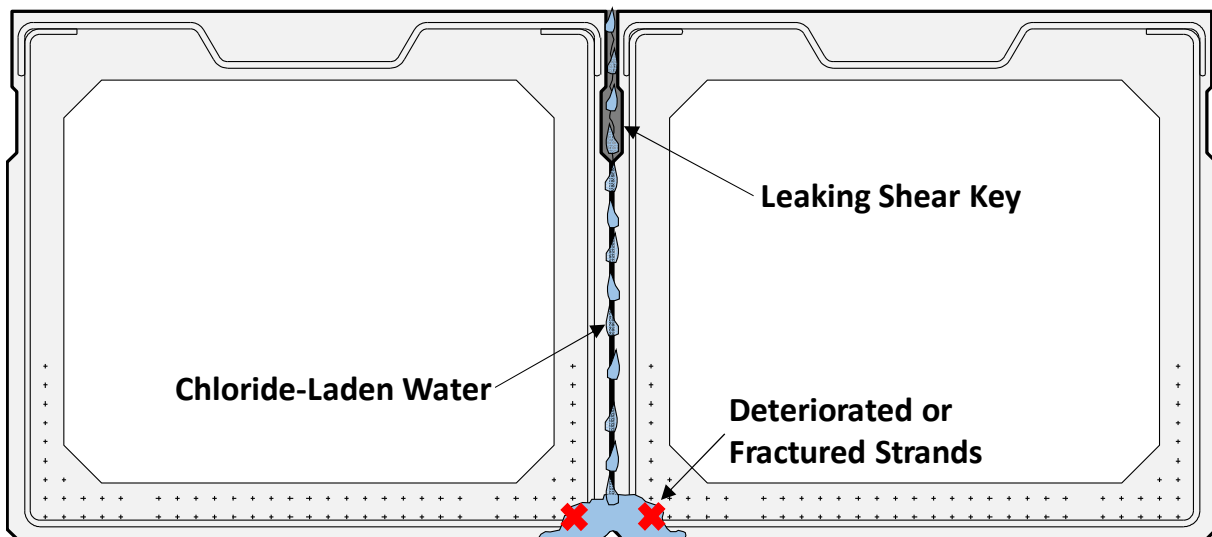


Figure 1.1: Process of Deterioration at Bottom Corners of Box Beams



Figure 1.2: Elkhart, Indiana, Bridge No. 102 CR 35 over Little Elkhart River

With the high volume of bridges reaching the end of their service lives around the same time, it is necessary to find a way to at least temporarily extend the service lives of these bridges since replacing all of them at once would be financially impractical. In the interest of determining the optimal solution to mitigate these flexural deficiencies described above, FRP strengthening systems were identified as a possible solution for extending the lives of these bridges. The FRP strengthening systems would be used to regain the flexural capacity lost due to corrosion of the prestressing strands. To design a feasible strengthening system, geometric constraints due to the nature of adjacent precast box beam bridges would have to be considered in the development of a research program focused on FRP strengthening of these members. These constraints include:

- No access to the sides of the box beam members
- Limited access to the ends of the box beam members
- 1-in. concrete clear cover below the stirrups (see Figure 1.3)
- 1.5-in. center-to-center spacing of the prestressing strands (see Figure 1.3)

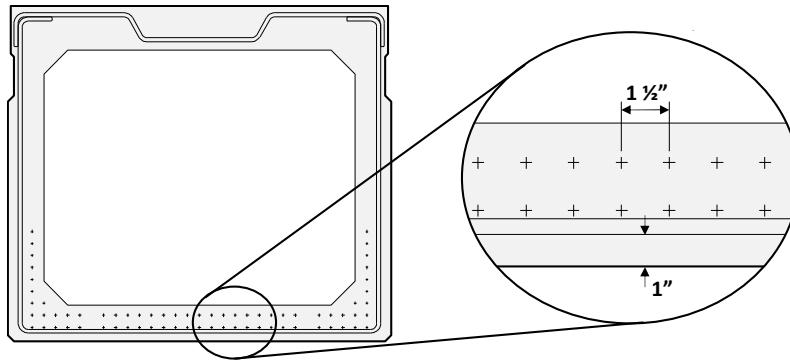


Figure 1.3: Geometric Constraints

To successfully strengthen the members while meeting the constraints listed above, two FRP flexural strengthening systems were identified as feasible solutions: externally bonded FRP unidirectional sheets and near-surface-mounted FRP strips. These two systems can be designed to provide a comparable amount of flexural strength while giving the researchers an opportunity to compare the effectiveness and feasibility of two possible solutions.

1.2 Project Scope and Objectives

Although the inception of the study was formulated based on the issues observed in the field with deteriorating adjacent box beam bridges, the generalized nature of the experimental study detailed in this document allows the results to be applied more broadly to other existing reinforced concrete members in need of flexural strengthening. This document is not intended to be a comprehensive analysis of the mechanics of FRP systems nor a complete review of all types of FRP strengthening systems, but rather the intention of this document is to add to the growing experimental FRP research for structural applications.

The objectives of the experimental program described in this document are as follows:

- Directly compare the effectiveness of two flexural strengthening methods: externally bonded FRP sheets and near-surface-mounted FRP strips
- Assess the ability of the two repair methods to restore the strength and stiffness of artificially weakened laboratory specimens

- Investigate anchorage techniques of externally bonded FRP sheets to the flexural tension side of a member
- Verify FRP application procedures

The experimental program described in this document is part of a larger research project with the objective of developing a guidebook that will provide general recommendations for the application of FRP systems to bridges in Indiana. This document presents the details of laboratory experiments performed to better understand the behavior of FRP flexural strengthening systems applied to existing reinforced concrete members.

1.3 Organization

An introduction to FRP strengthening systems is presented in Chapter 2, including descriptions of the two strengthening systems used in the experimental program. Furthermore, the procedure for calculating the flexural strength of members strengthened with the FRP systems is presented. In Chapter 3, the experimental program is detailed, including the logistics of specimen fabrication and testing. The results from the experimental program are outlined in Chapter 4. This chapter also includes an analysis of the experimental data. Lastly, the summary of the experimental program and resulting conclusions are provided in Chapter 5.

CHAPTER 2. INTRODUCTION TO FRP FLEXURAL STRENGTHENING SYSTEMS

2.1 Introduction

A brief introduction to common fiber reinforced polymer (FRP) materials, systems, and techniques for flexural strengthening is provided in this chapter. Specific focus will be placed on the strengthening systems that were selected for the beam testing program that is detailed in Chapters 3 and 4. Furthermore, the design calculations for these FRP systems per ACI 440.2R-17 will be covered.

2.2 Overview

In order to best understand the essence of the experimental program detailed in Chapter 3 and 4, basic background information about the FRP strengthening systems used in the experimental program will be presented in this chapter. In this section, a basic introduction to FRP strengthening systems is provided, and the systems evaluated through the experimental program detailed in Chapters 3 and 4 are also introduced. Although only the basic principles will be outlined in the current chapter, a more detailed review of FRP materials and systems as well as case studies of FRP systems currently installed on in-service bridges in Indiana is provided in Pevey (2018).

2.2.1 Common FRP Materials

FRP strengthening systems consist of a high-tensile strength fiber and a binding resin to form a reinforced matrix. According to ACI 440.2R-17, typical strengthening fibers used in FRP systems are either carbon, glass, or aramid, while common binding resins include epoxy, polyesters, and vinyl esters. The combination of these two constituent materials is determined based on the intended strengthening characteristics of the FRP strengthening system (ACI 440.2R-17). The properties of carbon, glass, and aramid fibers combined with an epoxy into a cured laminate are provided in Table 2.1.

Table 2.1: FRP Material Properties (adapted from ACI 440.2R-17, as presented in Pevey 2018)

FRP System (w/ epoxy)	Young's Modulus (ksi)	Ultimate Strength (ksi)	Rupture Strain (in./in.)
Carbon (high-strength)	15,000 - 21,000	130 - 150	0.010 - 0.015
Glass (E-glass)	3,000 - 6,000	75 - 200	0.015 - 0.030
Aramid (high-performance)	7,000 - 10,000	100 - 250	0.020 - 0.030

The ranges of data provided in Table 2.1 are given for a 40-60% fiber volume fraction of cured laminate (i.e., the properties of the FRP system are dependent on the ratio of fiber to resin) (ACI 440.2R-17). The constituent materials used in the experimental program outlined in this document were limited to carbon fiber and epoxy resin due to the common use of carbon fiber in FRP strengthening applications currently in service today. Carbon fiber is often preferred to other options due to its relatively high strength and stiffness.

2.2.2 Common FRP Systems for Flexural Strengthening

Fiber reinforced polymer (FRP) flexural strengthening systems, due to their relatively high strength-to-weight ratios and ease of application in relation to conventional materials, offer a practical solution to increasing the flexural capacity of existing reinforced concrete members. These systems come in the form of bi-directional FRP meshes, unidirectional FRP sheets (or “fabrics”), circular FRP bars, and rectangular FRP bars (or “strips”). The two FRP flexural strengthening systems used in the experimental program included externally bonded sheets and near-surface-mounted strips, as shown in Figure 2.1.

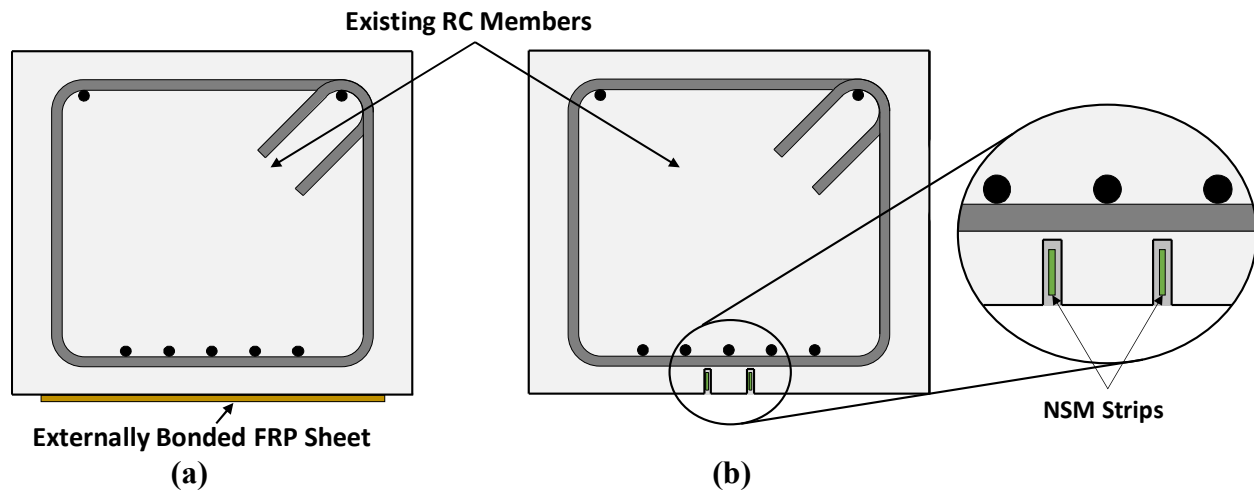


Figure 2.1: FRP Flexural Strengthening Systems Investigated During Experimental Program – (a) Externally Bonded Sheets; (b) Near-Surface-Mounted (NSM) Strips

For flexural strengthening, both systems presented in Figure 2.1 are added to the tension face of an existing reinforced concrete member. Externally bonded sheets and near-surface-mounted strips will be further discussed in Sections 2.3 and 2.4, respectively.

2.2.3 Behavior of FRP Composites and FRP Flexurally-Strengthened Elements

The addition of FRP composites to flexurally strengthen an existing reinforced concrete member provides additional strength to the member, but this typically is coupled with a reduced ductility. The added strength from the FRP strengthening system will be further discussed and quantified in Section 2.5.

2.3 Externally Bonded Sheets

Externally bonded FRP sheets can be adhered to the tension face of a flexural member to increase its flexural capacity. According to Section 3.2 of ACI 440.2R-17, sheets can either be presaturated with a binding resin offsite and packaged for transportation or saturated in the field just prior to application onto the structure. For the sheets that are saturated in the field, there are two methods of adhering the sheets onto the concrete substrate: wet-layup and dry-layup. Wet-layup is the process of saturating the dry fiber sheet with the binding resin prior to adhering the sheet onto the surface of the concrete, while dry-layup is the process of saturating the dry fiber sheet once it has already been placed onto the concrete surface (Pevey 2018).

Surface preparation is required for all areas of the concrete substrate that will receive the FRP sheet. Areas of deteriorated concrete shall be repaired and all concrete prepared to a specified concrete surface profile (CSP) of 3 by acid etching, grinding, abrasive (sand) blasting, or steel shotblasting as required by Section 3.3.C of ICRI 330.2-2016. This preparation ensures a sound concrete substrate and appropriate roughness for bonding of the FRP laminate to the surface.

2.3.1 Anchorage Systems

To ensure the externally bonded FRP strengthening system is secured in place, an anchorage system is needed. An anchorage system is an additional component to the primary externally bonded sheet which aides in developing the full capacity (or rupture strain) of the sheet. Orton et al. (2008) determined that anchorage systems can improve the material efficiency of carbon fiber reinforced polymer (CFRP) retrofits. Although there have been numerous studies on the effect of anchorage on the behavior of FRP-strengthened reinforced concrete members, no widely accepted standard for anchorage design currently exists. As stated in ACI 440.2R-17, “because no anchorage design guidelines are currently available, the performance of any anchorage system should be substantiated through representative physical testing.” According to Pevey (2018), for some state departments of transportation, the determination of appropriate anchorage techniques is dependent upon information from the supplier of the FRP system. Unlike metallic anchors, FRP material-based anchorage systems that include anchors made from FRP are noncorrosive. Common anchorage systems are described in the following subsections with the primary focus being on the anchorage systems in which the anchors are composed of FRP material.

2.3.1.1 U-Wrap Anchors

U-wrap anchors consist of supplemental FRP sheets that are used to anchor the primary externally bonded FRP sheet in place. These anchors are oriented perpendicular to the longitudinal axis of the primary externally bonded FRP sheet (see Figure 2.2). For flexural strengthening systems, such anchors can fully enclose all four sides of the beam but usually only wrap around three sides (U-wrap anchors) due to limited access to the top surface of the member. The application of a U-wrap anchor to an inverted test specimen is provided in Figure 2.2(a). An elevation of the three-sided U-wrap anchor is provided in Figure 2.2(b).

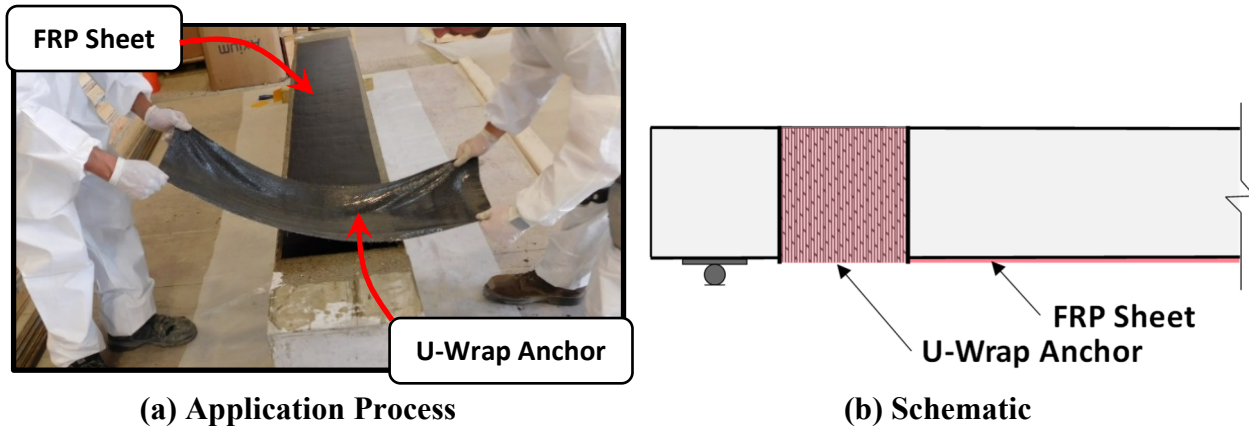


Figure 2.2: U-Wrap Anchor

Additional surface preparation is required for this anchorage system. In order to reduce stress concentrations in the FRP sheet at the corners of the member, it is required by ICRI 330.2-2016 and ACI 440.2R-17 that all corner and sharp edges be rounded to a minimum radius of 0.5 in. where FRP is to be wrapped.

2.3.1.2 FRP Anchors

Also known as fan anchors, spike anchors, or simply fiber anchors, FRP anchors consist of a bundle of fibers saturated with a binding resin. Both “spike” and “fan” are accurate descriptions of this anchor as the saturated bundle of fibers is inserted (or “spiked”) through the externally bonded sheet into a pre-drilled hole in the concrete substrate and then spread (or “fanned”) out onto the surface of the externally bonded FRP sheet. An example of the use of FRP anchors is shown in Figure 2.3.

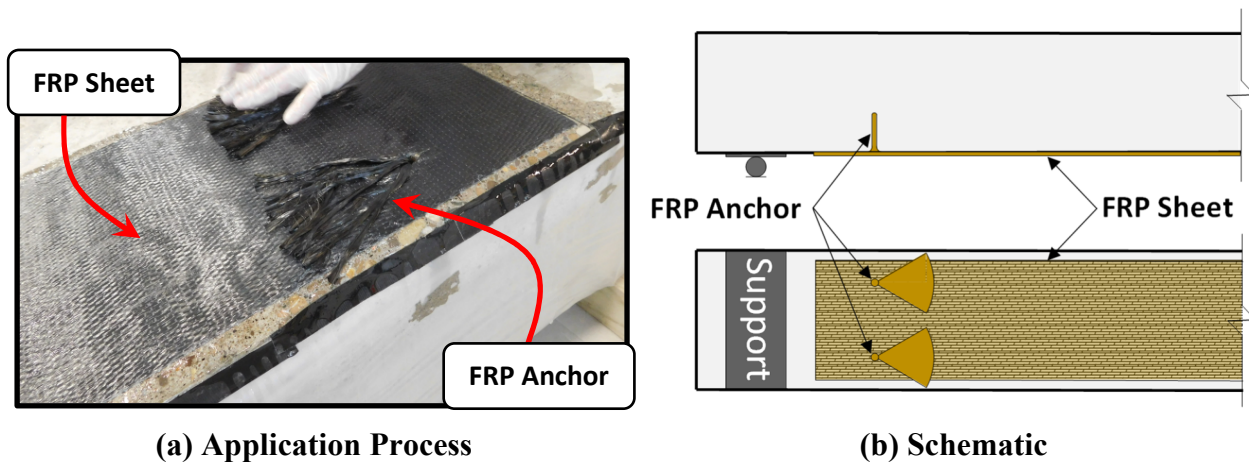


Figure 2.3: FRP Anchors

Although there is limited guidance for the design of FRP anchors, some past research has shown that these anchors can be used effectively if properly sized. After conducting an experimental study using carbon fiber reinforced polymer anchors, Quinn (2009) achieved satisfactory anchor performance when the following details were used:

- Anchor holes drilled at least 4-in. into the member with an area 40% larger than the area of the material used for the anchor
- Anchor holes rounded to a minimum radius of 0.5-in.
- The area of the FRP anchor should be twice the area of the primary FRP sheet in which it is anchoring
- The splayed portion of the FRP anchor extended at least 0.5-in. outside the primary FRP sheet onto the concrete surface at an angle no greater than 60 degrees
- Two square sheets applied onto the FRP anchor, the first with its fibers oriented perpendicular to the primary FRP sheet and the second oriented parallel to the primary FRP sheet

While U-wrap anchors rely solely on the bond between the anchored sheet and the concrete substrate, the geometry of fiber anchors allow for both friction forces and bearing forces to develop in the force transfer mechanism between the anchored sheet and the concrete substrate as described in Pham (2009) (see Figure 2.4).

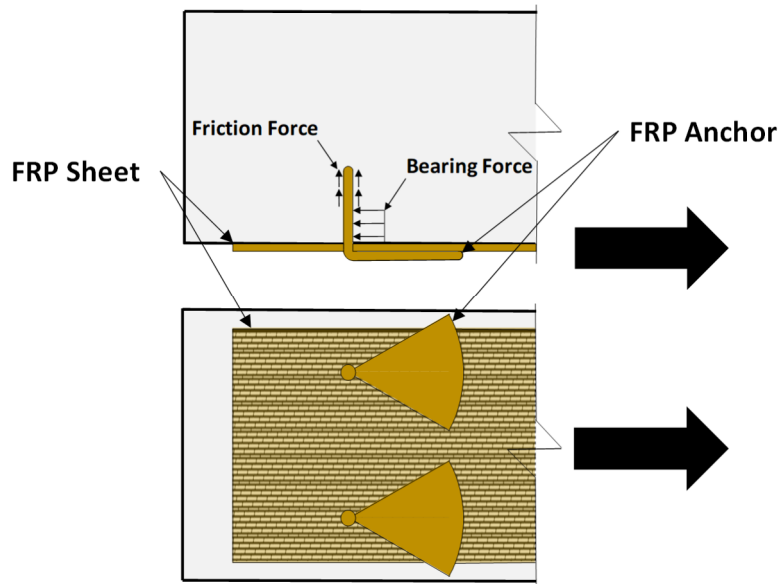


Figure 2.4: FRP Anchor Force Transfer (adapted from Pham 2009)

In addition to the surface preparation required for the externally bonded FRP sheet, surface preparation is required for FRP anchors. Anchor holes must be pre-drilled in the concrete substrate to receive the anchors. The drilling of these holes requires the contractor to have knowledge of the layout of the steel reinforcement in the existing member through either existing plans or the use of specialized equipment (e.g. ground penetrating radar). Furthermore, the edges of the drilled holes need to be rounded to a minimum radius of 0.5-in. as required by ICRI 330.2-2016 and ACI 440.2R-17 to reduce the stress concentration where the anchor exits the hole.

2.3.1.3 Other Anchorage Systems

According to ACI 440.2R-17, other possible anchorage systems include mechanical fasteners, FRP strips, and U-anchors (FRP near-surface-mounted bars used to anchor externally bonded sheets). Mechanical fasteners may include steel plates and threaded rods (Pevey 2018). Further information about these other anchorage systems can be found in Pevey (2018).

2.3.1.4 Anchorage Systems Investigated During Experimental Program

The experimental program was developed with the intention to investigate the effectiveness of both U-wrap anchors and FRP anchors. Based on their proven effectiveness in past experimental studies, these two anchorage systems were selected as the best candidates to successfully anchor

an externally bonded FRP strengthening system to deteriorated adjacent box beams (or spread box beams in the case of the U-wrap anchors).

2.4 Near Surface Mounted Strips

In contrast to externally bonded systems, near-surface-mounted (NSM) systems are installed within the cross section of the concrete member. FRP applied in this manner can be in the form of circular bars or rectangular bars (strips). Rectangular strips were used in the experimental program detailed in Chapters 3 and 4, as can be seen in Figure 2.5. Although circular bars could have been used, rectangular strips were readily available by the manufacturer for the purposes of the experimental program. Furthermore, a strip with the same width as the diameter of a bar provides more cross-sectional area than the bar. The components of this FRP strengthening system (NSM strips and epoxy grout) can be seen in Figure 2.5(a) during the application process to an inverted test specimen.

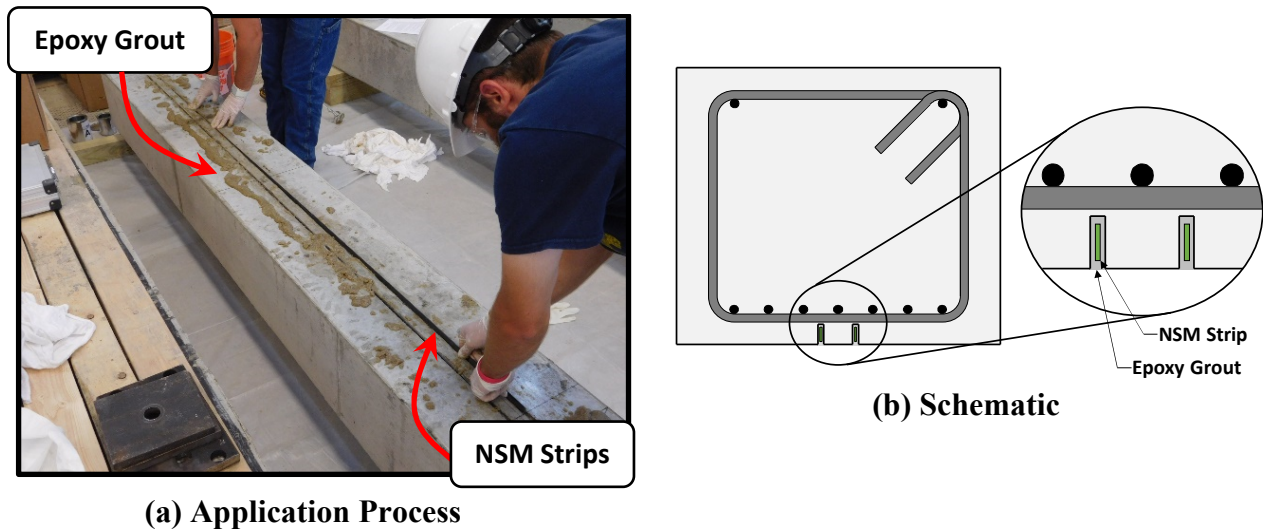


Figure 2.5: Near-Surface-Mounted (NSM) Strengthening System

For this system to be applied for flexural strengthening, grooves are saw-cut down the length of the tension face of the member for the NSM reinforcement to then be placed. Referencing Hassan and Rizkalla (2003), Section 14.3 of ACI 440.2R-17 suggests dimensions of the grooves based on the size of the FRP reinforcement (see Figure 2.6). Furthermore, ACI 440.2R-17 states that the minimum clear spacing between two grooves should be at least twice the depth of the

groove. Moreover, it is suggested that the clear edge distance measured from the groove be four times the depth of the groove to minimize a potential debonding failure (ACI 440.2R-17). The suggested groove dimension ($1.5d_b$ or $1.5b_b$) into the section of the existing member becomes important when determining if the strengthening system is applicable to a situation given the layout of the steel reinforcement in the existing member. For example, if the required depth into the section of the existing member is greater than the concrete cover, then proper use of the strengthening system may not be possible. An epoxy grout is inserted in the grooves to bond the FRP reinforcement to the concrete substrate.

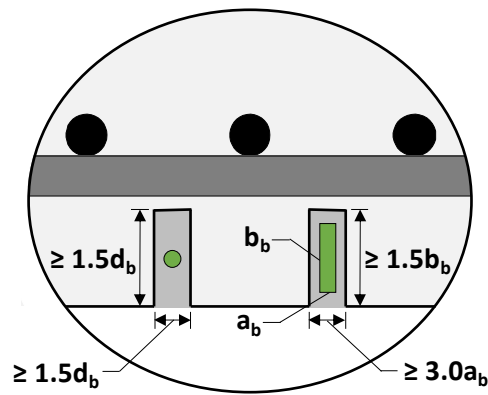


Figure 2.6: Minimum Groove Dimensions for NSM Reinforcement (adapted from ACI 440.2R-17)

Because this FRP strengthening system is within the cross section of the member, it has the advantage of being protected from some environmental factors that other strengthening systems may face. With this comes the disadvantage of forcing the contractor to destructively modify the existing member that will receive the NSM reinforcement, creating the need to accurately know the location of the existing steel reinforcement and avoid damaging it during installation.

2.5 Calculation of Nominal Flexural Strength

The process of calculating the nominal flexural strength of an FRP-strengthened reinforced concrete member in accordance with ACI 440.2R-17 is presented in this section. As with typical flexural analysis of a reinforced concrete beam, the nominal flexural strength of a section is determined by the internal coupling moment generated by the compressive and tensile forces

developed by the constituent materials that resist externally applied moments. For FRP-strengthened sections, an additional tensile force from the FRP is added to the analysis.

Before calculating the nominal flexural strength, a basic understanding of the possible failure modes for an FRP-strengthened section should be discussed. The design procedures presented in Section 10.1.1 of ACI 440.2R-17 account for the following failure modes:

- Concrete crushes in compression prior to yielding of the reinforcing steel
- Reinforcing steel yields in tension followed by FRP rupture
- Reinforcing steel yields in tension followed by concrete crushing in compression
- Concrete cover delamination due to shear/tension
- FRP debonds from the concrete substrate prior to FRP rupture

The internal strain and stress distributions for an FRP-strengthened reinforced concrete section at nominal moment capacity as given in ACI 440.2R-17 are presented in Figure 2.7. Because there are multiple possible failure modes for an FRP-strengthened section, the equivalent rectangular compressive stress block (Whitney stress block) approximation for concrete is not always applicable. Therefore, a nonlinear concrete stress distribution is also presented in Figure 2.7. As suggested in Section 10.2.10 of ACI 440.2R-17, the Whitney stress block is often acceptable to use because it yields “reasonably accurate results” regardless of the failure mode (ACI 440.2R-17). For the strength analysis provided henceforth in this section, the parameters associated with the Whitney stress block will be used.

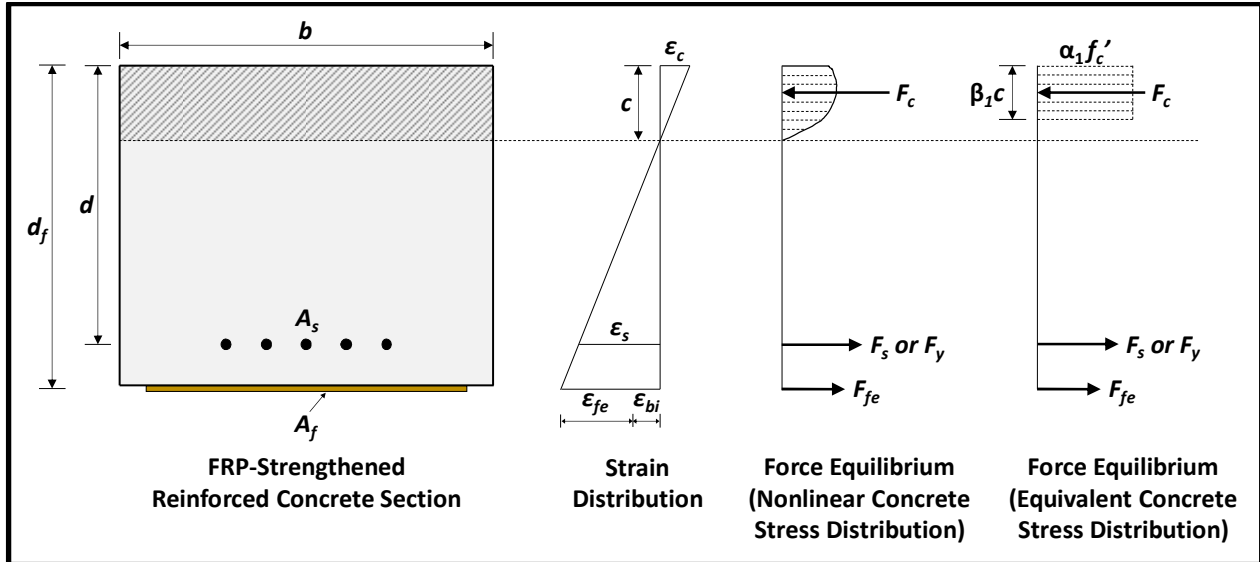


Figure 2.7: Internal Strain and Stress Distribution for FRP-Strengthened Reinforced Concrete Section at Nominal Moment Capacity (adapted from ACI 440.2R-17)

For the strength analysis of an FRP-strengthened section, a few key assumptions are required as stated in Section 10.2.1 of ACI 440.2R-17:

- Material properties, reinforcement details, and dimensions of the existing member being strengthened are used in design calculations
- Plane sections remain plane (i.e., material strains are proportional to their respective distance from the neutral axis)
- Strain compatibility is maintained between FRP reinforcement and the concrete
- Within the adhesive, or epoxy, layer, shear deformations are assumed to be negligible
- Compressive strain in the concrete is limited to 0.003 at failure
- Tensile strength of the concrete is neglected
- A linear-elastic stress-strain relationship is assumed for FRP reinforcement

To properly design an FRP-strengthened member, it is required to ensure the factored nominal flexural strength of the section, ϕM_n , can resist the applied factored moment at that section, M_u . This design check is represented by Equation 2-1 as follows (Eq. 10.1 of ACI 440.2R-17):

$$\phi M_n \geq M_u \quad (2-1)$$

where:

$$\begin{aligned}\phi &= \text{strength reduction factor, see Equation 2-2} \\ M_n &= \text{nominal flexural strength (in.-lb)} \\ M_u &= \text{factored moment at a section (in.-lb)}\end{aligned}$$

The strength reduction factor, ϕ , is calculated in accordance with Equation 2-2 and is a function of the strain in the extreme layer of steel tension reinforcement, ϵ_t , at the nominal moment capacity. Because of the ductility the member can achieve when the net tensile strain in the extreme layer of steel reinforcement at nominal strength is at least 0.005, a strength reduction factor of 0.90 is specified for a value of ϵ_t greater than or equal to 0.005. Strains less than 0.005 (i.e., a less ductile section) correspond to a smaller reduction factor based on Equation 2-2 (Eq. 10.2.7 of ACI 440.2R-17):

$$\phi = \begin{cases} 0.90 \text{ for } \epsilon_t \geq 0.005 \\ 0.65 + \frac{0.25(\epsilon_t - \epsilon_{sy})}{0.005 - \epsilon_{sy}} \text{ for } \epsilon_{sy} < \epsilon_t < 0.005 \\ 0.65 \text{ for } \epsilon_t \leq \epsilon_{sy} \end{cases} \quad (2-2)$$

where:

$$\begin{aligned}\epsilon_t &= \text{net tensile strain in extreme tension steel reinforcement at} \\ &\quad \text{nominal strength (in./in.)} \\ \epsilon_{sy} &= \text{strain corresponding to yield strength of steel reinforcement} \\ &\quad \text{(in./in.)}\end{aligned}$$

The nominal flexural strength, M_n , is calculated in accordance with Equation 2-3 as follows (Eq. 10.2.10d of ACI 440.2R-17):

$$M_n = A_s f_s \left(d - \frac{\beta_1 c}{2} \right) + \psi_f A_f f_{fe} \left(d_f - \frac{\beta_1 c}{2} \right) \quad (2-3)$$

where:

A_f	=	area of FRP reinforcement (in. ²)
A_s	=	area of nonprestressed steel tension reinforcement (in. ²)
β_1	=	factor relating depth of equivalent rectangular compressive stress block to depth of neutral axis, see Equation 2-4
c	=	distance from extreme compressive fiber to neutral axis (in.)
d	=	distance from the extreme compression fiber to centroid of nonprestressed steel tension reinforcement (in.)
d_f	=	depth to outermost layer of FRP reinforcement (in.)
f_{fe}	=	effective stress in the FRP reinforcement (psi)
f_s	=	tensile stress in steel reinforcement (psi)
ψ_f	=	FRP strength reduction factor (0.85 for flexure, as recommended by ACI 440.2R-17)

The factor relating the depth of the equivalent rectangular compressive stress block (Whitney stress block) to the depth of the neutral axis, β_1 , is a function of the compressive strength of the concrete. It is calculated in accordance with Equation 2-4 as follows (Table 22.2.2.4.3 of ACI 318-19):

$$\beta_1 = \begin{cases} 0.65 & \text{if } f'_c \geq 8000 \\ 0.85 - \frac{0.05(f'_c - 4000)}{1000} & \text{if } 4000 < f'_c < 8000 \\ 0.85 & \text{if } 2500 \leq f'_c \leq 4000 \end{cases} \quad (2-4)$$

where:

$$f'_c = \text{specified compressive strength of concrete (psi)}$$

In order to account for potential debonding of the FRP reinforcement, the debonding strain is estimated. The value is limited by a percentage of the design rupture strain. The debonding strains for externally bonded and near-surface-mounted reinforcement are calculated using Equations 2-5 and 2-9, respectively.

The debonding strain of externally bonded FRP reinforcement, ϵ_{fd} , is calculated by Equation 2-5 as follows (Eq. 10.1.1 of ACI 440.2R-17):

$$\epsilon_{fd} = 0.083 \sqrt{\frac{f'_c}{nE_f t_f}} \leq 0.9\epsilon_{fu} \text{ (in. -lb)} \quad (2-5)$$

where:

E_f	=	tensile modulus of elasticity of FRP (psi)
n	=	number of plies of FRP reinforcement
t_f	=	nominal thickness of one ply of FRP reinforcement (in.)
ϵ_{fu}	=	FRP design rupture strain (in./in.), see Equation 2-6

The value of ϵ_{fd} is limited by $0.9\epsilon_{fu}$ in Equation 2-5 in consideration of rupture of the FRP.

To determine the FRP design rupture strain, ϵ_{fu} , used in Equations 2-5, the ultimate rupture strain reported by the manufacturer must be reduced by the environmental reduction factor, C_E . This is calculated in Equation 2-6 as follows (Eq. 9.4b of ACI 440-2R-17):

$$\epsilon_{fu} = C_E \epsilon_{fu}^* \quad (2-6)$$

where:

C_E	=	environmental reduction factor, see Table 2.2
ϵ_{fu}^*	=	ultimate FRP rupture strain reported by the manufacturer (in./in.)

Similarly, the ultimate rupture stress reported by the manufacturer, f_{fu}^* , is reduced by the environmental reduction factor, C_E , to obtain the FRP design rupture stress, f_{fu} . This is calculated by Equation 2-7 as follows (Eq. 9.4a of ACI 440-2R-17):

$$f_{fu} = C_E f_{fu}^* \quad (2-7)$$

where:

- f_{fu} = FRP design rupture stress (psi)
 f_{fu}^* = ultimate FRP rupture stress reported by the manufacturer (psi)

The environmental reduction factor, C_E , is specified in ACI 440.2R-17 for various exposure conditions. The values as given in ACI 440.2R-17 are presented in Table 2.2.

Table 2.2: Environmental Reduction Factor (from ACI 440.2R-17)

Exposure Conditions	Fiber Type	Environmental Reduction Factor, C_E
Interior exposure	Carbon	0.95
	Glass	0.75
	Aramid	0.85
Exterior exposure (bridges, piers, and unenclosed parking garages)	Carbon	0.85
	Glass	0.65
	Aramid	0.75
Aggressive environment (chemical plants and wastewater treatment plants)	Carbon	0.85
	Glass	0.50
	Aramid	0.70

The tensile modulus of elasticity of FRP, E_f , is calculated by Equation 2-8 as follows (Eq. 9.4c of ACI 440.2R-17):

$$E_f = \frac{f_{fu}}{\varepsilon_{fu}} \quad (2-8)$$

The assumed debonding strain of near-surface-mounted FRP reinforcement, ε_{fd} , is calculated in Equation 2-9 as recommended in Section 10.1.1 of ACI 440.2R-17:

$$\varepsilon_{fd} = 0.7\varepsilon_{fu} \quad (2-9)$$

Although the value for ε_{fd} in Equation 2-9 is recommended, ACI 440.2R-17 states that the value “may vary from $0.6\varepsilon_{fu}$ to $0.9\varepsilon_{fu}$.”

To achieve the adequate development of the near-surface-mounted FRP reinforcement, the bonded length of the bar or strip should exceed the development length, ℓ_{db} , calculated by Equations 2-10 and 2-11 as follows (Eq. 14.3a and 14.3b of ACI 440.2R-17):

$$\ell_{db} = \frac{d_b}{4\tau_b} f_{fd} \quad \text{for circular reinforcement (bars)} \quad (2-10)$$

$$\ell_{db} = \frac{a_b b_b}{2(a_b + b_b)(\tau_b)} f_{fd} \quad \text{for rectangular reinforcement (strips)} \quad (2-11)$$

where:

d_b	=	diameter of the circular FRP reinforcement (in.)
τ_b	=	average bond strength for FRP bars (psi)
a_b	=	smaller cross-sectional dimension for rectangular FRP bars (in.)
b_b	=	larger cross-sectional dimension for rectangular FRP bars (in.)
f_{fd}	=	debonding stress of the FRP reinforcement (psi)

Next, the effective strain in the FRP reinforcement at failure, ε_{fe} , is determined by Equation 2-12. The middle term in Equation 2-12 gives the strain in the FRP when the concrete crushes in compression. If the middle expression is less than the value of ε_{fd} , then the controlling failure mode is concrete crushing. In order to use Equation 2-12, a neutral axis value must first be assumed. This value is later refined using Equation 2-16. The value of ε_{fe} is calculated by Equation 2-12 as follows (Eq. 10.2.5 of ACI 440.2R-17):

$$\varepsilon_{fe} = \varepsilon_{cu} \left(\frac{d_f - c}{c} \right) - \varepsilon_{bi} \leq \varepsilon_{fd} \quad (2-12)$$

where:

ε_{cu}	=	0.003 (maximum usable compressive strain in the concrete)
--------------------	---	---

ϵ_{bi} = existing substrate strain at the time FRP is applied
(assuming cracked section properties)

Once the effective strain is determined, the effective stress in the FRP, f_{fe} , can be calculated using the tensile modulus of elasticity, E_f , using Equation 2-13 as follows (Eq. 10.2.6 of ACI 440.2R-17):

$$f_{fe} = E_f \epsilon_{fe} \quad (2-13)$$

Next, strain in the steel reinforcement is calculated using similar triangles in the strain distribution schematic in Figure 2.7, resulting in Equation 2-14:

$$\epsilon_s = (\epsilon_{fe} + \epsilon_{bi}) \left(\frac{d-c}{d_f-c} \right) \quad (2-14)$$

The force in the steel reinforcement, assuming the steel has not yet yielded, is calculated in Equation 2-15:

$$f_s = E_s \epsilon_s \quad (2-15)$$

where:

E_s = modulus of elasticity of steel reinforcement (psi)

In order to refine the value of the neutral axis depth, c , force equilibrium must be satisfied. Equation 2-16 can be reorganized in order to solve for a refined value of c (Equation 10.3.1.6f in ACI 440.2R-17).

$$\alpha_1 f_c' \beta_1 b c = A_s f_s + A_f f_{fe} \quad (2-16)$$

where:

α_1 = equivalent compressive stress block factor, taken as 0.85

The initial calculation of Equation 2-12 requires the neutral axis depth to be assumed. With an assumed neutral axis depth, material forces can be determined using similar triangles in the strain distribution schematic in Figure 2.7. Then the force equilibrium equation can be used to solve for a new neutral axis depth with the given forces. Once the new neutral axis depth is determined with Equation 2-16, it can be plugged back into Equation 2-12 to acquire a more accurate estimation of the neutral axis depth. This refinement process is repeated until both Equations 2.12 and 2.16 are satisfied, thus giving the actual depth of the neutral axis, c .

Finally, the nominal flexural strength of the section can be accurately calculated using Equation 2-3 once the actual depth of the neutral axis is determined. Equation 2-1 is then checked to ensure a satisfactory FRP design.

2.6 Research Need

Despite the increasing popularity of the use of FRP for structural concrete applications, there remains a need for additional guidance for the design of FRP strengthening systems, especially for anchorage systems. Because there are limited guidelines for anchoring FRP strengthening systems, experimental research is needed to compile the necessary data to provide guidance for future designs. The experimental program described in the following chapters will aim to add to this developing research with a specific focus on strengthening box beam bridge members.

CHAPTER 3. EXPERIMENTAL PROGRAM

3.1 Introduction

An experimental program was developed to directly compare the performance of two FRP flexural strengthening systems in regard to the increase in strength and stiffness provided to reinforced concrete beam members. The feasibility of using the strengthening systems on box beam bridges in the field is also considered. A total of 22 beam specimens were fabricated in the laboratory and tested in flexure. The experimental program is described in detail within this chapter.

3.2 Specimen Design

As described in Section 1.1, adjacent precast concrete box beam bridges are prone to deterioration that may lead to flexural deficiencies (Frosch et al. 2020a, 2020b). To evaluate the effectiveness of potential flexural strengthening methods for box beams, laboratory specimens were designed and fabricated with common box beam characteristics in mind. To specifically create specimens that are representative of common box beams in Indiana, the specimens were designed to mimic characteristics of the 1960s era WS-42 standard box beam (see Figure 3.1). The WS-42 box beam from INDOT's 1961 standard drawings (see Appendix B) was chosen to provide the general details of typical box beams in the field that are now experiencing deterioration. Although prestressed reinforcement was not used in the test program, other significant variables from the WS-42 box beam were incorporated into the research. Variables such as reinforcement spacing and concrete cover were held constant in order to simulate limitations involved with installing and anchoring the FRP strengthening systems.

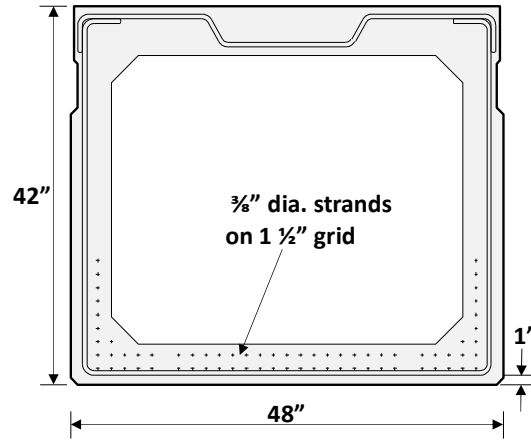


Figure 3.1: WS-42 Box Beam Cross Section (INDOT 1961 Standard Set)

The 22 reinforced concrete beam specimens were rectangular in cross section with a depth of 12 in. and a width of 14 in., as shown in Figure 3.2. The specimens were designed with one layer of longitudinal tension (i.e., bottom) reinforcement consisting of No. 3 Grade 60 bars spaced at 1.5 in. The number of bars in each specimen was varied, as described later in this section. Two No. 3 Grade 60 longitudinal reinforcing bars were also included in all of the specimens near the compression face of the member and acted as hanger bars for the stirrups. Each specimen was designed with 20 No. 3 Grade 60 stirrups spaced at 6 in. along the member length. The shear reinforcement ensured that a shear failure would be precluded. It should be noted that a bottom cover dimension of 1 in., longitudinal reinforcement with a diameter of 3/8 in., and a reinforcement grid spacing of 1.5 in. were not only standard for the 1960s WS-42 box beam but were typical for all standard adjacent precast concrete box beams used in that era (see Appendix B). A total length of 120 in. was selected for all specimens based on an approximate scaled ratio of the WS-42 cross-sectional dimensions with consideration of the typical span lengths of adjacent box beam bridges in Indiana (Frosch et al. 2020a). General specimen details are provided in Figure 3.2.

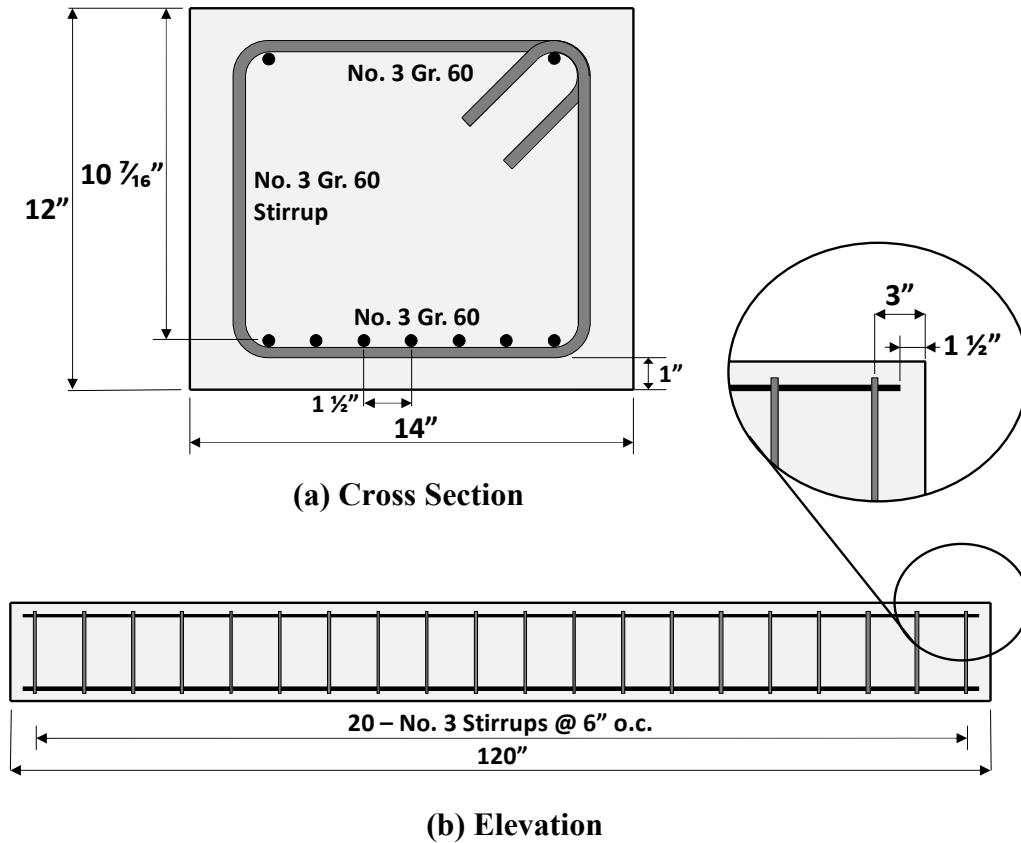


Figure 3.2: General Specimen Dimensions

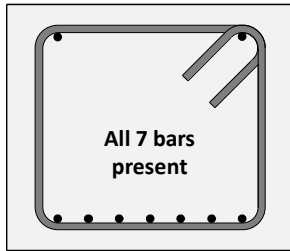
The experimental program consisted of three primary groups of beams and an additional pilot group of four initial test beams. For the purposes of this discussion, the state of each specimen at the time of fabrication is referred to as its “simulated field condition” (see Figure 3.3). The details of each specimen are summarized in Table 3.1.

Table 3.1: Test Matrix

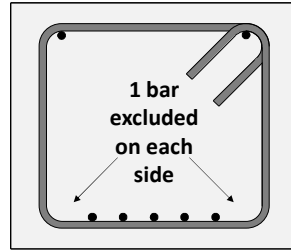
Group	Specimen ID	Simulated Field Condition			FRP Strengthening System							
		Control (C)	Artificially Deteriorated (D)			Externally Bonded Sheet (EB)			Near-Surface-Mounted Strips (NSM)			No FRP
		[I] All 7 bars present	[II] 1 bar excluded on each side	[III] 1 bar cut at midspan on each side	[I] 2 bars excluded on one side	[1] FRP anchors along length	[2] FRP anchors at ends	[3] U-Wrap anchors at ends	[1] 2 strips centered on beam	[2] 2 strips under excluded bars	[3] 2 strips offset from excluded bars	
0 (Pilot)	0-C ¹											
	0-EB.2											
	0-EB.3											
	0-NSM.1											
1	1-C											
	1-D											
	1-EB.1											
	1-EB.2											
	1-NSM.1a											
	1-NSM.1b ²											
2	2-C											
	2-D											
	2-EB.1											
	2-EB.2											
	2-NSM.1											
3	3-C											
	3-D											
	3-EB.1											
	3-EB.2											
	3-NSM.1											
	3-NSM.2											
3-NSM.3												

¹Pin-roller support condition

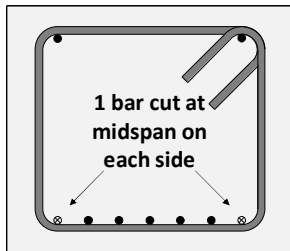
²Epoxy grout and NSM strips applied overhead



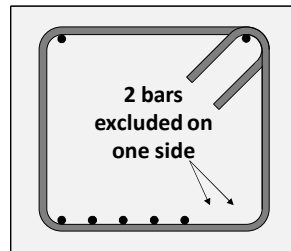
(a) Control



(b) Artificially Deteriorated Type I



(c) Artificially Deteriorated Type II



(d) Artificially Deteriorated Type III

⊗ = cut reinforcing bar

Figure 3.3: Simulated Field Conditions

As indicated in Table 3.1, each specimen group contained one full-strength control specimen with seven longitudinal tension reinforcing bars in addition to a number of specimens that were intentionally weakened in a manner that was specific to the group in which they belonged. This intentional weakening of select specimens was designed to simulate the conditions caused by common deterioration patterns experienced by box beams in the field. Therefore, the weakened specimens are referred to as “artificially deteriorated.” Artificial deterioration was accomplished by either excluding or cutting longitudinal tension reinforcing bars at the time of fabrication. Excluded reinforcing bars (Types I and III, refer to Table 3.1 and Figure 3.3) simulated extensively deteriorated reinforcement that is no longer effective in flexure. Cut reinforcing bars (Type II) simulated locally fractured reinforcement. For each cut bar, the location of the cut was at midspan to simulate a worst-case scenario of fractured longitudinal reinforcement due to deterioration. Of the artificially deteriorated specimens in each group, one was tested in its simulated field condition while all others were strengthened prior to testing with one of the two FRP strengthening systems as described in Section 2.2 (externally bonded sheet or near-surface-mounted strips). The strengths provided by the two FRP strengthening systems were determined in accordance with ACI 440.2R-17 with the objective of fully regaining the capacity of the control specimen. The specimens were designed so that the calculated flexural capacities resulting from each of the two FRP systems are similar, allowing practical comparisons to be made between FRP strengthening systems within each group. ACI 318-19 was used to calculate the capacities of the control specimens and the artificially deteriorated specimens that were left unstrengthened.

The artificially deteriorated Type I specimens simulated box beams with deterioration near both bottom corners that led to the reinforcement near the corners to be ineffective. For the artificially deteriorated Type III specimens, the objective was to simulate unsymmetrical deterioration of reinforcement with the intention of evaluating how the location of the near-surface-mounted strengthening system, in relation to the excluded reinforcement, affected the overall performance of the specimen. All three types of artificial deterioration were designed to result in the same nominal capacity at midspan in order to facilitate comparisons of similarly strengthened specimens between different groups.

A color scheme is used in Table 3.1 to help highlight similarities between specimen types as well as distinguish variations of each strengthening system. Within the specimen ID column, all control specimens with seven longitudinal tension bars are shown in blue. In the same column, all specimens tested in the weakened, or artificially deteriorated, state are shown in beige. The externally bonded FRP-strengthened specimens are shown in either light yellow or gold, depending on the anchorage configuration. The exception to the color scheme of the externally bonded FRP strengthening system is Specimen 0-EB.3, which is shown in pink and will be discussed further in Section 3.3.1.3. The near-surface-mounted FRP strengthening system is shown in three shades of green, depending on the location of the NSM strips. This color scheme will be used in upcoming figures, tabulated results, and plots for clarity.

Each specimen was given an identification tag that identifies the specimen by group number, specimen type (Control – C, Artificial Deterioration – D, Externally Bonded – EB, Near-Surface-Mounted – NSM), and, if applicable, strengthening system subset number. The strengthening system subset number refers to specific anchorage details for the externally bonded specimens and the location of the strips for the NSM specimens. These details of the strengthening systems are described in Sections 3.3.1 and 3.3.2, respectively. An example of a specimen identification label is provided in Figure 3.4 for Specimen 1-EB.2.

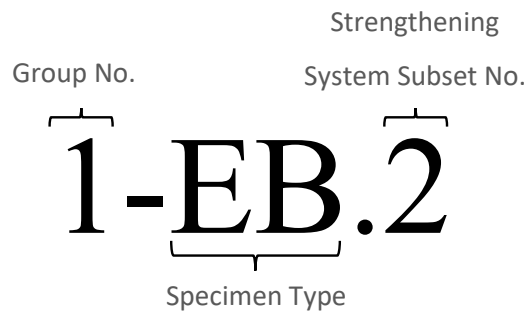


Figure 3.4: Specimen Identification Label

3.3 FRP Strengthening System Details

The following subsections present the details of the two FRP strengthening systems included in the experimental program: externally bonded FRP sheets and near-surface-mounted FRP strips. The configuration of each system is described, and the anchorage methodologies evaluated for the externally bonded FRP system are introduced.

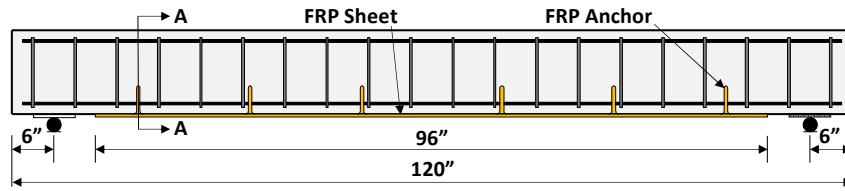
3.3.1 Externally Bonded (EB) Sheet Details

A total of eight specimens received one layer of a unidirectional FRP sheet that was adhered, or externally bonded (EB), to the tension face of the specimen along the longitudinal axis. All sheets were 12-in. wide (2-in. narrower than the beam width) and 96-in. long. As described in Section 2.3.1, a variety of anchorage methods can be implemented to anchor the FRP sheet to the concrete substrate and develop the rupture capacity. To further investigate the performance of the EB sheets, three different anchorage methods were evaluated in the experimental program. These anchorage methods are as follows, listed in ascending order of strengthening system subset number:

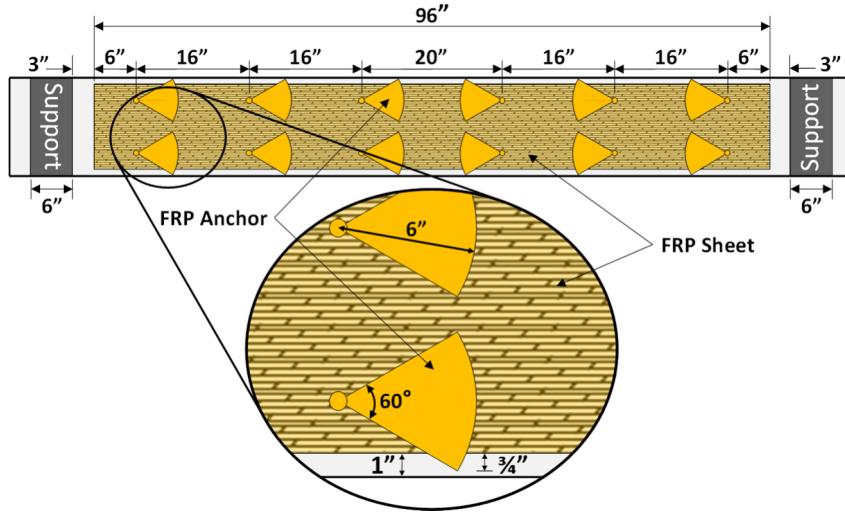
1. FRP anchors along the length of the sheet (EB.1)
2. FRP anchors at the ends of the sheet (EB.2)
3. U-wrap anchors at the ends of the sheet (EB.3)

3.3.1.1 FRP Anchors Along the Length (EB.1)

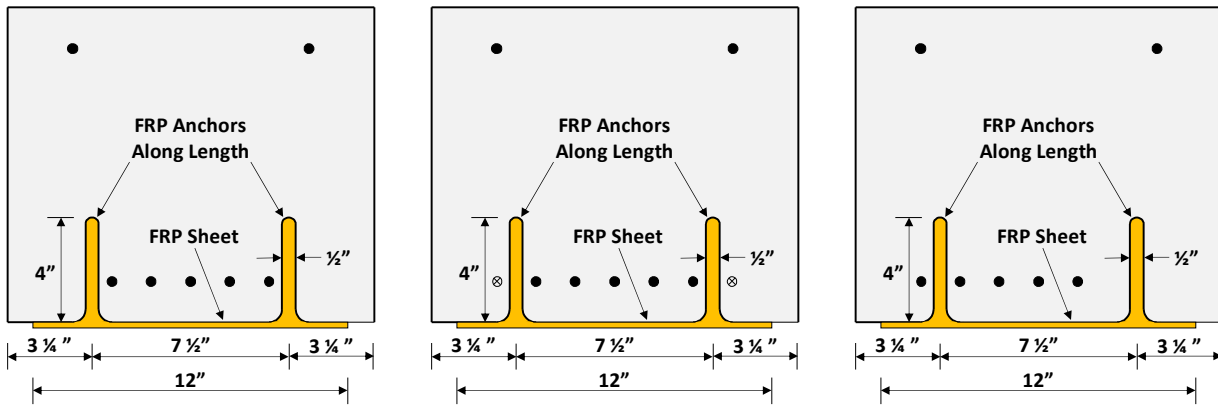
Details of the EB.1 strengthening system with FRP anchors along the length of the externally bonded sheet are provided in Figure 3.5. Six pairs of anchors were installed at the spacings shown in Figure 3.5(b). The placement of the supports in the test setup, described in Section 3.7, are shown for reference. The support plates were 36 in. by 6 in., which provided a 3-in. gap between the edge of the plate and the termination of the FRP strengthening system. Similar to the experimental tests conducted by Quinn (2009), each of the 12 anchors had a fan length of 6 in. and a fan angle of 60 degrees. The embedment depth of the anchors was 4 in. based on the research by Quinn (2009). Each anchor extended beyond the edge of the sheet by 3/4 in., as indicated. This dimension also complies with the guidelines from Quinn (2009) that suggest this dimension be at least 0.5 in. Each pair of anchors was covered with two 12-in. by 12-in patches cut from the same FRP sheet as the primary longitudinal sheet. The first patch placed over the anchors had fibers oriented transversely to the longitudinal sheet, and the second patch had fibers oriented parallel to the longitudinal sheet, as recommended by Quinn (2009). The placement of the patches is shown in Figure 3.5(d). The application of the EB.1 strengthening system will be discussed further in Section 3.6.1.1.



(a) Elevation View



(b) Plan View – Tension Face

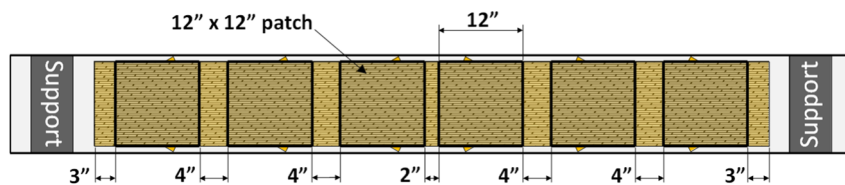


(i) 1-EB.1

(ii) 2-EB.1

(iii) 3-EB.1

(c) Section A-A

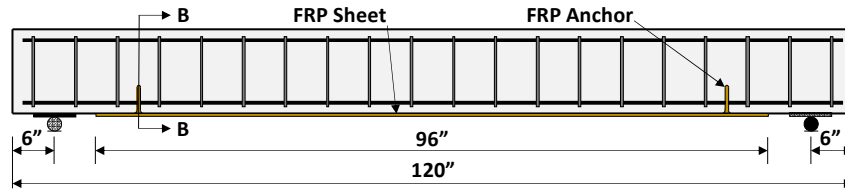


(d) Final Configuration (with 12-in. by 12-in. Patches)

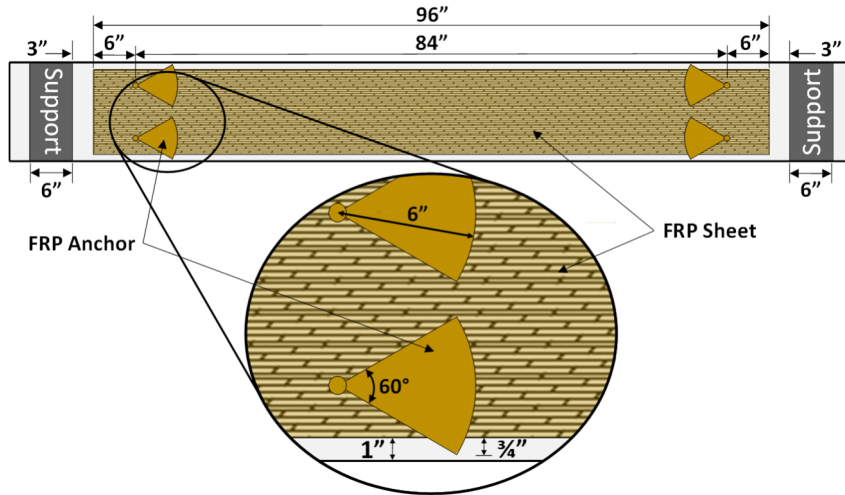
Figure 3.5: EB.1 Strengthening System

3.3.1.2 FRP Anchors at the Ends (EB.2)

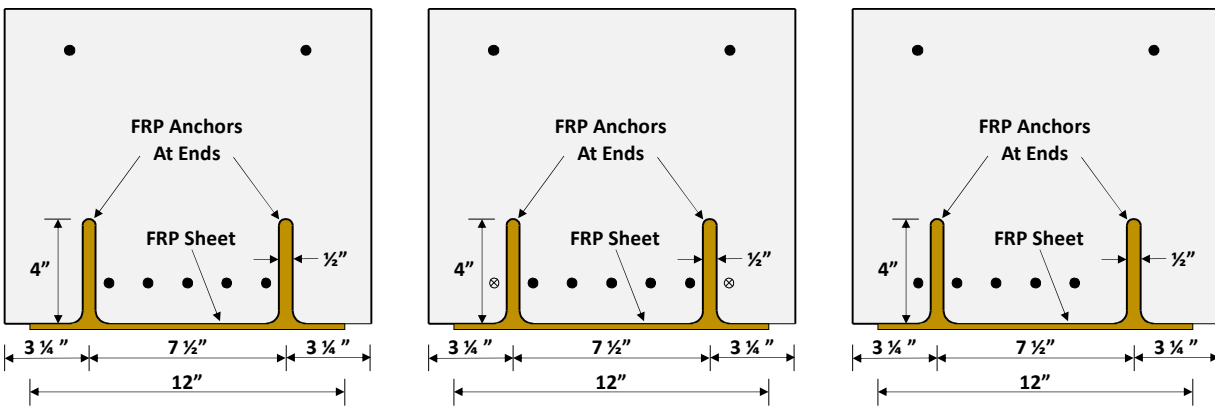
Details of the EB.2 strengthening system with FRP anchors only at the ends of the externally bonded sheet are provided in Figure 3.6. As shown, a pair of anchors was installed 6 in. from each end of the longitudinal sheet. The anchor details were the same as those described for the EB.1 system. Again, two patches with fibers oriented transversely and parallel to the longitudinal sheet were placed over each anchor pair as shown in Figure 3.6(d). The application of the EB.2 strengthening system will be discussed further in Section 3.6.1.1.



(a) Elevation View



(b) Plan View – Tension Face

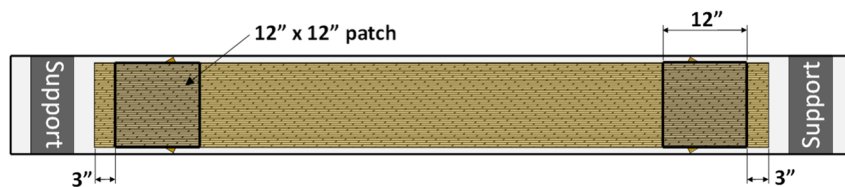


(i) 1-EB.2

(ii) 0-EB.2 and 2-EB.2

(iii) 3-EB.2

(c) Section B-B

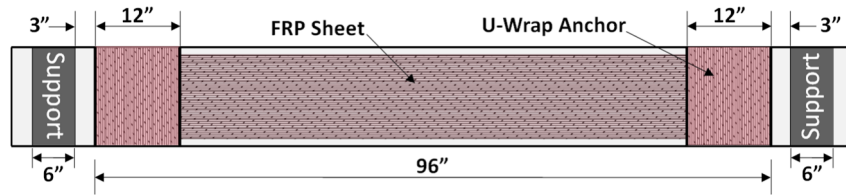
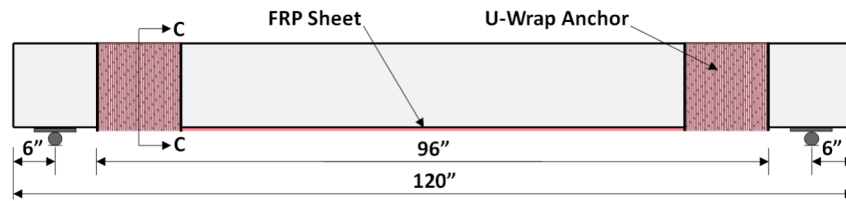


(d) Final Configuration (with 12-in. by 12-in. Patches)

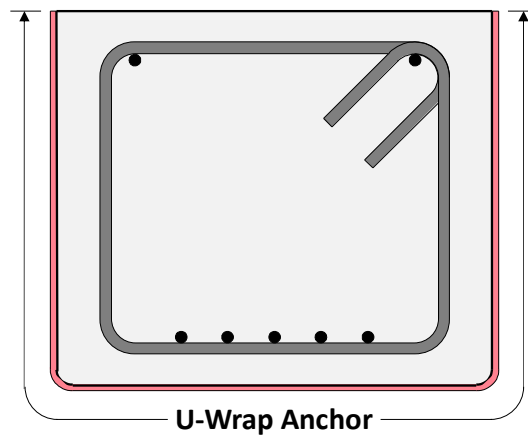
Figure 3.6: EB.2 Strengthening System

3.3.1.3 U-Wrap Anchors (EB.3)

Details of the EB.3 strengthening system with U-wrap anchors at the ends of the externally bonded sheet are provided in Figure 3.7. The U-wrap anchor provided at each end of the longitudinal sheet was 12-in. wide and extended over the full depth of the cross section as shown. The fibers of the U-wrap anchors were oriented perpendicular to the fibers of the longitudinal sheet. The application of the EB.3 strengthening system will be discussed further in Section 3.6.1.2. It should be noted that the U-wrap anchors were only included for one specimen (0-EB.3) in the pilot group (see Table 3.1). Due to the relatively inferior performance of the specimen and the fact that U-wraps cannot be installed on adjacent box beams in the field, this anchorage system was not included in the three primary specimen groups of the experimental program. Additional details of the performance of the specimen with U-wrap anchors are presented in Section 4.4.



(b) Plan View – Tension Face

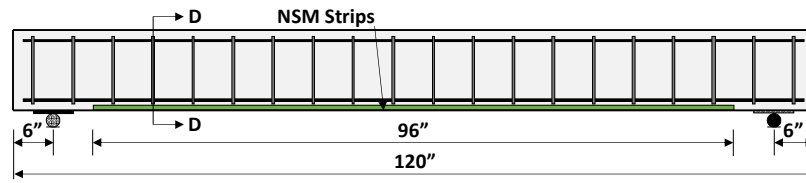


(c) Section C-C

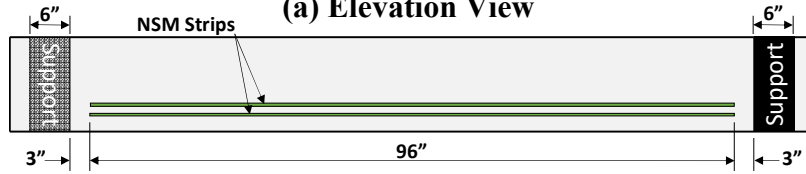
Figure 3.7: EB.3 Strengthening System

3.3.2 Near-Surface-Mounted (NSM) Strip Details

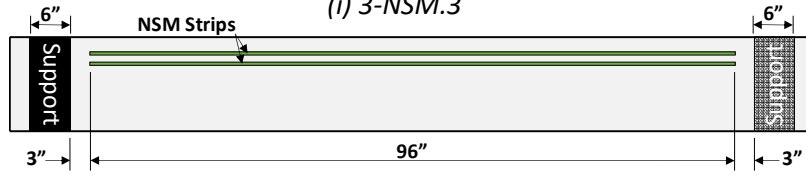
A total of seven specimens were strengthened with two near-surface-mounted FRP strips that were inserted into the section along the tension face of the member as shown in Figure 3.8. The cross sections of the rectangular strips had a nominal width of 0.079 in. and a nominal depth of 0.63 in., and each strip was 96 in. long. All strips were inserted to the same depth, centered inside a 0.875-in. deep groove cut into the cross section of the tension face of the specimen (see Figure 3.8(c)). Per ACI 440.2R-17, the suggested depth of a groove for a rectangular strip is 1.5 times the largest dimension of the strip. Therefore, the suggested depth of the groove is 0.945 in. for the NSM strips used in the experimental program. Since the specimens had a concrete cover of only 1.0 in., it was decided to test the specimens with strips inserted into a shallower groove with a depth of 0.875 in. to prevent cutting into a stirrup. All strips were centered on the longitudinal axis of the specimen with the exception of Specimens 3-NSM.2 and 3-NSM.3 (see Figure 3.8(b)). As previously discussed, the artificially deteriorated Type III specimens (see Figure 3.3(d)) were designed to simulate unsymmetrical deterioration of reinforcement to provide the means to evaluate the effects of the placement of NSM strips relative to the missing bars. The variation of the NSM strips relative to the missing bars is intended to simulate a field condition in which it would not be practical to place the NSM strips directly under the deteriorated reinforcement (i.e., insufficient concrete cover or excessive concrete spalling). The placement of the NSM strips relative to the missing bars of the Type III specimens (3-NSM.1, 3-NSM.2, and 3-NSM.3) is illustrated in Figure 3.8(c). The application of the NSM strengthening system will be discussed further in Section 3.6.2.



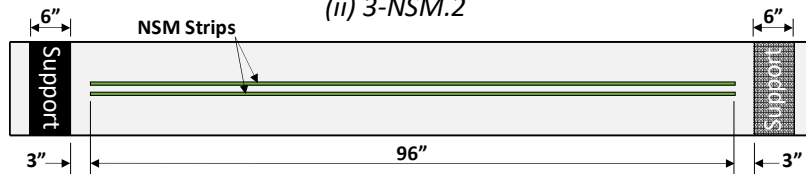
(a) Elevation View



(i) 3-NSM.3

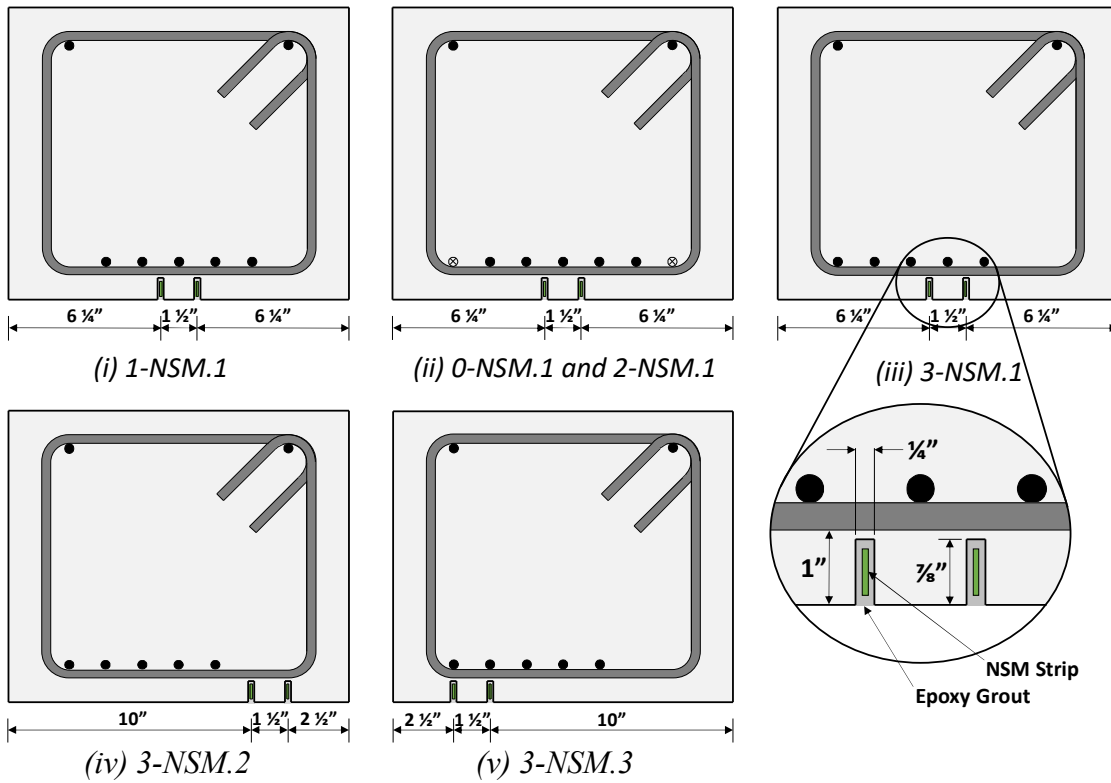


(ii) 3-NSM.2



(iii) 0-NSM.1, 1-NSM.1a, 1-NSM.1b, 2-NSM.1, and 3-NSM.1

(b) Plan View – Tension Face



(c) Section D-D

Figure 3.8: NSM Strengthening System

In Table 3.1, two specimens with NSM strips are included in Group 1. These specimens (1-NSM.1a and 1-NSM.1b) are essentially identical except for the orientation of the beams when the NSM strips were installed and the type of epoxy used to install the strips. Further details of the installation procedure and epoxy are provided in Section 3.6.2.

3.4 Material Properties

The following subsections provide the material properties and other details of the concrete, steel reinforcement, and fiber reinforced polymer systems used during the experimental program.

3.4.1 Concrete

All concrete used to cast the specimens was delivered to the laboratory by a local ready-mix producer. The concrete mixture design is provided in Table 3.2. The concrete was normalweight concrete with a target 28-day compressive strength of 4000 psi. The target slump was 4 in.

Table 3.2: Concrete Mixture Design

Material		S.G.	Quantity (lb/yd ³)
Cement	Type 1 Cement (ASTM C150)	3.15	520
Course Agg.	#8 Gravel (INDOT)	2.70	1850
Fine Agg.	Natural Sand	2.65	1458
Water		1.00	250.5
Entrapped Air		-	-
Water/Cement Ratio		0.482	

A total of four casts were required to fabricate all specimens of the experimental program. The beams within each group of the primary groups of specimens (Groups 1, 2, and 3) were fabricated together during separate casts, while the pilot group was comprised of beams from another cast and a specimen fabricated along with the Group 1 specimens. During each cast, 6-in. by 12-in. concrete test cylinders were prepared in accordance with ASTM C192 and stored in the same conditions as the beam specimens. The compressive strength for each cast group was tested

at 7, 14, and 28 days as well as on the test day of the beam specimens in accordance with ASTM C39. Prior to the compressive strength tests, a concrete cylinder end grinder was used to level the ends of each cylindrical test specimen so that they were parallel and plane. Furthermore, splitting tensile and modulus of elasticity tests were conducted in accordance with ASTM C496 and ASTM C469, respectively, on the day of each flexural test on a beam specimen. For each material test that was conducted, at least two cylinders were tested and the results were averaged. The typical compressive strength gain of the concrete is provided in Figure 3.9.

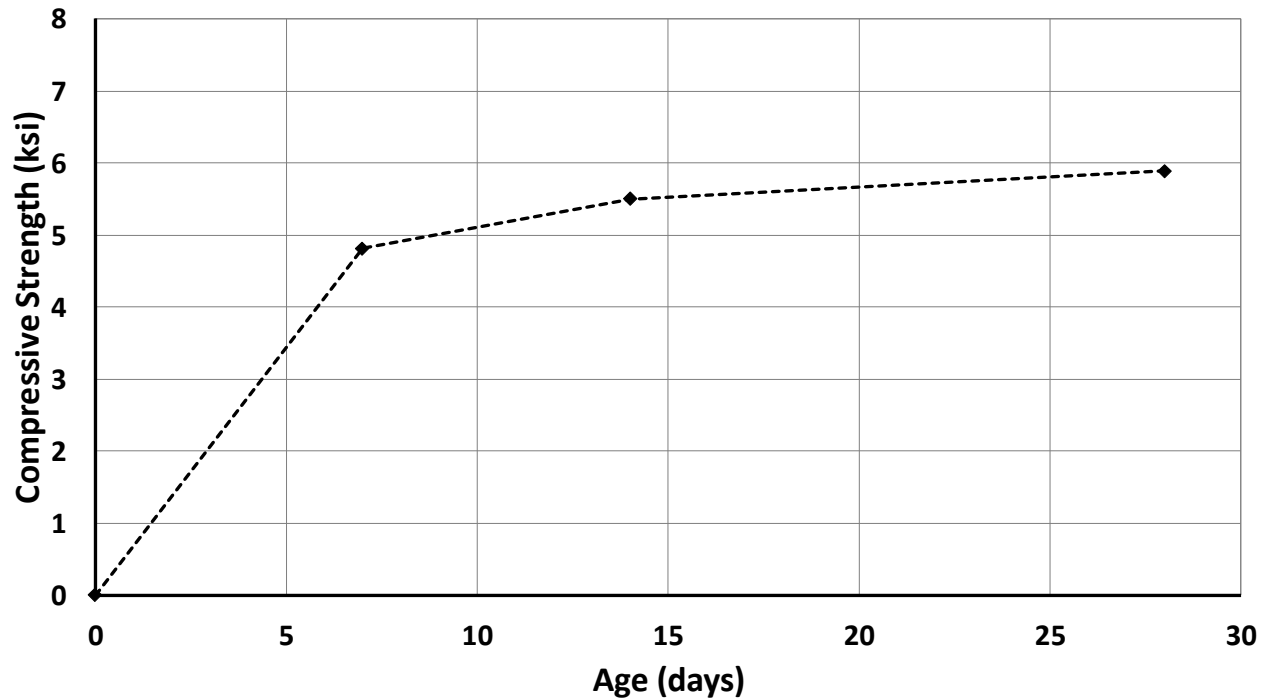


Figure 3.9: Typical Concrete Strength Gain over 28 Days

3.4.2 Steel Reinforcement

ASTM A615 Grade 60 reinforcing steel was used for both the longitudinal bars and the stirrups. All longitudinal reinforcing steel used in the experimental program was rolled from the same heat. Steel tensile strength tests were performed on three sample coupons from the No. 3 longitudinal reinforcing bars using a universal testing machine. A digital imaging correlation (DIC) system was used to gather strain data and produce stress-strain curves. The resulting curves for each of the three samples are provided in Figure 3.10. By considering an average value based on the three sample tests, the yield stress of the longitudinal reinforcement was determined to be

67.5 ksi. Further discussion about the yield stress used in strength calculations and an analysis tool developed for the research program is provided in Section 4.3.1.

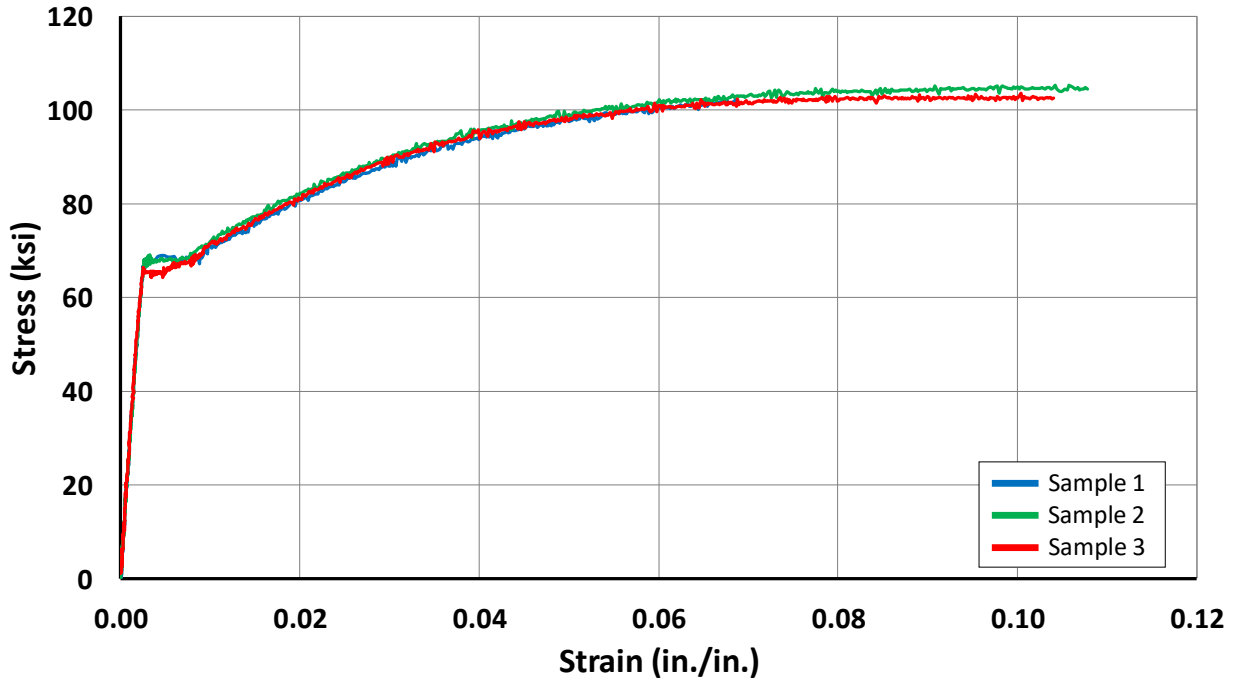


Figure 3.10: Stress-Strain Response of Longitudinal Reinforcement Samples

3.4.3 Fiber Reinforced Polymer (FRP) Systems

Each of the two strengthening systems used in the test program consisted of a carbon fiber strengthening component and a constituent material that bonded the component to the concrete substrate. Material properties as reported by the manufacturer of each system are listed in Table 3.3. These values are used for calculating the capacity of the FRP systems. The material properties for the externally bonded FRP sheet are given as the properties of the cured laminate consisting of the fabric and epoxy. The design value for the thickness of the cured laminate as reported by the manufacturer is 0.02 in. The FRP rope was used for the FRP anchors. The material properties of the FRP rope combined with the cured epoxy are reported. The material properties listed for the NSM strengthening system consider only the dry carbon fiber strips. In the table, A_f is the area of the FRP reinforcement, f_{fu}^* is the ultimate tensile strength of the FRP reinforcement, ε_{fu}^* is the ultimate rupture strain of the FRP reinforcement, and E_f is the tensile modulus of elasticity of the FRP. This notation and the definitions are consistent with those given in ACI 440.2R-17. The value

of A_f given in Table 3.3 for the externally bonded FRP sheet is the total nominal cross-sectional area of the cured laminate installed on the tension face of the EB specimens (EB.1, EB.2 and EB.3). For the FRP rope, the value of A_f is the nominal cross-sectional area of one anchor combined with epoxy that is used in the EB specimens (EB.1 and EB.2). The value of A_f listed for the NSM reinforcement is the nominal cross-sectional area of a single FRP strip.

Table 3.3: FRP Strengthening System Components and Design Values

Strengthening System	Components	Constituent Materials	A_f (in. ²)	f_{fu}^* (ksi)	ϵ_{fu}^*	E_f (ksi)
Externally Bonded (EB)	FRP Sheet	FRP Fabric ¹ + Epoxy ³	0.24	105	0.01	8200
	FRP Anchor	FRP Rope ² + Epoxy ³	0.1	304	0.016	33,300
Near-Surface-Mounted (NSM)	NSM Strips	FRP Tape ⁴ + Epoxy Grout ^{5,6}	0.049	325	0.0181	18,000

¹SikaWrap Hex 117C Unidirectional Carbon Fiber Fabric

²SikaWrap FX-50 C Unidirectional Carbon Fiber Rope

³Sikadur Hex 300 Impregnating Resin

⁴Hughes Brothers Aslan 500 #2 Carbon Fiber Reinforced Polymer Tape

⁵Pilgrim Permocoat Magmaflow Grout-Pak CF Epoxy Grout

⁶Unitex Pro-Poxy 400 Anchoring Gel

As indicated in the footnotes to Table 3.3, two different epoxies were used in the test program for installing the NSM strips, yet only Specimen 1-NSM.1b received the Unitex Pro-Poxy 400 Anchoring Gel. The relatively high viscosity of the Unitex Pro-Poxy 400 Anchoring Gel allowed for the application process to be performed overhead. Installation of the NSM strips and use of the two epoxies is described further in Section 3.6.2.

3.5 Specimen Construction

In order to fabricate the specimens for the experimental program, formwork was first designed and built. Formwork used to cast each specimen was constructed from lumber. Phenolic plywood was used as the casting surface. Phenolic plywood was chosen so that the forms could be cleaned and reused multiple times. Although the number of specimens in each cast group varied, Figure 3.11 provides a photograph of a typical set of forms.

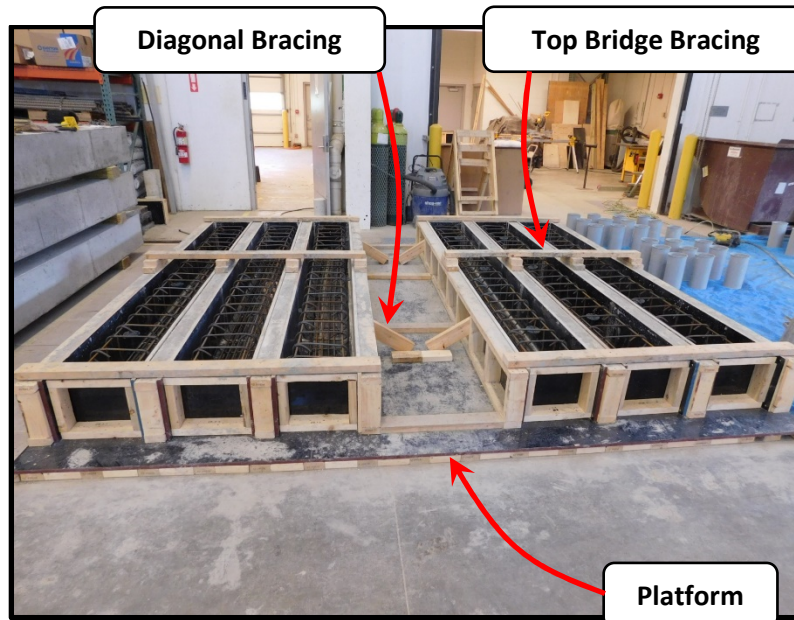


Figure 3.11: Formwork for Casting a Typical Group of Specimens

A completed reinforcement cage installed in one of the forms is shown in Figure 3.12. As indicated in the figure, spacer wheels and bar chairs were used to make certain that the reinforcement cages would not shift during casting and ensured the specified cover dimensions were met.

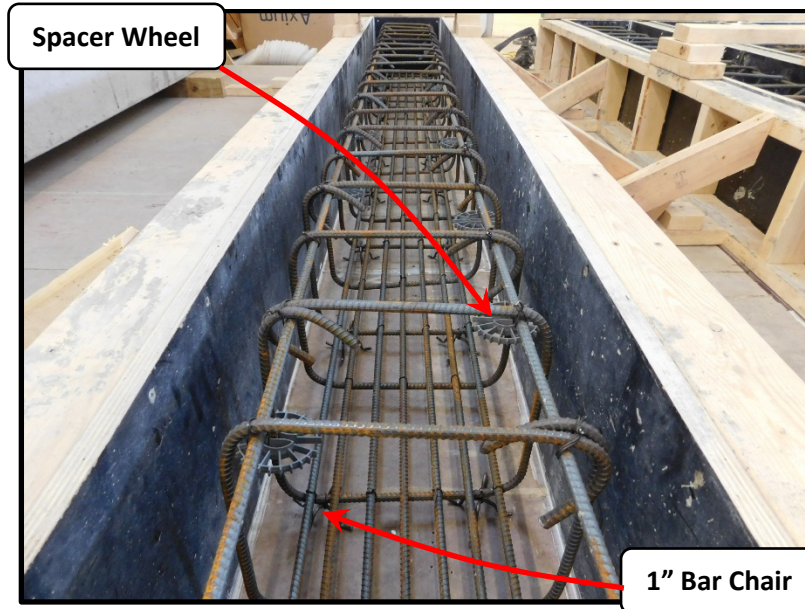


Figure 3.12: Reinforcing Cage in Forms

Concrete was poured directly from the concrete truck into the forms. To ensure proper consolidation, concrete immersion vibrators were used as can be seen in Figure 3.13(a). Then, the concrete was carefully finished with hand floats (see Figure 3.13(b)).



(a) Vibrating Concrete into Place



(b) Finishing Concrete

Figure 3.13: Casting Process

Before the end of the casting day, the freshly cast specimens were covered with wetted burlap blankets (see Figure 3.14(a)), followed immediately by a plastic tarp to contain the moisture

(see Figure 3.14(b)). After seven days, the burlap and tarp coverings were removed and the specimens were removed from the forms.



(a) Burlap Blankets



(b) Plastic Tarp

Figure 3.14: Curing Process

3.6 FRP Strengthening System Application Procedures

The application procedures for the FRP strengthening systems included in the experimental program are described in the following subsections. With the exception of Specimen 1-NSM.1b, the beams were inverted prior to the application of the FRP sheets or strips in order to easily access the tension face. After application of an FRP system was completed, the strengthening system was allowed to cure for a minimum of 7 days before the beam was tested.

3.6.1 Externally Bonded Sheets

3.6.1.1 Surface Preparation and FRP Application

For all bond-critical applications of externally bonded strengthening systems, concrete substrate preparation must be performed. As shown in Figure 3.15(a), the surface area of concrete to which the FRP was to be applied was first roughened with a grinding wheel to a concrete surface profile (CSP) of 3. Concrete surface profiles, ranging from 1 to 10, are defined by ICRI 310.2R-2013. ICRI 330.2-2016 states that concrete surfaces are to be prepared to a surface profile not less than CSP 3 for externally bonded FRP fabric. This is also consistent with ACI 440.2R-17. A set of CSP chips were used as a reference to verify adequate surface roughness. Furthermore, as

pictured in Figure 3.15 (b and c), 0.5-in. diameter holes with a depth of 4 in. were drilled into the concrete for the FRP anchors at the locations indicated in Figures 3.5(a and b) and 3.6(a and b) to comply with the recommendation from Quinn (2009) stating that anchor holes should be 40% larger than the area of the FRP anchor. To reduce stress concentrations in the FRP at the edges of the holes, a rotary tool was used to round the edges to a minimum radius of 0.5 in., as specified by ICRI 330.2-2016 and ACI 440.2R-17 (Figure 3.13(d)). Finally, a wire brush and compressed air were used to clean the holes and concrete surface to remove dust and foreign particles before the FRP was applied.

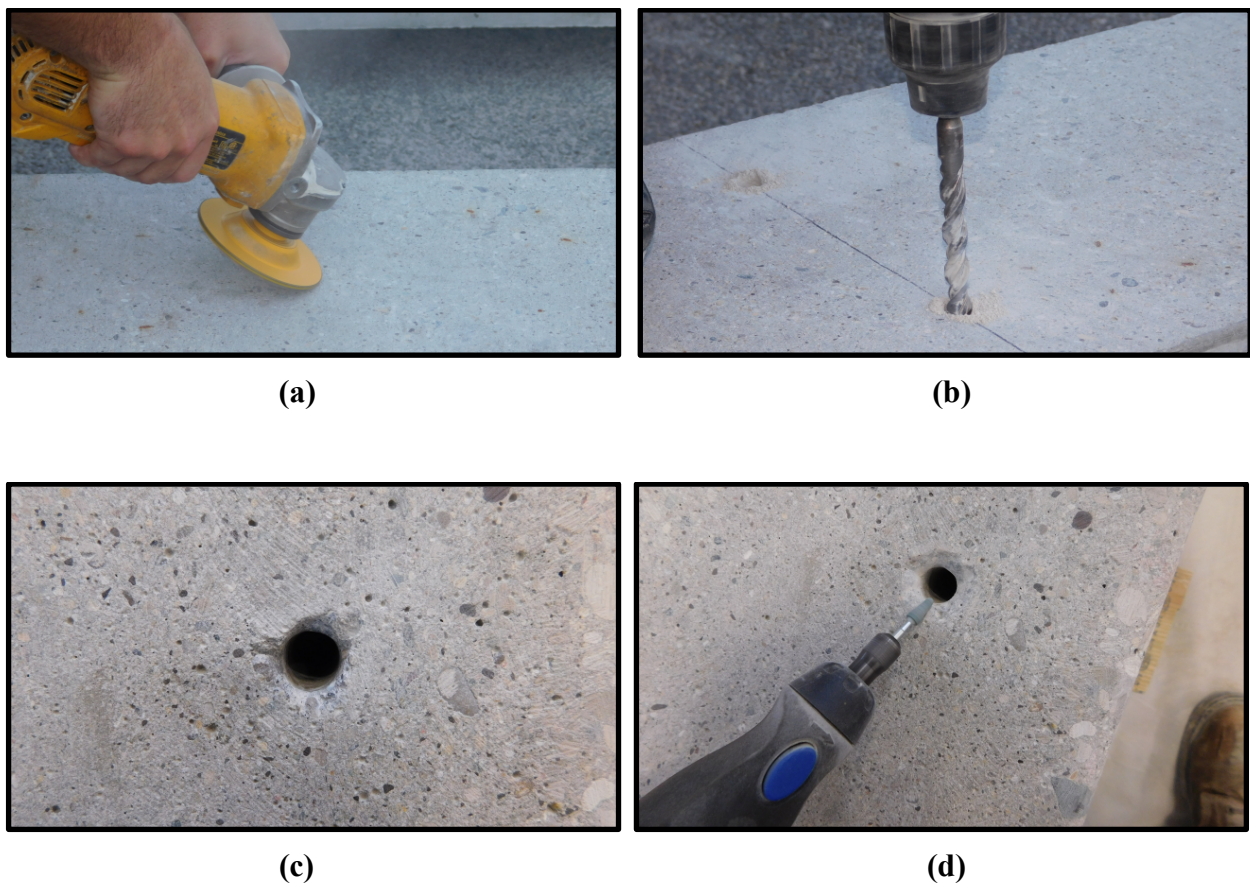


Figure 3.15: Surface Preparation for Externally Bonded Strengthening System – (a) grinding the concrete substrate; (b) drilling anchor holes; (c) drilled anchor hole prior to rounding the edges; (d) rounding the edges of the anchor hole

A wet-layup application process was implemented in which the dry carbon fiber fabric was impregnated with epoxy prior to placement onto the prepared and sealed concrete surface. The process of sealing the concrete surface simply involves applying a thin layer of the epoxy onto the

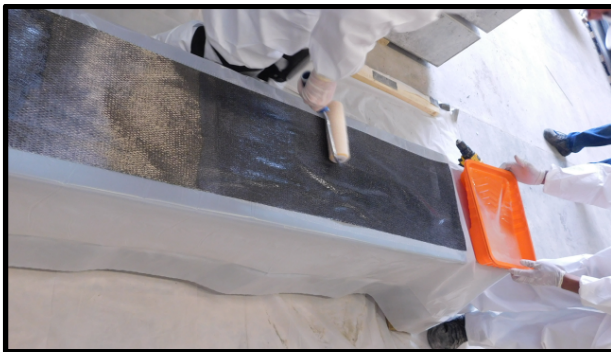
surface using a common paint roller to fill any air voids and ridges, resulting in a level resin layer (Figure 3.16(a)). Next, spare FRP rope material, saturated with epoxy, was used to prepare the concrete surface inside the pre-drilled anchor holes (Figure 3.16(b)). Then, prior to installing the fiber sheet on the specimen, it was impregnated with the same epoxy used to seal the concrete surface (Figure 3.16(c)). This process was performed using the same roller type that was used to apply the thin layer of epoxy onto the concrete surface. The sheet was then placed on the tension face of the specimen (Figure 3.16(d)). Once in place, plastic laminating rollers were used to ensure the fibers were fully impregnated with epoxy and to smooth out any air pockets (Figure 3.16(e)). After fully impregnated, squeegees were used to remove excess epoxy from the sheet (Figure 3.16(f)).



(a)



(b)



(c)



(d)



(e)



(f)

Figure 3.16: Application of Externally Bonded Sheets– (a) sealing the concrete surface; (b) coating the inside of the drilled holes with epoxy; (c) impregnating the dry fiber sheet with epoxy; (d) placing impregnated fiber sheet onto sealed concrete surface; (e) smoothing out air pockets; (f) removing excess epoxy with squeegee

3.6.1.2 Installation of FRP Anchors and Patches

After the FRP longitudinal sheets were applied, the FRP anchors were installed. The details of the anchors are provided in Figures 3.5(b) and 3.6(b). In order to insert the FRP anchors through the longitudinal sheet applied to the beam and into the section of the specimen, a razorblade was used to separate the fibers in the sheet to expose the drilled holes (Figure 3.17(a)), resulting in the condition shown in Figure 3.17(b). Each anchor was cut from the FRP rope and had a total length of 10 in. consisting of a 4-in. embedment depth and 6-in. fan length (Figure 3.17(c)). A steel double loop rebar tie was used to hold the fibers of an individual anchor together near the end that was to be inserted into a hole on the tension face of the beam. Prior to installing an anchor in the beam, the anchor was fully submerged into a container of epoxy. The FRP anchor was then inserted into the hole in the beam (Figure 3.17(d)). The rebar tie aided with inserting the anchors and was left with the anchor inside the holes. Once inserted, the anchor was fanned out at a 60-degree angle (Figure 3.17(e)). As shown in Figure 3.17(f), additional epoxy was applied to the anchor using a paint brush with special consideration given to ensuring the fibers toward the center of the bundle were fully saturated.



(a)



(b)



(c)



(d)



(e)



(f)

Figure 3.17: Installation of FRP Anchors for Externally Bonded Strengthening System – (a) separating fibers to expose anchor hole; (b) exposed anchor holes; (c) cut FRP anchors; (d) inserting FRP anchor into hole; (e) fanning out anchor fibers; (f) saturating anchors

After the FRP anchors were installed, two 12-in. by 12-in. patches, the first with the fibers oriented transversely to the longitudinal sheet and the second with the fibers oriented parallel to the longitudinal sheet, were subsequently placed over the top of the FRP anchors as shown in

Figure 3.18. The patches were prepared and installed in a similar manner as the longitudinal FRP sheets. The patches were first saturated using a roller (Figure 3.18(a)) and then placed over the top of the two anchors (Figure 3.18(b)). As with the longitudinal sheets, a plastic laminating roller and squeegee were used to ensure the fibers were fully impregnated with epoxy, smooth out any air pockets, and remove excess epoxy from the patch. A patch with the final anchor configuration is shown in Figure 3.18(c).

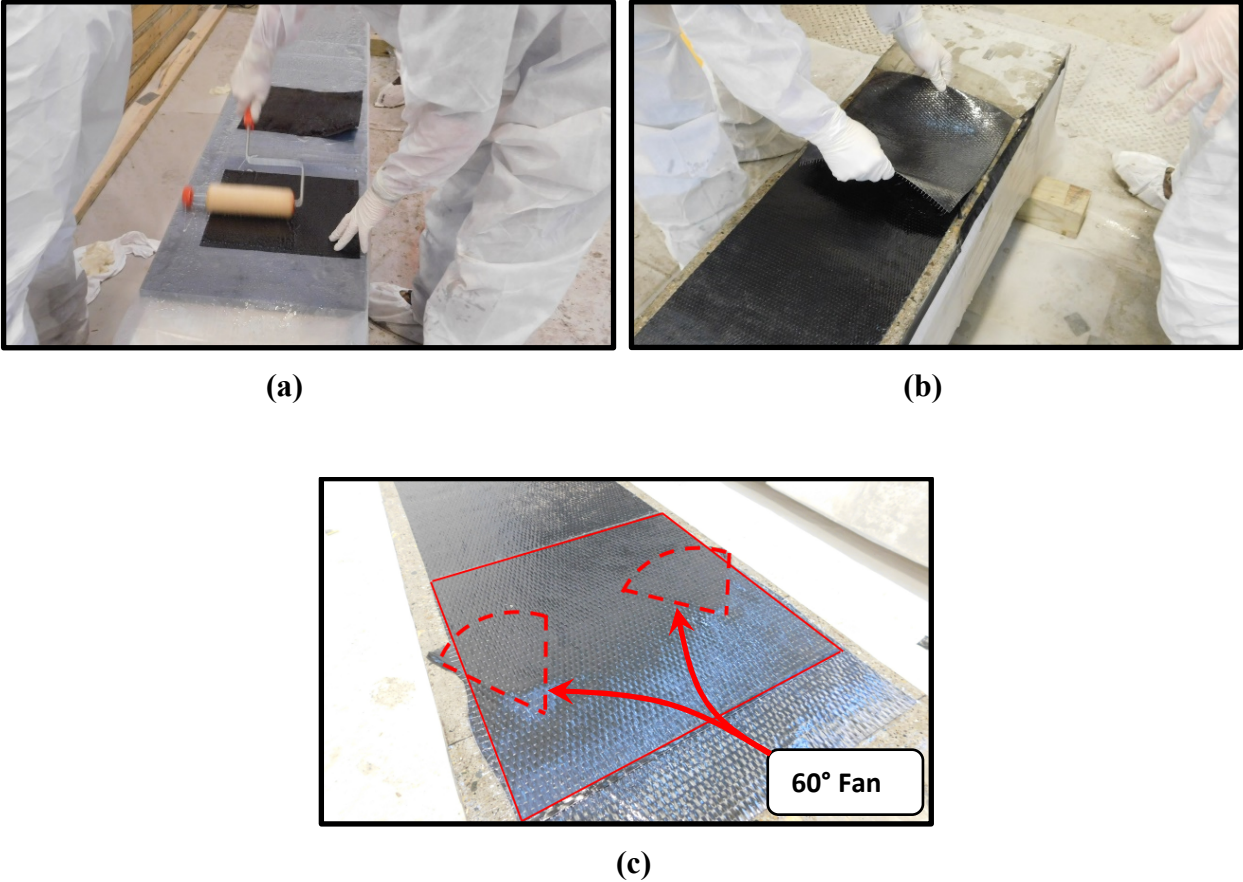


Figure 3.18: Application of Patches over FRP Anchors – (a) impregnating the dry fiber square sheet with epoxy; (b) placing square sheet over anchors; (c) patch with final anchor configuration

3.6.1.3 Installation of FRP U-Wrap Anchors (EB.3)

As will be described further in Chapter 4, U-wrap anchors were tested in the pilot group (Specimen 0-EB.3) but were determined to be inferior to FRP anchors located near the ends of the longitudinal sheet. For installation of the U-wrap anchors, a grinding wheel was used to roughen

the concrete substrate along the sides of the specimen where the anchors were to be installed to a concrete surface profile (CSP) of 3 (ICRI 310.2R-2013). According to ICRI 330.2-2016 and ACI 440.2R-17, outside corners and sharp edges over which FRP sheets are wrapped should be rounded to a minimum radius of 0.5 in. The grinding wheel was used to round the appropriate edges to the specified radius of 0.5 in. as shown in Figure 3.19.



(a) Rounding Edges



(b) Verifying Minimum Radius

Figure 3.19: Additional Surface Preparation for U-Wrap Anchors

Application of the longitudinal FRP sheet on the specimen with U-wrap anchors followed the same wet-layup procedure described in Section 3.6.1.1 (Figure 3.20(a)). The application of the U-wrap anchors also followed this procedure (Figure 3.20(b)).



(a) Applying Longitudinal Sheet



(b) Applying U-Wrap Anchor

Figure 3.20: Application of FRP on Specimen with U-Wrap Anchors

3.6.2 Near-Surface-Mounted Strips: Surface Preparation and FRP Application

The strips of the near-surface-mounted strengthening system are to be completely enclosed in the section of the beam. Grooves were therefore required to be cut along the length of the tension face. A tuckpointing grinder with a 0.25-in. thick diamond cutting blade was used to cut grooves into the specimen that were 0.25-in. wide and 0.875-in. deep. The dimensions of the NSM strips were 0.079-in. wide by 0.63-in. tall. As shown in Figure 2.6, the suggested depth of a groove for a rectangular strip is at least 1.5 times the largest dimension of the strip according to ACI 440.2R-17. Due to the relatively shallow clear cover at the tension face of the beam members, a depth of 0.875-in. was used to prevent cutting into a stirrup. Similarly, ACI 440.2R-17 suggests that the width of a groove for a rectangular strip be at least 3.0 times the smallest dimension of the strip. Therefore, the 0.25-in. wide groove meets this suggested dimension because it is larger than 3.0 times 0.079-in., or 0.237-in. The clear groove spacing of 1.25-in. (see Figure 3.8) was based on the spacing of the steel reinforcement in the member. This is inconsistent with the suggestions in ACI 440.2R-17 which would require the clear groove spacing to be 1.75-in. in this case. A steel angle was clamped onto the specimen as shown in Figure 3.21 in order to ensure a straight line was cut at a constant depth. Once both of the grooves were cut, compressed air was used to remove any dust and particles before the FRP strips were inserted into the grooves.

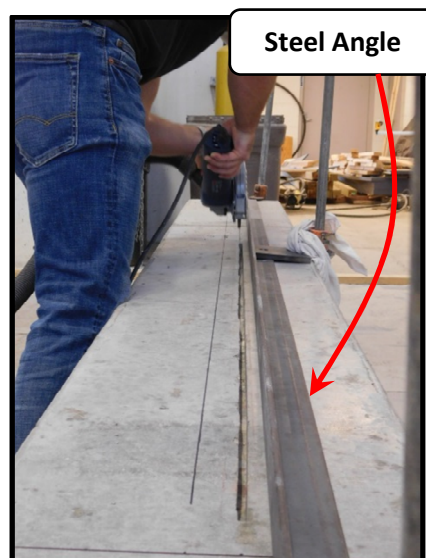


Figure 3.21: Cutting NSM Grooves

Next, epoxy grout was poured to fill approximately one quarter of the groove (Figure 3.22(a)). Each NSM strip was then put into place by moving it back and forth in a sawing motion to ensure satisfactory bond was achieved between the epoxy grout and the concrete substrate (Figure 3.22(b)). The strips were inserted such that they were approximately centered within the depth of the groove. Epoxy grout was then pushed into the groove and leveled to match the surface of the specimen. Excess epoxy grout was removed using a squeegee as shown in Figure 3.22(c).



(a) Filling Groove with Epoxy Grout



(b) Inserting NSM Strip



(c) Squeegeeing Excess Epoxy Grout
Figure 3.22: Installation of NSM Strips

Specimen 1-NSM.1b was added to the test program in order to verify the feasibility of applying the epoxy overhead. Photographs of the application are provided in Figure 3.21. Unitex

Pro-Poxy 400 Anchoring Gel was used in lieu of the Pilgrim Permocoat Magmaflow Grout-Pak CF Epoxy Grout, which was used for all other NSM specimens in the test program. After consulting with the manufacturer of the NSM strips, the Unitex Pro-Poxy was chosen for the overhead application due to its high viscosity. A dispenser gun was used to inject the epoxy into each groove (Figure 3.23(a)). Once the groove was roughly halfway filled with epoxy, the NSM strip was inserted such that it was approximately centered within the depth of the groove (Figure 3.23(b)). Excess epoxy was squeegeed away and added where needed so that the epoxy was level with the surface of the specimen. Overall, the installation was successful, and once the installation was completed, no sagging of the epoxy from the grooves was observed.



(a) Filling Groove with Epoxy

(b) Inserting NSM Strip

Figure 3.23: NSM Overhead Application

3.7 Test Setup and Procedure

Each of the 22 beam specimens was monotonically loaded to failure in four-point bending using the loading configuration shown in Figure 3.24. The test setup used for the tests is illustrated in Figure 3.25, and a photograph of the setup is provided in Figure 3.26.

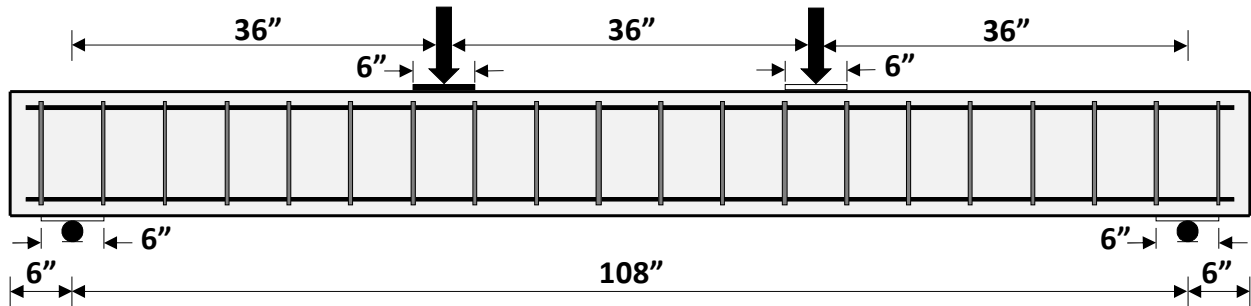


Figure 3.24: Loading Configuration

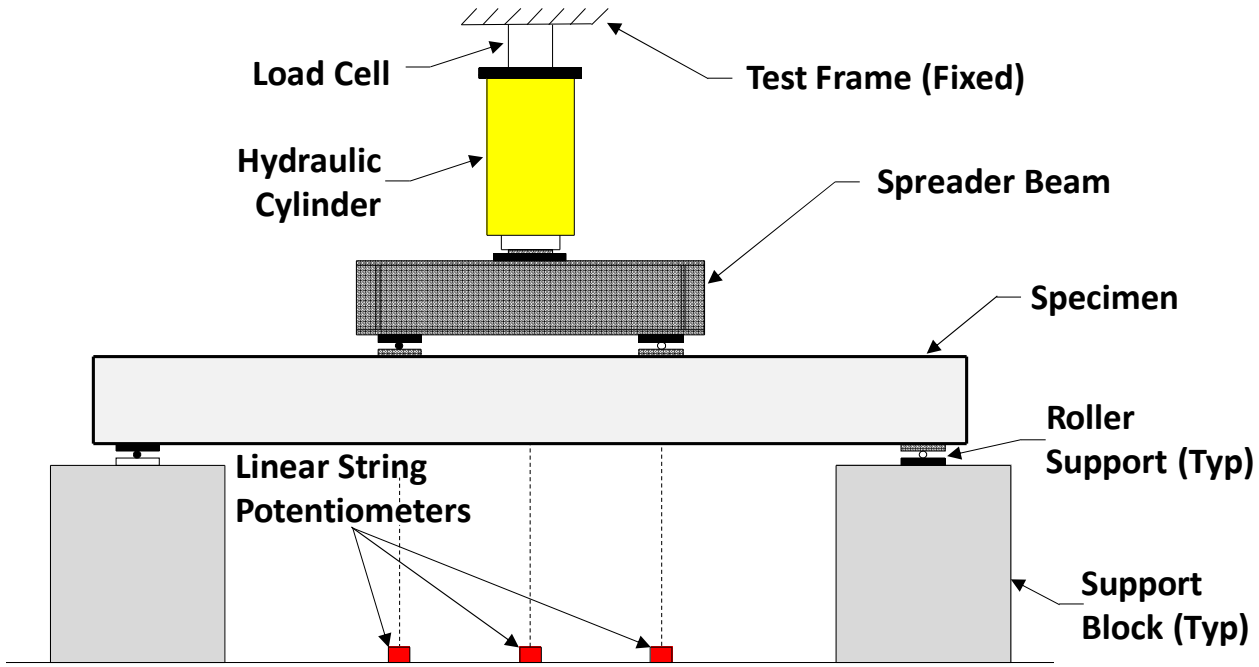


Figure 3.25: Elevation View of Test Setup

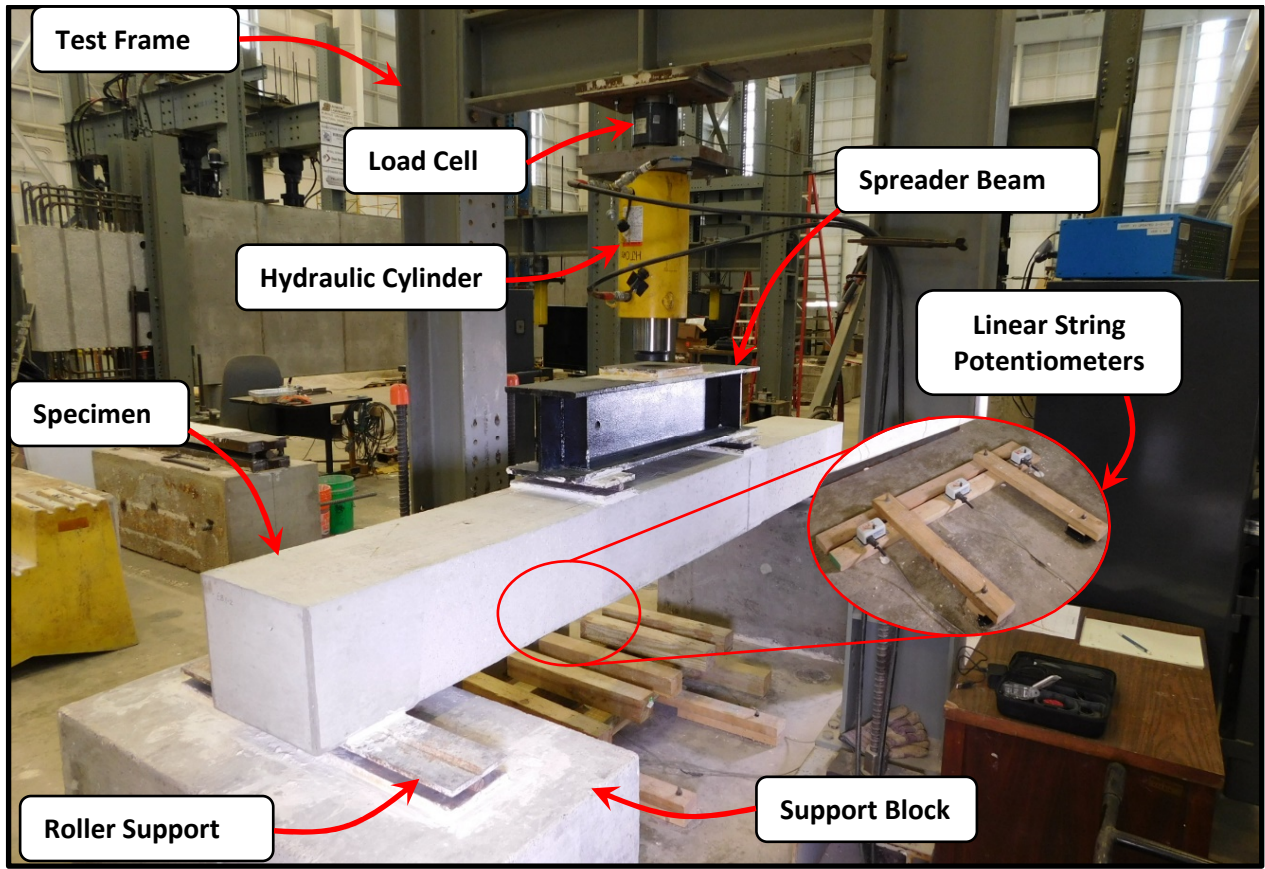


Figure 3.26: Photograph of Test Setup

As indicated in Figures 3.25 and 3.26, a hydraulic cylinder was used to apply load through a spreader beam to the third points of the specimens. A load cell with a 55-kip capacity was installed in series with the hydraulic cylinder in order to directly measure the total load applied to the beam. Rollers were used under the spreader beam at each point of load application to the specimen. The load plates on the specimen extended across the 14-in. width of the member. The specimen was supported on roller supports at both ends to allow for equal elongation of the tension face in both directions, thus producing a symmetric deflected shape. Linear string potentiometers were used to capture displacements at midspan and under the load points by measuring displacements of the bottom edge of one side of the member relative to a stationary point on the ground. For the specimens in Group 3, displacements at these three locations along the length of the member (midspan and under the load points) were measured on both bottom edges of the member in order to capture any differential displacements between the sides due to the eccentric reinforcement within these specimens.

At the beginning of each test, the specimen was loaded to 5 kip (2.5 kip at each load point) followed by 1-kip increments, or load steps, until flexural cracking was observed and marked with felt-tipped markers. The load was then increased to the next multiple of 3 kip and cracks were marked. Additional load was then applied in 3-kip increments until failure occurred. Once yielding was observed in unstrengthened specimens with no FRP, load steps were defined by each additional 0.5 in. of midspan displacement instead of 3-kip load increments until failure occurred. Cracks were marked and photographs were taken at the end of each load step with the exception of the load steps immediately preceding an imminent failure due to safety concerns. Failure of the unstrengthened specimens was characterized by concrete crushing in the compression region, accompanied by a decrease in load-carrying capacity. Failure of the FRP-strengthened specimens occurred when the beams experienced a sudden drop in load-carrying capacity due to the rupture of the FRP. A high-speed camera, capturing images at 4000 frames per second, was used to better understand failure modes of the specimens with externally bonded FRP (see Figure 3.27).



Figure 3.27: High-Speed Camera

3.8 Summary

This chapter outlined the experimental program focused on the flexural strengthening of beam specimens. Details of 22 specimens fabricated in the laboratory were provided. Furthermore, the steps followed to prepare the beams for testing, including the application of the chosen FRP systems (i.e., externally bonded FRP and near-surface-mounts FRP) were outlined. The next chapter discusses the results from the experimental program, and important comparisons between the two FRP strengthening systems are presented to develop conclusions that help fulfill the project objectives.

CHAPTER 4. EXPERIMENTAL RESULTS AND DISCUSSION

4.1 Introduction

Experimental results from the 22 beam tests described in Chapter 3 are presented in this chapter. An overview of the experimental results is first introduced. Next, the development of load-deflection plots based on theoretical analysis is presented. The analysis results are compared to experimental results throughout the chapter. Details of the behavior of the specimens and the performance of the FRP strengthening systems are then discussed along with comparisons between specimens in terms of strength, stiffness, and ductility. The experimental results are described in the following order:

- Results from pilot tests (Group 0)
- Results by specimen type (Control - C, Artificially Deteriorated - D, Externally Bonded - EB, and Near-Surface-Mounted - NSM)
- Results by group (Groups 1-3)

Lastly, the primary observations from the test program are summarized.

4.2 Overview of Experimental Results

The results from the experimental program are summarized in Table 4.1. Each specimen is represented in the table by its identification label. The color scheme described in Section 3.2 is used for clarity. The table includes the concrete compressive strength on test day, f_c (reported to the nearest 10 psi per ASTM C39); maximum load applied during the test, P_{test} , and the corresponding moment, M_{test} ; nominal flexural capacity, M_n , and the corresponding applied load, P_n ; the ratio of the experimental moment capacity to the nominal moment capacity, M_{test}/M_n ; the ratio of the experimental capacity of a member to the experimental capacity of the corresponding control specimen in the same group, M_{test}/M_c ; and the midspan deflection at the maximum applied load. The value of M_n was calculated based on nominal flexural strength provisions in ACI 318-19 for the unstrengthened specimens and ACI 440.2R-17 for the specimens strengthened with FRP. It should be noted that the environmental reduction factor, C_E , in Section 9.4 of ACI 440.2R-17 is taken as 1.0 throughout this chapter due to the controlled environment in the laboratory. Furthermore, the Whitney stress block was consistently used for all M_n calculations, even for the

FRP specimens with capacity governed by rupture of the FRP. This methodology was determined to provide reasonable strength estimates as noted in ACI 440.2R-17 and discussed in Section 2.5. The value of P_n is the magnitude of one of the two point loads that corresponds to M_n at the midspan of the member with consideration of the additional moment imposed at midspan due to both the self-weight of the specimen and the weight of the spreader beam. In other words, the moment due to P_n plus the moments due to the specimen self-weight and spreader beam weight add to M_n . The value of P_{test} is the maximum load applied to the specimen during the test and corresponds to one of the two point loads applied to the member as indicated by the load cell. The value of M_{test} is the total moment at midspan when P_{test} is applied. It therefore includes the moment from P_{test} plus the moments due to the specimen self-weight and spreader beam weight.

Table 4.1: Test Results

Group	Specimen ID	Concrete Strength, f_c (psi)	M_{test} (kip-ft)	P_{test} (kip)	M_n (kip-ft)		P_n (kip)		M_{test} / M_n		M_{test} / M_c	Midspan Deflection at Max Load, Δ (in.)
					$\psi_f = 0.85$	$\psi_f = 1.0$	$\psi_f = 0.85$	$\psi_f = 1.0$	$\psi_f = 0.85$	$\psi_f = 1.0$		
0 (Pilot)	0-C ¹	6370	59.59	19.11	45.92 ³		14.56		1.30		1.00	3.29
	0-EB.2	6110	79.96	25.90	47.08 ⁴	49.65 ⁴	14.94	15.80	1.70	1.61	1.34	1.76
	0-EB.3	6120	62.95	20.23	47.09 ⁴	49.65 ⁴	14.94	15.80	1.34	1.27	1.06	1.30
	0-NSM.1	6140	77.11	24.95	50.07 ⁴	53.17 ⁴	15.94	16.97	1.54	1.45	1.29	1.61
1	1-C	6820	59.80	19.18	46.11 ³		14.62		1.30		1.00	3.23
	1-D	6560	44.68	14.14	33.88 ³		10.54		1.32		0.75	3.63
	1-EB.1	6920	54.91	17.55	47.33 ⁴	49.91 ⁴	15.02	15.88	1.16	1.10	0.92	0.81
	1-EB.2	6680	71.71	23.15	47.26 ⁴	49.84 ⁴	15.00	15.86	1.52	1.44	1.20	1.63
	1-NSM.1a	6490	70.81	22.85	50.20 ⁴	53.31 ⁴	15.98	17.02	1.41	1.33	1.18	1.72
	1-NSM.1b ²	7030	58.54	18.76	50.38 ⁴	53.51 ⁴	16.04	17.08	1.16	1.09	0.98	1.10
2	2-C	6020	59.41	19.05	45.77 ³		14.50		1.30		1.00	3.45
	2-D	6000	45.40	14.38	33.67 ³		10.47		1.35		0.76	1.63
	2-EB.1	6630	60.10	19.28	47.25 ⁴	49.82 ⁴	15.00	15.86	1.27	1.21	1.01	0.68
	2-EB.2	6800	72.79	23.51	47.29 ⁴	49.87 ⁴	15.01	15.87	1.54	1.46	1.23	1.25
	2-NSM.1	6390	82.87	26.87	50.16 ⁴	53.28 ⁴	15.97	17.01	1.65	1.56	1.39	1.82
3	3-C	6330	56.83	18.19	45.90 ³		14.55		1.24		1.00	2.88
	3-D	6680	44.47	14.07	33.92 ³		10.55		1.31		0.78	3.63
	3-EB.1	7270	58.36	18.70	47.42 ⁴	50.00 ⁴	15.05	15.91	1.23	1.17	1.03	0.96
	3-EB.2	7210	71.62	23.12	47.40 ⁴	49.98 ⁴	15.05	15.91	1.51	1.43	1.26	1.69
	3-NSM.1	6750	68.56	22.10	50.29 ⁴	53.41 ⁴	16.01	17.05	1.36	1.28	1.21	1.62
	3-NSM.2	6570	69.25	22.33	50.23 ⁴	53.35 ⁴	15.99	17.03	1.38	1.30	1.22	1.56
	3-NSM.3	6620	65.50	21.08	50.25 ⁴	53.36 ⁴	16.00	17.04	1.30	1.23	1.15	1.43

¹Pin-roller support condition

²Epoxy grout and NSM strip applied overhead

³Calculated in accordance with ACI 318-19

⁴Calculated in accordance with ACI 440.2R-17

In Table 4.1, two values of M_n and P_n are given for all specimens strengthened with FRP. The two strength values correspond to ψ_f values of 0.85 and 1.0. In ACI 440.2R-17, ψ_f is a reduction factor applied to the FRP within the equation for M_n . The value recommended for ψ_f within ACI 440.2R-17 is 0.85. For a thorough comparison of calculated and experimental strengths, the values of M_n and P_n were calculated with the inclusion of the recommended value and also with the value of ψ_f taken as 1.0.

As explained in Section 3.7, the deflection of the test beams was measured at midspan and at each load point. For the Group 3 specimens, the deflection was measured at each of these three locations using two linear potentiometers at each side of the member. For these specimens, the

midspan deflection at the maximum applied load listed in Table 4.1 and subsequent tables in this chapter is the average reading from the two potentiometers at midspan. The test results presented in Table 4.1 will be discussed in detail within the following sections.

Throughout this chapter, the behavior of the specimens is presented in load-displacement (P - Δ) plots. In the plots, the applied load, P , represents one of the point loads applied to the beam (see Figure 4.1) and is shown on the y-axis consistently from 0 to 60 kip. The midspan deflection, Δ , is shown on the x-axis from 0 in. to 2 in., 0 in. to 4 in., or 0 in. to 6 in. depending on the ductility of the specimens. In general, the FRP-strengthened specimens were loaded until the FRP ruptured and no longer contributed to the load carrying capacity of the member. The specimens not strengthened with FRP (i.e., C and D specimens) were loaded until extensive concrete crushing was observed along with a drop in load-carrying capacity. For the plots showing test results of specimens from multiple test groups, all specimens from Group 0 are plotted in purple. Similarly, all specimens from Group 1 are plotted in red, Group 2 in green, and Group 3 in blue. Furthermore, in plots displaying the response curves for a specific specimen type, a red dotted line is provided to show the load P_n corresponding to the calculated nominal flexural strength for that specimen type, which is calculated using the greatest measured concrete compressive strength of the specimens represented in the plot. For the plots showing test results by group, the color scheme described in Section 3.2 is used in conjunction with illustrative cross sections inset within the plots in order to easily match the specimen to its response curve.

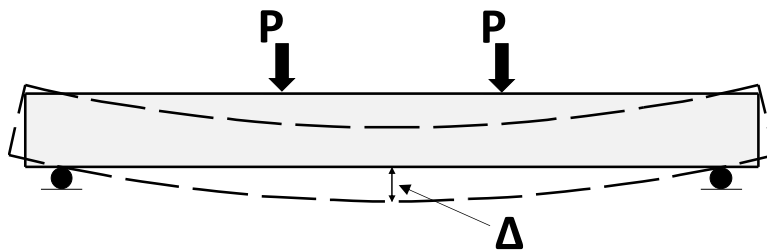


Figure 4.1: Applied Load, P , and Midspan Deflection, Δ

4.3 Load-Deflection Behavior from Analysis

An analysis tool was developed in Mathcad 15.0 to create theoretical load-deflection curves for specimens within the experimental program. The beam analyses provided results that allow key comparisons to be made with the experimental results of the test program. More specifically, one of the primary intentions of the analysis tool was to better understand the strains/stresses in the FRP of the test specimens and thus evaluate each strengthening system. Even though two FRP-strengthened specimens (0-EB.2 and 0-NSM.1) experienced some concrete crushing prior to rupture of the FRP, all strengthened specimens ultimately failed due to FRP rupture. That is, any crushing prior to rupture of the FRP did not result in a significant loss in load-carrying capacity. The estimated stress in the FRP at rupture obtained from the analysis results is useful in gaining a better understanding of the performance of the strengthening systems. The analysis also allowed the approximate stresses in the steel reinforcement at failure of the specimens to be estimated. Comparisons of the theoretical load-deflection curves to the response curves based on tests demonstrated the viability of using simple models to approximate the flexural behavior of FRP-strengthened members.

4.3.1 Input Values

The analysis tool considered the geometric information of each specimen as well as the stress-strain properties of the following materials: concrete, steel, and FRP. To calibrate the model, some material properties were adjusted based on the experimental data in order to best model the behavior of the strengthening systems.

For concrete in compression, the stress-strain relationship was based on the Hognestad (1951) model, as indicated in Figure 4.2 and given as

$$f_c = f'_c \left[2 \frac{\varepsilon}{\varepsilon_0} - \left(\frac{\varepsilon}{\varepsilon_0} \right)^2 \right] \quad (4-1)$$

Here, the value of the concrete strain at peak stress, ε_0 , was assumed to be equal to

$$\epsilon_0 = \left(1 + \frac{\sqrt{2}}{2}\right) \frac{f'_c}{E_c} \quad (4-2)$$

where E_c is taken as $57,000\sqrt{f'_c}$ (psi). This formula for ϵ_0 assumes that E_c is the secant modulus defined by the slope of a line through the origin and the point corresponding to $0.5f'_c$ on the stress-strain curve. The value of the concrete strength, f'_c , was input for each specimen based on cylinder tests described in Section 3.4.1. The concrete model assumed an ultimate concrete strain of 0.0038. Unlike the Hognestad (1951) model, which incorporates a linear descending branch, the parabolic relationship given above was used to define the entire concrete curve in compression.

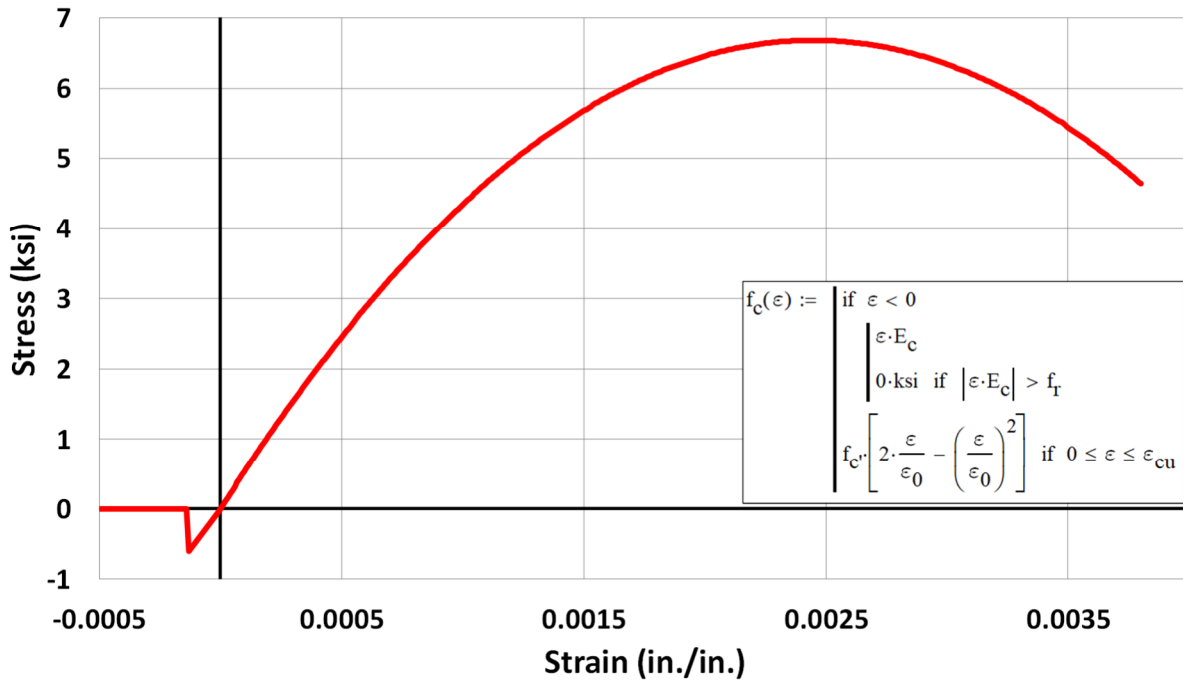


Figure 4.2: Stress-Strain Model for Concrete

For concrete in tension, the stress-strain curve was assumed to be linear with a slope of $57,000\sqrt{f'_c}$ (psi) until the modulus of rupture, f_r , was reached, as indicated in Figure 4.2. The modulus of rupture was taken as $7.5\sqrt{f'_c}$ (psi).

The stress-strain relationship for the steel reinforcement in tension used in the analysis tool, presented in Figure 4.3, was based on the tensile tests conducted on reinforcing bar samples

described in Section 3.4.2. With the full response of the bars obtained using DIC, the assumed stress-strain relationship for the analysis was first defined in a manner that followed the responses obtained through the tests. The yield strength, f_y , input into the model was calibrated once the load-deflection plots for the specimens output by the analysis tool were compared to results from the beam tests. To better fit the experimental results, it was decided to use the yield strength reported on the mill certificate for the reinforcing bars (70.199 ksi) rather than the average yield strength obtained from the tensile tests utilizing DIC (67.52 ksi). In other words, the yield strength reported on the mill certificate resulted in theoretical load-deflection plots that better matched the responses of test specimens. The assumed stress-strain relationship in the strain-hardening range used in the analysis tool was still based on the strain-hardening behavior of the reinforcement obtained from the DIC results. The stress-strain response from the bar tests are shown in Figure 4.3 along with the assumed stress-strain relationship incorporated into the analysis tool. In compression, the stress-strain relationship was assumed to be elastic-perfectly plastic with a yield strength of 70.199 ksi.

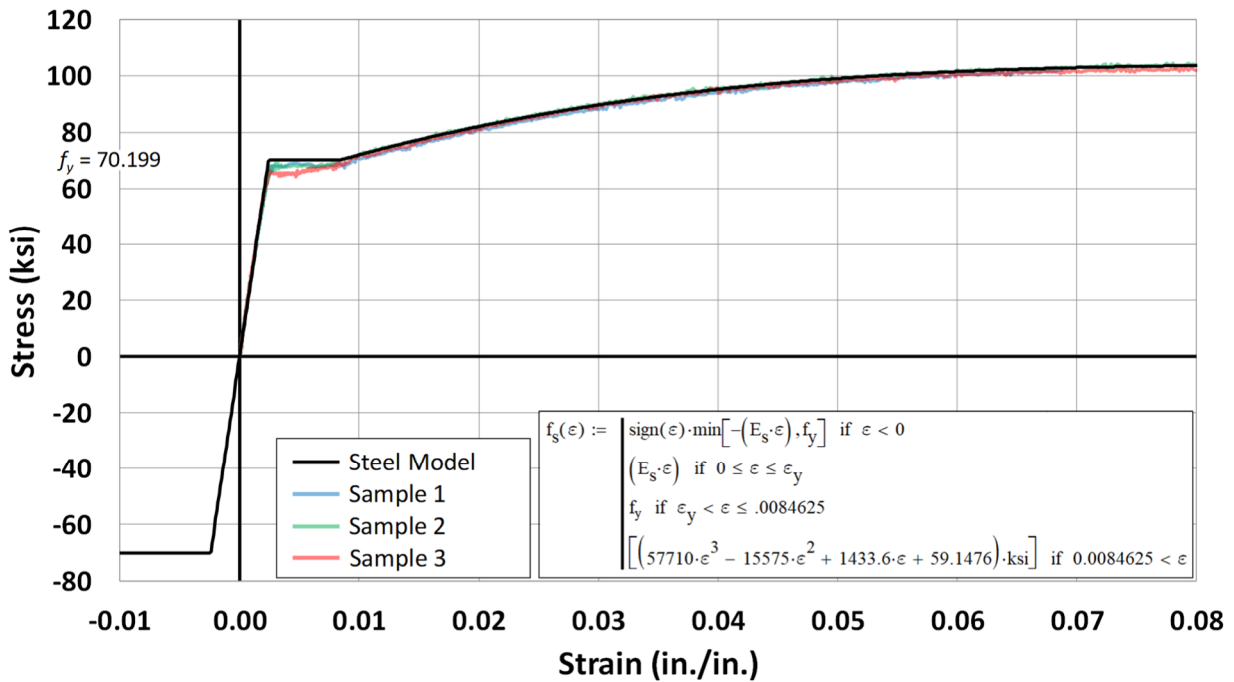


Figure 4.3: Stress-Strain Model for Steel Reinforcement

The stress-strain behaviors of the externally bonded FRP sheets and the near-surface-mounted FRP strips were assumed to be linear. Initially, the input values for the modulus of

elasticity were assumed to be equal to the values given on the product data sheets from the manufacturers of both the FRP sheets (8200 ksi) and strips (18,000 ksi). When the resulting theoretical load-deflection plots were compared to load-deflection plots from the beam tests, it was clear that these assumed stiffness values did not accurately reflect the effective stiffnesses of the FRP reinforcement used to strengthen the specimens. More specifically, the slopes of the theoretical and experimental load-deflection plots after yielding of the reinforcing bars did not correlate well. The values for the modulus of elasticity were therefore calibrated so that the post-yield slopes of the theoretical load-deflection plots and the experimental load-deflection plots are similar. It was determined that the effective stiffnesses of the FRP strengthening systems installed on the beams were greater than the design values initially assumed. The values used in the analysis tool were 8530 ksi for the externally bonded sheets and 21,000 ksi for the NSM strips. Determining the correct stiffness of the FRP is important for estimating the stress in the FRP at failure of the beam specimens, as described in Section 4.3.3. Because the analyses were used to estimate the stress in the FRP at failure, the tensile strengths of the FRP materials were selected to ensure that the failure load achieved by the experimental specimen being modeled was reached prior to rupture of the FRP in the analytical model.

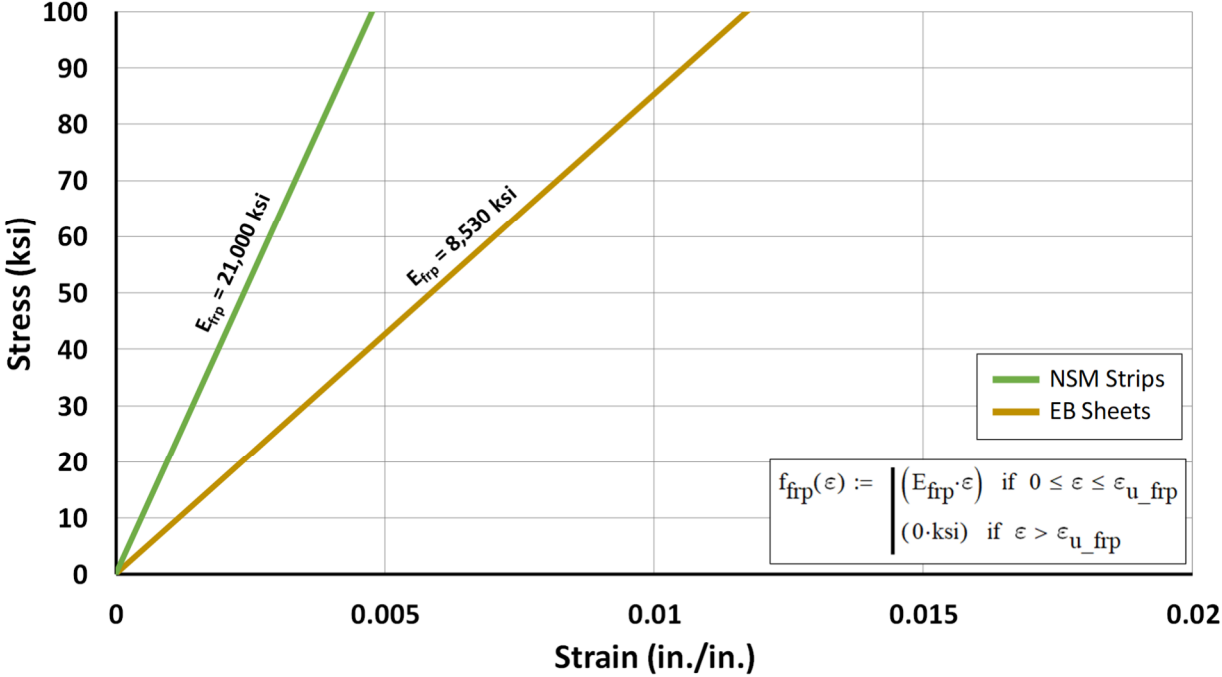


Figure 4.4: Stress-Strain Model for FRP

For the steel and FRP reinforcement, nominal areas for the bars, sheets, and strips were used within the analyses.

4.3.2 Analysis

To develop a theoretical load-deflection plot for specimens of the test program, the analytical tool first develops a moment-curvature plot considering a cross section of the member. By enforcing internal equilibrium, strain compatibility (i.e., plane sections remain plane and assuming strain compatibility between the concrete and the FRP and steel reinforcement), and the stress-strain responses described in the previous sections, corresponding moment and curvature values are found for increments of the concrete strain at the top fiber of the member ranging from 0 to the ultimate concrete strain. An example moment-curvature plot developed by the analytical tool in Mathcad 15.0 is shown in Figure 4.5.

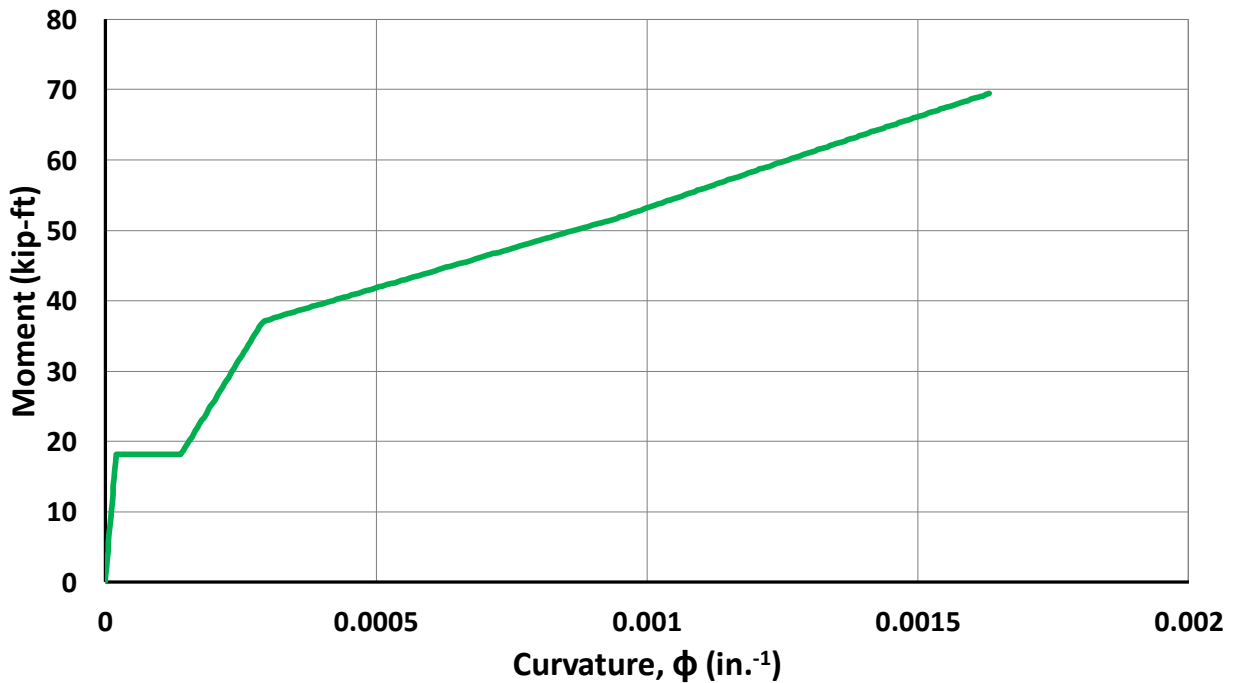


Figure 4.5: Example Moment-Curvature Plot

Because material strains and stresses at numerous stages are required to develop the moment-curvature plot for a member, the analysis tool can be used to obtain valuable information about the state of stresses and strains in the beam given any applied moment. For example, the tool

allows the strain in the reinforcing bars and the strain in the FRP sheets or strips to be easily obtained for any moment acting on the member cross section. Therefore, the tool can be used to determine the estimated state of stress in the FRP strengthening system at the experimentally-determined failure load. This value can then be compared to the effective stress in the FRP, f_{fe} , as defined by ACI 440.2R-17 or the tensile strength reported by the manufacturer, f_{fu}^* , effectively determining the efficiency of the FRP strengthening system installed on a beam specimen. The value of f_{fu}^* is defined by ACI 440.2R-17 and ACI 440.1R-15 as the average tensile strength of a sample of FRP specimens minus three times the standard deviation. An estimate of the stress in the reinforcing steel at the maximum applied load can also be obtained from the analysis tool. Because the reinforcing steel in the test specimens entered into the strain-hardening range, having an estimate of the actual stress in the steel at failure of the specimen is useful.

Using the moment-curvature plot along with the known bending moment diagram resulting from the three-point bending test configuration, the analytical tool develops a series of relationships describing the curvature over the length of the member for various increments of the applied load. An example of the curvature over the member length is given for Specimen 1-EB.2 under an applied load P of 10 kip in Figure 4.6.

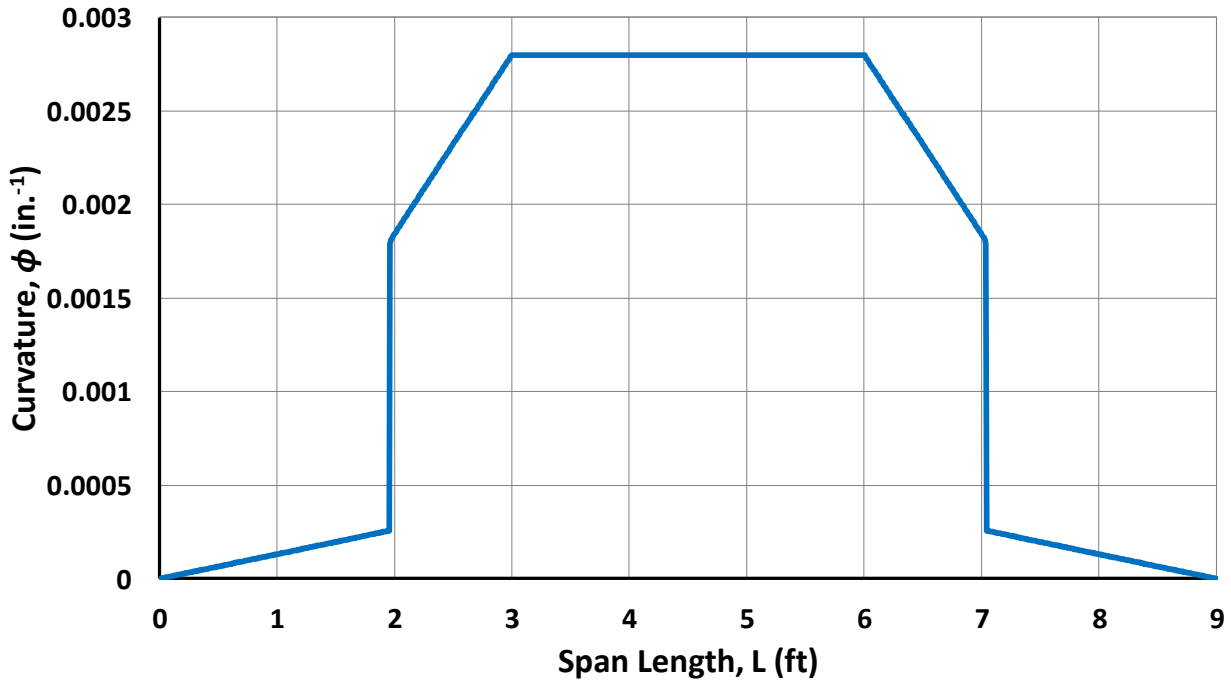


Figure 4.6: Example Plot of Curvature over Member Length

The analytical tool then applies the second moment-area theorem (Hibbeler 2012) to calculate the midspan deflection of the member being modeling for each increment of the applied load for which the curvature over the member length was determined. The equation used within the tool to calculate the midspan deflection, δ , is

$$\delta = \int_0^{L/2} \phi(x) \cdot x dx \quad (4-3)$$

where $\phi(x)$ is the curvature along the member length, x is the distance along the member measured from the support, and L is the beam span. It should be noted that the self-weight of the beam and the weight of the spreader beam was neglected within the theoretical analysis for simplicity.

4.3.3 Results

For each subsection in Section 4.5, figures are provided that compare the theoretical load-deflection plots from the analysis tool to the experimental load-deflection plots. It should be noted that the specimens with cut bars could not be accurately modeled, and therefore, theoretical load-deflection plots are not provided for these beams. Except for these specimens, the estimated stress

in the FRP from the analysis corresponding to the maximum applied load during the experiments, f_{f_max} , is reported within Section 4.5 along with the estimated stress in the steel reinforcement, f_s , corresponding to the maximum applied load.

As an example, both the theoretical and experimental load-deflection plots for Specimen 1-EB.2 are shown in Figure 4.7. The theoretical response is shown as a solid line up to the load that corresponds to an FRP stress equal to the effective stress f_{fe} calculated in accordance with ACI 440.2R-17. The response is shown as a dashed line beyond this point and is terminated at the load corresponding to the maximum load applied to the test specimen. Using the analytical tool, the value of the stress in the FRP reinforcement, f_{f_max} , and the stress in the steel reinforcement, f_s , corresponding to the maximum applied load is obtained assuming strain compatibility between the concrete and reinforcement. For Specimen 1-EB.2 these values are 148.19 ksi and 77.15 ksi, respectively. It is recognized that a discrepancy does exist between the theoretical and experimental responses as can be expected for most simple analytical models that are compared to results from structural tests. Nevertheless, the stress values obtained from the analysis provide a means to compare results from the tests and better understand the relative performance of the FRP strengthening systems. If the stress values were chosen based on the point in Figure 4.7 at which the theoretical curve corresponds to the midspan deflection of the specimen at the maximum load applied during the test, the values of f_{f_max} and f_s differ by 16.05 ksi and 1.66 ksi, respectively, relative to the values given above (148.19 ksi and 77.15 ksi). The values of f_{f_max} and f_s provided in the following sections should primarily be used to compare the results between specimens rather than taken as an accurate representation of the stresses reached by the materials. Theoretical and experimental load-deflection plots for all applicable specimens are provided in Appendix A along with a comparison between the values of f_{f_max} corresponding to the maximum applied load during the test and the values of f_{f_max} corresponding to the midspan deflections at the maximum load.

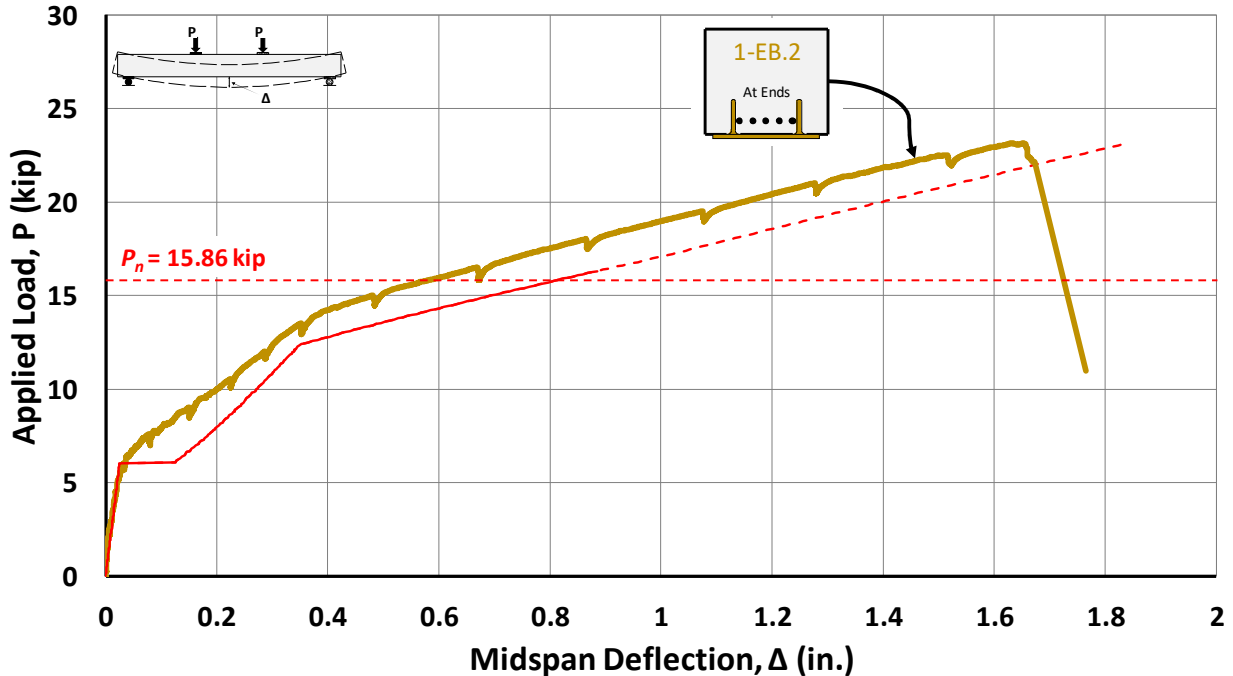


Figure 4.7: Example of Comparison of Theoretical and Experimental Responses

4.4 Pilot Specimen Test Results

As explained in Chapter 3, a group of four pilot beam tests were initially conducted in order to better understand the behavior of the FRP strengthening systems and to use the results to refine the experimental program to best achieve the specified objectives. The intention of the first beam tested, Specimen 0-C, was to verify that the testing configuration and associated instrumentation would perform as predicted. This test was conducted similar to all other tests except the beam supports consisted of a pin and a roller as opposed to two rollers. During the test on Specimen 0-C, it was noted that the tensile face of the beam elongated only in the direction of the roller, causing the hydraulic cylinder to slightly tilt towards the roller support due to the friction between the hydraulic cylinder and the spreader beam. It was then decided to change the support conditions to what is shown in Figure 4.1. The pilot tests for Specimens 0-EB.2, 0-EB.3, and 0-NSM.1 were intended to verify the general behavior of the FRP strengthening systems before continuing with the planned experimental program. The results from the four pilot tests are presented in Table 4.2 and Figure 4.8. The control specimen (Specimen 0-C) failed due to crushing of the concrete in the compression region after the longitudinal steel yielded and entered the strain-hardening range. Specimen 0-EB-3 failed due to rupture of the FRP sheet, while Specimens 0-NSM.1 and 0-EB.2

experienced some concrete crushing prior to the rupture of the FRP. This can be observed in Figure 4.8 where the load-deflection curves display a reduction in load-carrying capacity before the significant drop that corresponds to rupture of the FRP.

Table 4.2: Group 0 (Pilot) Test Results

Specimen ID	M_{test} (kip-ft)	M_n (kip-ft)		M_{test} / M_n		M_{test} / M_c	Steel Stress, f_s (ksi)	Rupture Stress, $f_{f,max}$ (ksi)	f_{fu}^* (ksi)	Effective Stress, f_{fe} (ksi)	$f_{f,max} / f_{fu}^*$	$f_{f,max} / f_{fe}$	Midspan Deflection at Max Load, Δ (in.)
		$\psi_f = 0.85$	$\psi_f = 1.0$	$\psi_f = 0.85$	$\psi_f = 1.0$								
0-C ¹	59.59	45.92 ²		1.30		1.00	88.47	-	-	-	-	-	3.29
0-EB.2	79.96	51.00 ³	54.28 ³	1.57	1.47	1.34	-	-	105	73.8	-	-	1.76
0-EB.3	62.95	51.00 ³	54.28 ³	1.23	1.16	1.06	73.88	117.18	105	73.8	1.12	1.59	1.30
0-NSM.1	77.11	50.36 ³	53.53 ³	1.53	1.44	1.29	-	-	325	228.1	-	-	1.61

¹Pin-roller support condition

²Calculated in accordance with ACI 318-19

³Calculated in accordance with ACI 440.2R-17

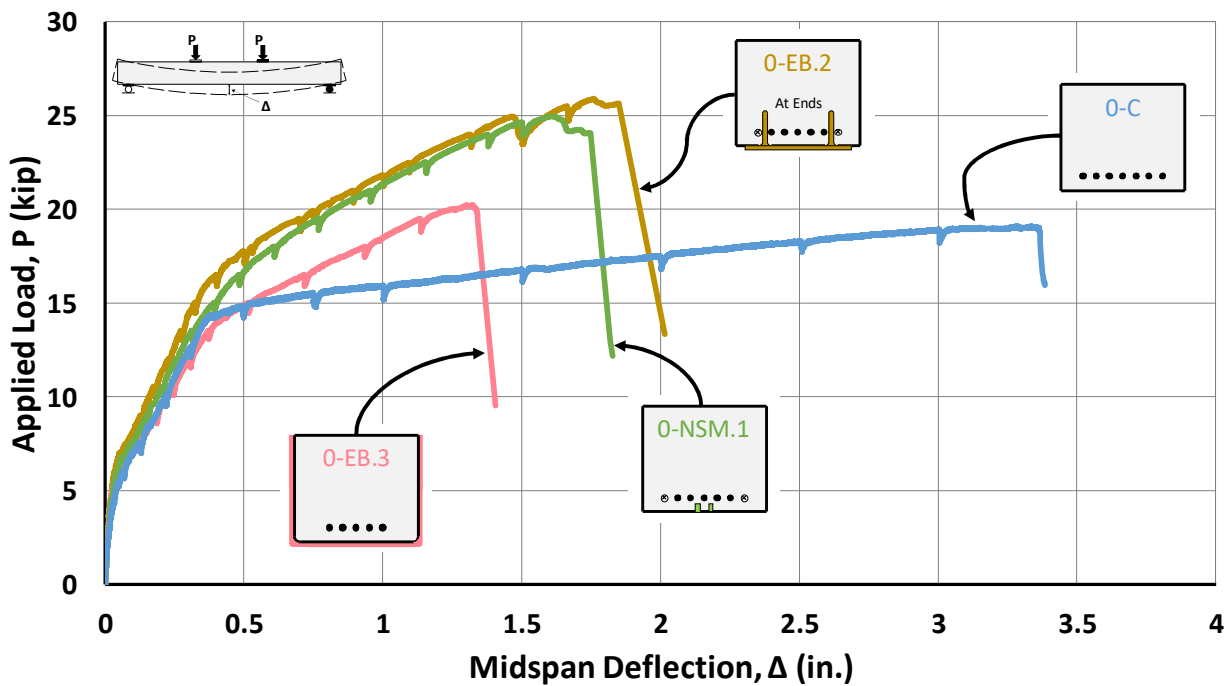


Figure 4.8: Applied Load vs. Midspan Deflection for Group 0 (Pilot) Specimens

In Table 4.2, $f_{f,max}$ and f_s are the estimated stresses in the FRP and steel reinforcement, respectively, obtained from the analytical tool and correspond to the maximum load applied to the test specimen. The value of f_{fu}^* is the ultimate tensile strength of the FRP reinforcement as reported by the manufacturer (see Table 3.3), and f_{fe} is the effective stress in the FRP reinforcement at

nominal flexural strength calculated in accordance with ACI 440.2R-17. Columns for the ratios f_{f_max}/f_{fe} and f_{f_max}/f_{fu}^* are also included in the table. These ratios are convenient values for evaluating the efficiency of the FRP systems. For the FRP-strengthened specimens in Table 4.2, Specimens 0-EB.2 and 0-NSM.1 contained cut reinforcement bars and, therefore, could not be accurately modeled using the analysis tool.

The longitudinal reinforcing bars in the FRP-strengthened pilot specimens differed among the beams. As indicated in Table 3.1 and the inset cross sections in Figure 4.8, Specimens 0-EB.2 and 0-NSM.1 included a bar cut at midspan on each side while Specimen 0-EB.3 had one bar excluded on each side. Therefore, direct comparisons between all three of the FRP-strengthened pilot specimens is not possible. Nevertheless, it is observed from Figure 4.8 that, although each specimen had a similar nominal moment capacity, M_n , as indicated in Table 4.2, all three of the strengthened specimens exceeded the strength of the control specimen. Further comparisons of the behavior of beams strengthened using various FRP systems and control specimens are provided in later sections of this chapter.

Although comparisons between the performance of the pilot test specimens with externally bonded sheets (0-EB.2 and 0-EB.3) cannot be directly compared, some valuable knowledge was gained during the pilot group testing based on how the strengthening systems behaved under load. The observed behavior of the specimens led to a modification of the experimental program. As explained in Chapter 3, the externally bonded longitudinal sheet of Specimen 0-EB.2 was anchored at its ends with FRP anchors, while the longitudinal sheet of Specimen 0-EB.3 was anchored at its ends with U-wrap anchors. Due to the observed behavior of Specimen 0-EB.3, it was decided to forego the U-wrap anchor design to allow for the testing of a different and possibly more viable anchorage configuration.

Comparing the performance of the three strengthened specimens as presented in Figure 4.8, the specimen with U-wrap anchors resulted in lower strength and ductility. This observation must be made with the understanding that the longitudinal reinforcement details differed among the specimens. Nevertheless, the difference in behavior contributed to the decision to explore other

anchorage options. Moreover, the application of U-wrap anchors to adjacent box beams in the field, a particular focus of this research, is not possible.

Another notable observation was made after investigating the condition of Specimen 0-EB.3 after failure. It was apparent that the U-wrap anchor reached its rupture strain during the test. As shown in Figure 4.9, the longitudinal sheet also ruptured at the location of the U-wrap. It should be noted that a small number of fibers along the edge of the sheet ruptured prior to the sudden rupture over the entire width of the longitudinal sheet. Nevertheless, it is unclear if the complete rupture across the width of one sheet contributed to the rupture of the other sheet as the video of the failure captured at a standard frame rate (i.e., 30 fps) shows the full rupturing of both sheets occurring seemingly simultaneously. Nevertheless, it is believed that the U-wrap anchor resulted in a reduction in strength and ductility relative to the other strengthened pilot specimens.

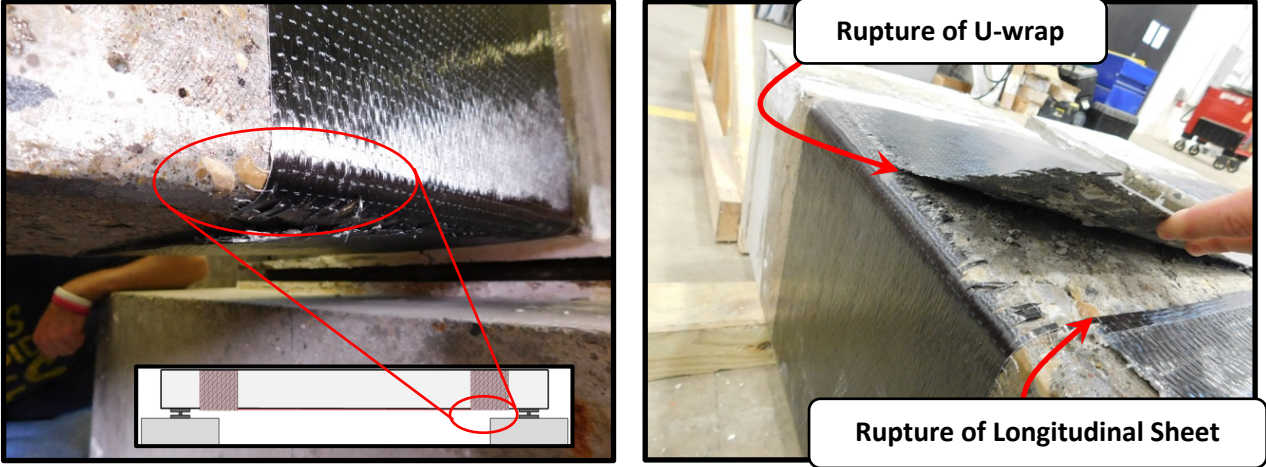


Figure 4.9: U-Wrap Anchor After Failure

The estimated stress in the longitudinal FRP sheet at midspan, f_{f_max} , for the specimen with U-wrap anchors is 117.18 ksi as indicated in Table 4.2. This value can be compared to the values of f_{f_max} calculated for similar specimens of the test program that are introduced in detail later. Specimens 1-EB.2 and 3-EB.2 were both detailed with two excluded steel reinforcing bars and were strengthened with an externally bonded FRP sheet anchored at its ends using FRP anchors. The values of f_{f_max} for Specimens 1-EB.2 and 3-EB.2 are 148.19 ksi and 147.27 ksi, respectively

(see Table 4.6). The values provide evidence that the U-wrap anchors may have led to a premature failure compared to the use of FRP anchors at the ends of the sheets.

During the tests on Specimens 0-EB.2 and 0-EB.3 of the pilot group, an important observation was made in regard to the behavior of the longitudinal FRP sheet as the applied load was increased. The FRP sheet started to debond from the concrete surface (see Figure 4.10). This apparent debonding was recognized by a crackling sound which was assumed to be the epoxy breaking its bond with the concrete substrate. The crackling sounds began to be observed sometime after the specimen had reached the cracking moment. To attempt to mitigate this debonding, specimens without U-wraps but with several FRP anchors along the length of the longitudinal sheet were added to the test program. This adjustment to the experimental program allowed the effect of the location of the FRP anchors on the performance of the strengthening system to be investigated. Complete details of the resulting specimens included in the experimental program are illustrated in Figure 3.5. The modification to the test program allowed for a more realistic solution to be tested in order to meet the objective of flexurally-strengthening adjacent box beam bridges. The strengthening system with FRP sheets anchored with FRP anchors does not require access to the sides of the box beam members.

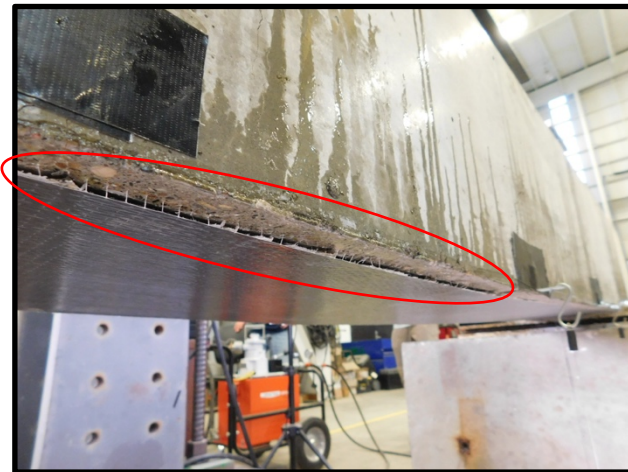


Figure 4.10: Partially Debonded FRP Sheet Between Anchor Points

Overall, the test results for Specimen 0-NSM.1 of the pilot group were satisfactory. No alteration was made to the design of the other NSM specimens in the experimental program as a result of the pilot tests.

4.5 Test Results By Specimen Type

4.5.1 Introduction

Direct comparisons between specimens of the same type (i.e., Control – C, Artificial Deterioration – D, Externally Bonded – EB, and Near-Surface-Mounted – NSM) are presented in this section. The behavior of the specimens with each strengthening system is also discussed. The test results help to identify reliable FRP systems for flexural strengthening.

4.5.2 Control (C) Specimens

A control specimen with seven No. 3 longitudinal tension bars was cast with each group of the test program. The results of the tests on the control specimens are summarized in Table 4.3. The corresponding response curves are provided in Figure 4.11. Despite the specimens being cast on different days and slight differences in the concrete strengths at the time of testing, consistency of the results for all four specimens is clearly evident. The specimens exhibited ductile behavior with failure characterized by crushing of concrete in the compression region. Due to the relatively low reinforcement ratio of the specimens ($\rho = A_s/b_wd = 0.53\%$), the strain in the longitudinal tension reinforcement entered the strain-hardening range for the steel. For this reason, M_{test} was on average 29% greater than M_n based on ACI 318-19, which was calculated using the measured yield stress of the bars ($f_y = 70.2$ ksi, refer to Section 4.3.1)

Table 4.3: Control Specimen Test Results

Specimen ID	M_{test} (kip-ft)	M_n (kip-ft)	M_{test} / M_n	Steel Stress, f_s (ksi)	Midspan Deflection at Max Load, Δ (in.)
0-C ¹	59.59	45.92 ²	1.30	88.47	3.29
1-C	59.80	46.11 ²	1.30	88.32	3.23
2-C	59.41	45.77 ²	1.30	88.81	3.45
3-C	56.83	45.90 ²	1.24	84.07	2.88

Mean: 1.29

Minimum: 1.24

Maximum: 1.30

¹Pin-roller support condition

²Calculated in accordance with ACI 318-19

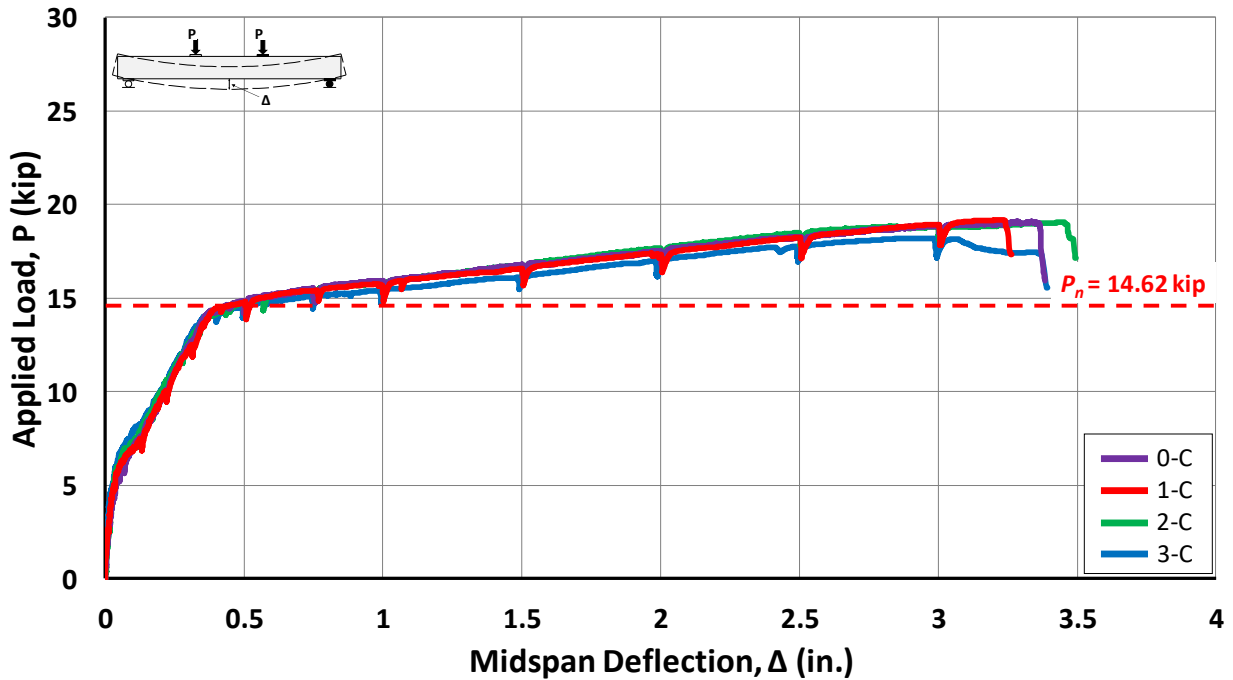


Figure 4.11: Applied Load vs. Midspan Deflection for Control Specimens

The theoretical load-deflection response developed by the analytical tool for the control specimens (f'_c taken as 6820 psi) is compared to the experimental curves in Figure 4.12. The theoretical load-deflection response is plotted up to the point corresponding to a concrete compressive strain of 0.0038 at the top fiber of the member. The response curve from analysis matches the experimental plots well, providing evidence of the suitability of the analysis tool to model reinforced concrete members under flexure.

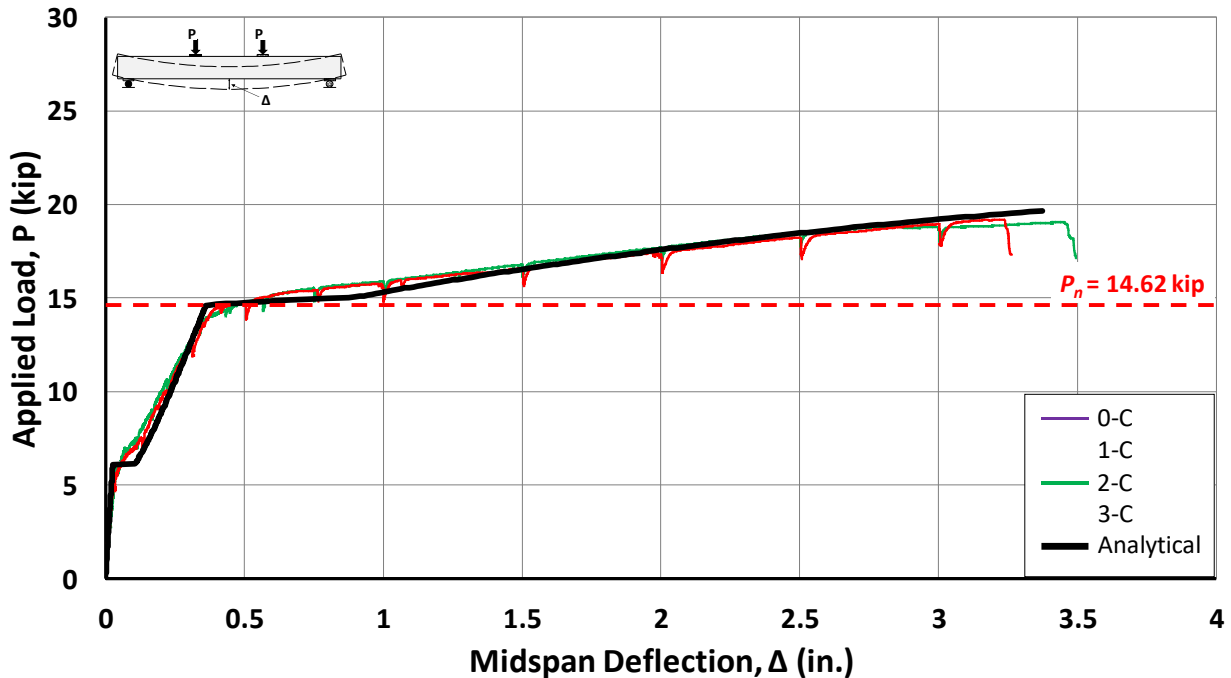


Figure 4.12: Comparison of Theoretical and Experimental Responses for Control Specimens

4.5.3 Artificially Deteriorated (D) Specimens

The test results for the three artificially deteriorated specimens that were left in their simulated field condition (i.e., not strengthened with FRP) are described in this section. Test data and experimental response curves are provided in Table 4.4 and Figure 4.13, respectively. Although each specimen had a different reinforcement layout (Artificial Deterioration Types I-III, refer to Figure 3.3), the three specimens were calculated to have approximately the same nominal capacity because the cut longitudinal reinforcing bars in Specimen 2-D were assumed to be ineffective at the location of the critical section for flexure (i.e., at midspan). The small variations in calculated values of M_n in Table 4.4 are only due to slight differences in the measured concrete compressive strengths. The flexural failure of each specimen was characterized by crushing of concrete in the compression region. Although the experimental moment capacities were very similar, Specimen 2-D with the two cut reinforcing bars exhibited the initiation of concrete crushing, accompanying by the opening of a wide flexural crack, considerably earlier compared to the other two specimens. As with the control specimens, the longitudinal reinforcing bars in the

artificially deteriorated specimens entered the strain-hardening range prior to ultimate failure (i.e., significant loss in load-carrying capacity) of the beams.

Table 4.4: Artificially Deteriorated Specimen Test Results

Specimen ID	M_{test} (kip-ft)	M_n (kip-ft)	M_{test} / M_n	Steel Stress, f_s (ksi)	Midspan Deflection at Max Load, Δ (in.)
1-D	44.68	33.88 ¹	1.32	89.17	3.63
2-D	45.40	33.67 ¹	1.35	-	1.63
3-D	44.47	33.92 ¹	1.31	88.67	3.63

Mean: 1.33

Minimum: 1.31

Maximum: 1.35

¹Calculated in accordance with ACI 318-19

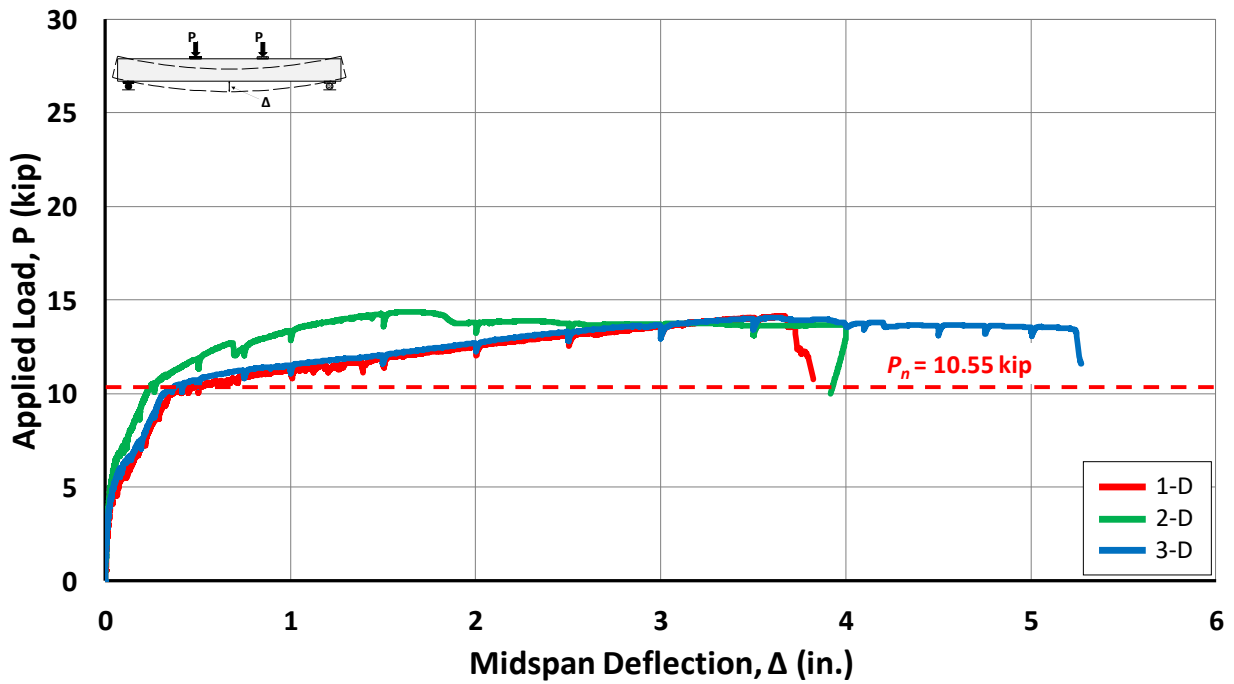


Figure 4.13: Applied Load vs. Midspan Deflection for Artificially Deteriorated Specimens

The behavior of Specimen 2-D represented in Figure 4.13 is notably different compared to the other specimens with two excluded reinforcing bars. Concrete began to crush at a midspan deflection of 1.63 in., only 45% of the deflection experienced by the other two specimens when concrete crushing initiated. This behavior was due to the concentration of curvature at the location of the cut bars (i.e., at midspan). A wide flexural crack developed at this location as the beam was loaded. The concentration of strain at the location of the crack caused the concrete in the compression region to begin to crush at a lesser deflection compared to the other two specimens. Each of the three artificially deteriorated specimens after failure are shown in Figure 4.14. The relatively large flexural crack at the midspan of Specimen 2-D is evident in Figure 4.14(b) in relation to the other artificially deteriorated specimens, which experienced a more uniform cracking pattern.

It is also observed that Specimen 2-D had higher post-cracking stiffness relative to the two other specimens due to the presence of the two cut reinforcing bars (see Figure 4.13). This higher relative stiffness of the specimen with cut reinforcement bars is important to note in this comparison in which the only variable was cut versus excluded bars. The difference in stiffness among the artificially deteriorated specimens can be used to explain some variations between the stiffnesses of FRP-strengthened specimens that are described in later sections of this chapter.

The load-deflection response obtained from the analytical tool for the artificially deteriorated specimens (f'_c taken as 6680 psi) is compared to the experimental load-deflection curves for the beams with excluded reinforcing bars in Figure 4.15. Here, the theoretical curve is plotted to the point corresponding to a concrete compressive strain of 0.0038. Again, the theoretical response curve closely corresponds to the experimental response curves.

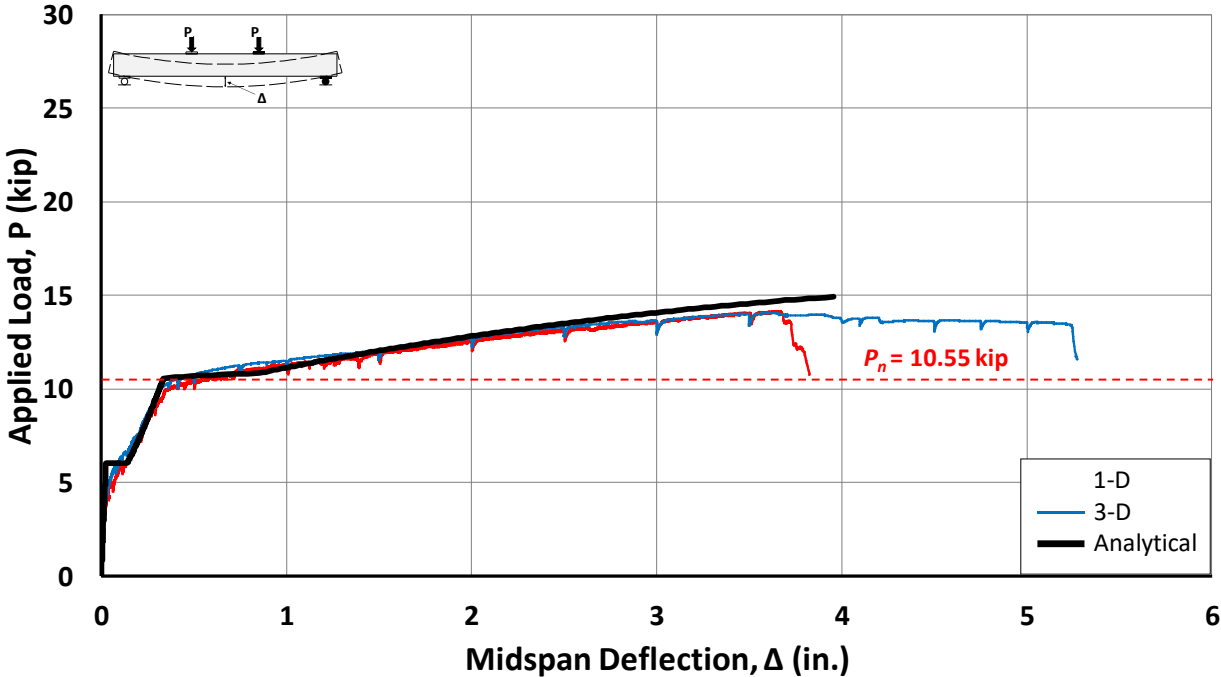


Figure 4.15: Comparison of Theoretical and Experimental Responses for Artificially Deteriorated Specimens

4.5.4 Externally Bonded (EB) FRP Sheet Specimens

The test results for the specimens with externally bonded FRP sheets show consistent differences in moment capacity between the two FRP anchor configurations (EB.1 with anchors along the length vs. EB.2 with anchors only at the ends). The results from the tests of both anchor configurations are described in the following subsections. Other than Specimen 0-EB.2 which experienced crushing of the concrete prior to FRP rupture, all EB specimens failed by rupture of the FRP sheets prior to concrete crushing regardless of the anchorage details. Important differences between the behaviors resulting from the anchorage details are described in Section 4.5.4.3.

4.5.4.1 FRP Anchors Along the Length of the FRP Sheet (EB.1)

The calculated strengths and experimental data for the EB.1 specimens are summarized in Table 4.5. All three EB.1 specimens exceeded their nominal moment capacity and experienced relatively similar failure moments. However, Specimen 1-EB.1 did not achieve the strength of the corresponding control specimens (Specimen 1-C). It should be noted that the midspan deflection at the maximum applied load for each of the three beams is much lower compared to the deflections of the corresponding unstrengthened specimens (at least approximately 58% less considering the strengthened and unstrengthened specimens from each group, see Table 4.4). Failure by rupture of the FRP sheet greatly reduced the ductility of the specimens. Table 4.5 again includes columns for steel reinforcement and FRP stress values. As previously explained, Specimen 2-EB.1 contained two cut reinforcing bars, and estimated stress values are therefore not included in the table as it is difficult to accurately quantify the contribution of the two cut bars.

Table 4.5: EB.1 Specimen Test Results

Specimen ID	M_{test} (kip-ft)	M_n (kip-ft)		M_{test} / M_n		M_{test} / M_c	Steel Stress, f_s (ksi)	Rupture Stress, $f_{f,max}$ (ksi)	f_{fu}^* (ksi)	Effective Stress, f_{fe} (ksi)	$f_{f,max} / f_{fu}^*$	$f_{f,max} / f_{fe}$	Midspan Deflection at Max Load, Δ (in.)
		$\psi_f = 0.85$	$\psi_f = 1.0$	$\psi_f = 0.85$	$\psi_f = 1.0$								
1-EB.1	54.91	51.29 ¹	54.58 ¹	1.07	1.01	0.92	70.60	88.19	105	73.8	0.84	1.19	0.81
2-EB.1	60.10	51.19 ¹	54.48 ¹	1.17	1.10	1.01	-	-	105	73.8	-	-	0.68
3-EB.1	58.36	51.40 ¹	54.70 ¹	1.14	1.07	1.03	71.97	100.00	105	73.8	0.95	1.36	0.96

Mean: 1.13 1.06

Minimum: 1.07 1.01

Maximum: 1.17 1.10

¹Calculated in accordance with ACI 440.2R-17

The response curves of the EB.1 specimens are provided in Figure 4.16. For each specimen, individual fibers of the longitudinal FRP sheet began to rupture once the applied load, P , reached approximately 15 kip. As can be seen by a larger initial drop in load, a larger amount of fibers ruptured at the maximum load for Specimens 1-EB.1 and 2-EB.1 while Specimen 3-EB.1 experienced a more gradual rupturing of the FRP sheet. Individual fibers continued to rupture with increasing applied load until the FRP fully ruptured across the width of the beam and all capacity from the FRP was lost. The plots in Figure 4.16 extend until this point. As expected based on the behavior of the artificially deteriorated specimens, Specimen 2-EB.1 with bars cut at midspan exhibited a greater stiffness compared to the other two specimens after the initial flexural cracking of the concrete occurred. The specimen also exhibited a slightly larger failure moment (9.45% greater than Specimen 1-EB.1) and reduced ductility compared to the beams with missing bars. Unlike the other EB.1 specimens, the flexural cracking behavior of Specimen 2-EB.1 was more closely related to Specimen 2-D due to the relatively larger cracks near midspan.

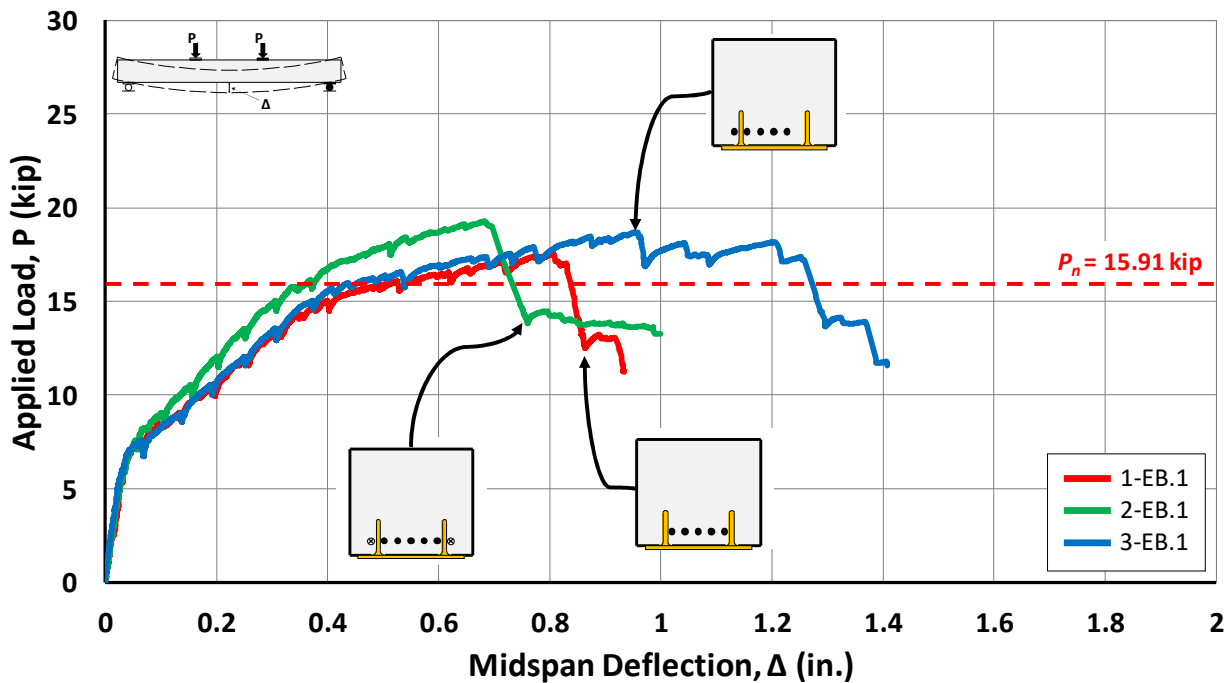


Figure 4.16: Applied Load vs. Midspan Deflection for EB.1 Specimens

The data in Figure 4.16 can be used to compare the behaviors of Specimen 1-EB.1 with one bar excluded near each corner and Specimen 3-EB.1 with two bars excluded near one corner.

The responses of the two specimens are similar up to the significant loss in load-carrying capacity experienced by Specimen 1-EB.1. Specimen 3-EB.1 displayed noticeably more deflection compared to Specimen 1-EB.1 before total rupture of the FRP sheet occurred across the width of the beam. However, this variability is not attributed to the eccentricity of the reinforcement but rather to the general variability of the FRP strengthening system.

From the results in Table 4.5, it is observed that the estimated stress in the FRP corresponding with the maximum applied load, f_{f_max} , surpassed the effective stress, f_{fe} , for both Specimens 1-EB.1 and 3-EB.1. However, for both beams, the value of f_{f_max} is less than the ultimate tensile strength of the cured FRP laminate, f_{fu}^* , reported by the manufacturer. It should be noted that the value of f_{fe} in the moment strength calculations based on ACI 440.2R-17 for all specimens represented in Table 4.5, as well as all other FRP-strengthened specimens of the flexural-strengthening experimental program, is governed by rupture of the FRP. In other words, in accordance with the design calculations, the value of f_{fe} is equal to $0.9E_f\varepsilon_{fu}$ for the EB specimens and $0.7E_f\varepsilon_{fu}$ for the NSM specimens, where E_f and ε_{fu} are the modulus of elasticity and design rupture strain, respectively, as reported by the manufacturer (see Table 3.3). A comparison of the theoretical load-deflection curve from the analysis tool is compared to the experimental load-deflection responses in Section 4.5.4.3.

Failure photos for each of the three tests are provided in Figure 4.17. The longitudinal FRP sheet ruptured in a similar location (near midspan) for all three specimens. After further investigation of the ruptured FRP sheet of the three specimens, it was determined that the location of the rupture was consistently at one of the FRP anchor points located closest to midspan (see Figure 4.18). It could not be visually verified while testing but it is assumed that the FRP first ruptured near the anchor points due to the increased stress concentration at that location.



(a) 1-EB.1



(b) 2-EB.1



(c) 3-EB.1

Figure 4.17: EB.1 Specimens After Failure

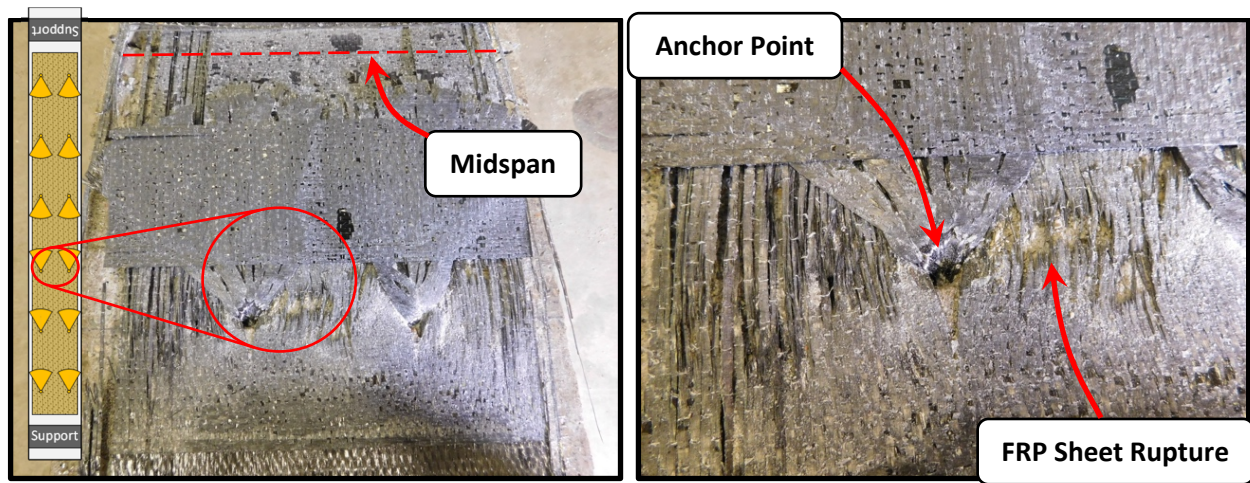


Figure 4.18: Typical FRP Sheet Rupture at Anchor Point – EB.1 Specimens

4.5.4.2 FRP Anchors at the Ends of the FRP Sheet (EB.2)

The results of the tests on the four EB.2 specimens are summarized in Table 4.6, and the corresponding load-deflection plots are presented in Figure 4.19. In contrast to the three EB.1 specimens that experienced incremental rupturing of the FRP sheet across the width of the sheet, all four EB.2 specimens experienced a failure characterized by an abrupt rupture of the longitudinal FRP sheet. In other words, the fibers within the FRP sheets suddenly ruptured across the width of the specimen, with the possible exception of a small number of fibers along the edge of the sheet rupturing prior to this event. As previously noted, Specimen 0-EB.2 experienced crushing of the concrete just prior to FRP rupture. Along with the failure behavior of the EB.2 specimens being different from that of the EB.1 specimens, the numerical results were also different. The EB.2 specimens consistently reached larger capacities compared to their EB.2 counterparts and also achieved larger midspan deflections prior to failure.

Table 4.6: EB.2 Specimen Test Results

Specimen ID	M_{test} (kip-ft)	M_n (kip-ft)		M_{test} / M_n		M_{test} / M_c	Steel Stress, f_s (ksi)	Rupture Stress, $f_{f,max}$ (ksi)	f_{fu}^* (ksi)	Effective Stress, f_{fe} (ksi)	$f_{f,max} / f_{fu}^*$	$f_{f,max} / f_{fe}$	Midspan Deflection at Max Load, Δ (in.)
		$\psi_f = 0.85$	$\psi_f = 1.0$	$\psi_f = 0.85$	$\psi_f = 1.0$								
0-EB.2	79.96	51.00 ¹	54.28 ¹	1.57	1.47	1.34	-	-	105	73.8	-	-	1.76
1-EB.2	71.71	51.21 ¹	54.50 ¹	1.40	1.32	1.20	77.15	148.19	105	73.8	1.41	2.01	1.63
2-EB.2	72.79	51.25 ¹	54.54 ¹	1.42	1.33	1.23	-	-	105	73.8	-	-	1.25
3-EB.2	71.62	51.38 ¹	54.68 ¹	1.39	1.31	1.26	77.07	147.27	105	73.8	1.40	2.00	1.69

Mean: 1.45 1.36
 Minimum: 1.39 1.31
 Maximum: 1.57 1.47

¹Calculated in accordance with ACI 440.2R-17

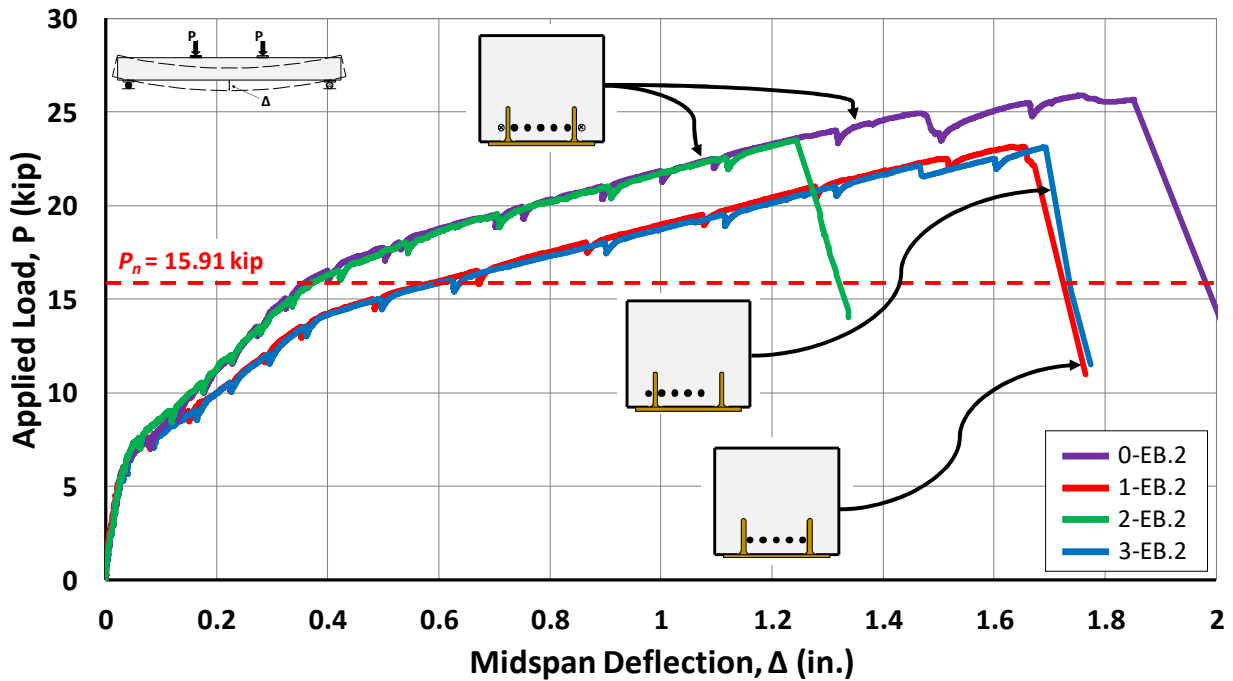


Figure 4.19: Applied Load vs. Midspan Deflection for EB.2 Specimens

The increased stiffness of the two specimens with cut reinforcing bars (Specimens 0-EB.2 and 2-EB.2) compared to the two specimens with excluded reinforcing bars (Specimens 1-EB.2 and 3-EB.2) is shown by the response curves in Figure 4.19. Another important observation is the variations in ductility and failure loads between Specimens 0-EB.2 and 2-EB.2 presented in this figure. Because the details of these specimens were similar, these differences are assumed to be attributable to variability in the properties of the FRP laminate and sensitivity to small variations in the application process. Considering the relatively large midspan deflection reached by

Specimen 0-EB.2, variations in the ductility of the FRP-strengthening beams do not seem to be dependent on whether longitudinal bars were cut or excluded to create the simulated field conditions of the members. It can also be noted that, with less deflection achieved before the end of the test, the cracking near midspan was less severe for Specimens 0-EB.2 and 2-EB.2 compared to Specimen 2-D of the artificially deteriorated group. It should be noted that cracking patterns after failure cannot be directly compared for all Group 2 specimens since deflections at failure were not all the same, yet general comparisons are still valuable. When comparing the cracking patterns between specimens with cut bars to those with excluded bars, the specimens with cut bars experienced relatively larger cracks near midspan.

The responses of Specimens 1-EB.2 and 3-EB.2 displayed in Figure 4.19 are nearly identical, indicating that the eccentricity of the steel reinforcement did not impact the behavior of the specimens. As discussed in Section 4.5.4.1, this provides further evidence that the difference in deflections achieved by Specimens 1-EB.1 and 3-EB.1 is likely due to variability of the FRP strengthening system and not due to the eccentricity of the steel.

The two EB.2 specimens with longitudinal bars excluded (Specimens 1-EB.2 and 3-EB.2) were modeled using the analysis described in Section 4.2. Based on this analysis, the FRP sheets for both of these specimens were estimated to have reached a strain value at the maximum applied load, f_{f_max} , that is twice the effective stress, f_{fe} , calculated in accordance with ACI 440.2R-17 (see Table 4.6). Again, the value of f_{fe} is calculated based on rupture of the FRP governing the failure of the member. The estimated values of f_{f_max} also exceed the tensile strength reported by the manufacturer, f_{fu}^* . The values of the ratio f_{f_max}/f_{fu}^* for the specimens are quite large and are again best understood in a relative sense compared to the results of other test specimens rather than as an accurate representation of the actual stress achieved by the FRP. A comparison of the theoretical load-deflection response from the analysis tool is compared to the experimental load-deflection curves in Section 4.5.4.3.

Photos of each EB.2 specimen after failure are provided in Figures 4.20 through 4.23. While the longitudinal FRP sheet ruptured consistently at one of the FRP anchor points located closest to midspan for all of the EB.1 specimens, the location of the ruptured longitudinal FRP

sheet varied between the EB.2 specimens. The FRP sheet on Specimens 0-EB.2 and 1-EB.2 ruptured at the location of the end anchor while the sheet on Specimens 2-EB.2 and 3-EB.2 ruptured near midspan. Considering the data in Table 4.6 and the plots in Figure 4.19, no correlation is found between the location of the FRP rupture and the overall efficiency (i.e., resulting failure load and ductility) of the strengthening system.



(a) South End



(b) North End



(c) Crack Pattern

Figure 4.20: Specimen 0-EB.2 After Failure



(a) South End



(b) North End



(c) Crack Pattern

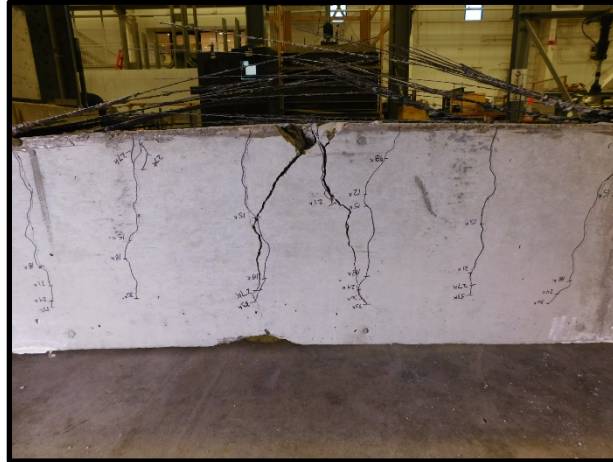
Figure 4.21: Specimen 1-EB.2 After Failure



(a) View 1



(b) View 2



(c) View 3

Figure 4.22: Specimen 2-EB.2 After Failure



(a) View 1



(b) View 2



(c) View 3

Figure 4.23: Specimen 3-EB.2 After Failure

Footage from the high-speed camera was used to verify that the failure of Specimen 1-EB.2 was, in fact, due to rupture of the longitudinal FRP sheet and not due to insufficient anchorage. An image of the north support for Specimen 1-EB.2 just prior to rupture of the FRP sheet (besides a small number of fibers at the edge of the sheet that had ruptured before the image was taken) is provided in Figure 4.24(a). The image in Figure 4.24(b) shows the rupture of the longitudinal FRP sheet, potentially due to the stress concentration at the northwest anchor.

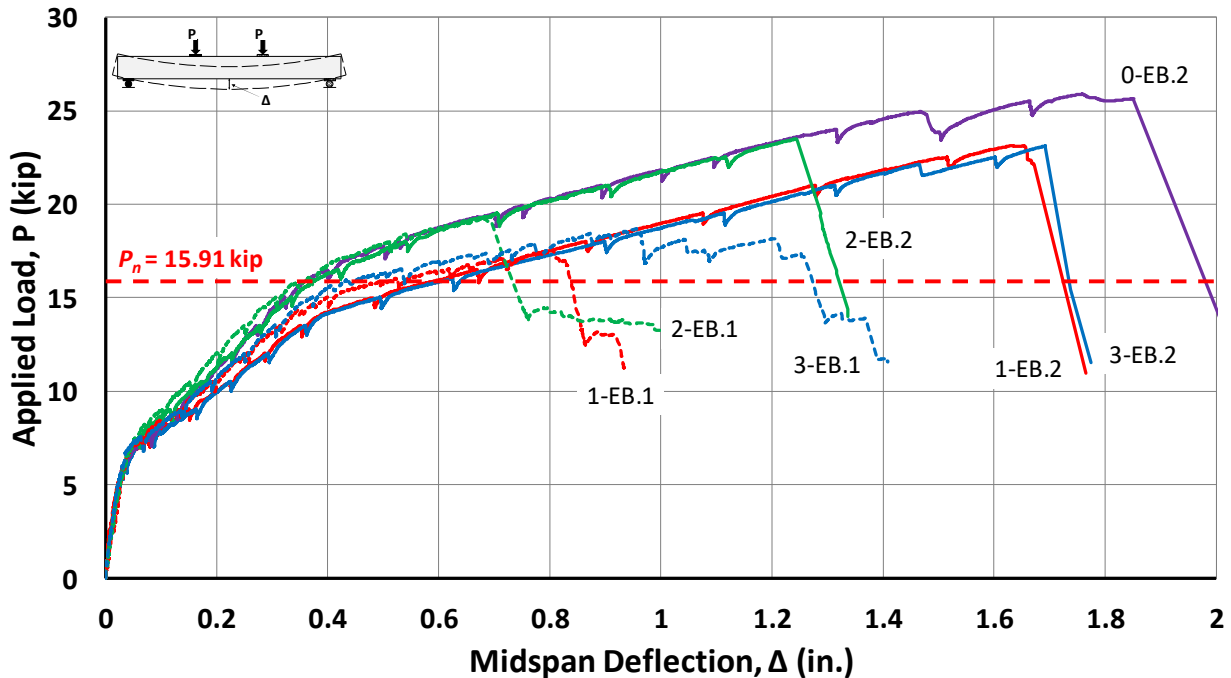


Figure 4.25: Applied Load vs. Midspan Deflection for EB.1 and EB.2 Specimens

Several important comparisons can be made from the data in Table 4.7 and Figure 4.25. Comparing the specimens from Groups 1, 2, and 3 with the same simulated field conditions, the experimental moment capacity, M_{test} , is 25% greater on average for the EB.2 specimens compared to the EB.1 specimens. Similarly, the midspan deflection at the maximum applied load is 87% greater on average for the EB.2 specimens compared to the EB.1 specimens from Groups 1, 2, and 3 with the same simulated field condition. The estimated values of the stress in the FRP sheets at the maximum applied load, f_{f_max} , for corresponding specimens analyzed using the procedure outlined in Section 4.2 (1-EB.1 vs. 1-EB.2 and 3-EB.1 vs. 3-EB.2) also provide an important comparison. Assuming the FRP stress can be calculated based on strain compatibility, the value of f_{f_max} is 68% and 47% greater for the specimens with anchors only at the ends of the sheet compared to the specimens with anchors along their lengths for Groups 1 and 3, respectively. Based on the analysis, the FRP sheets on the EB.2 specimens reached twice the calculated effective stress, f_{fe} , while the EB.1 specimens still surpassed the effective stress but only by an average of approximately 28%. Furthermore, the values of f_{f_max} exceed f_{fu}^* for the EB.2 specimens but not for the EB.1 specimens. Based on these comparisons along with the observed rupture of the sheets on the EB.1 specimens occurring at one of the FRP anchor points located closest to midspan, the

early failure of the EB.1 specimens is attributed to stress concentrations in the FRP sheets near the anchor points near midspan. It is noted that rupture of the FRP sheet was observed near an anchor at the end of the member for two of the EB.2 specimens. However, the strength of the member did not reflect a premature failure. This is likely because the anchor points were located at a position along the beam at which little bending moment is experienced.

To compare the theoretical load-deflection curve from the analysis tool with the behavior of the test specimens, a plot of the theoretical curve for the externally bonded case (f'_c taken as 7270 psi) is provided in Figure 4.26 along with the experimental load-deflection plots for the applicable EB specimens. Again, the value of f_{f_max} for a member is obtained from the analysis tool for the maximum load applied to the experimental specimen during the test.

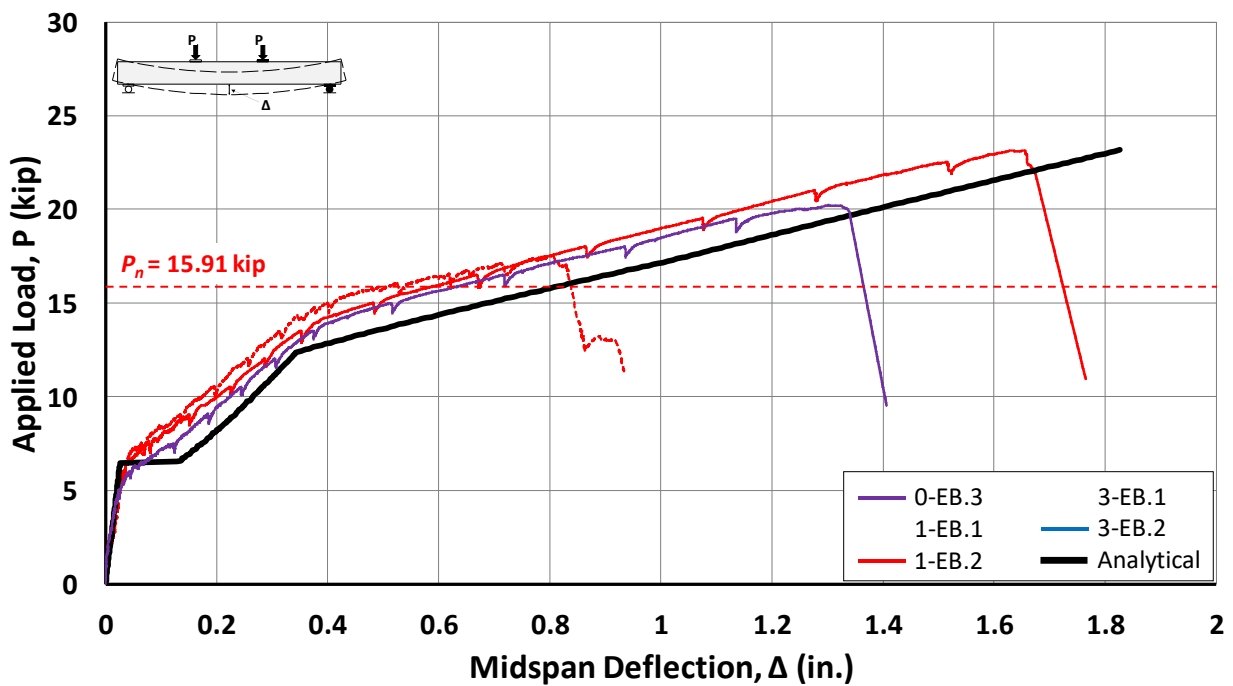


Figure 4.26: Comparison of Theoretical and Experimental Responses for Externally Bonded Specimens

4.5.5 Near-Surface-Mounted (NSM) FRP Strip Specimens

The test results of the seven near-surface-mounted FRP strengthened specimens are provided in Table 4.8. The response curves for all NSM.1 specimens are provided in Figure 4.27. The NSM strips were centered on the cross section for these specimens. Three NSM specimens were included in Group 3 to evaluate the effect of the placement of the FRP strips relative to the location of excluded longitudinal reinforcing bars. For clarity, the response of the Group 3 specimens are shown separately from the other specimens in Figure 4.28. The curve for Specimen 3-NSM.1 is therefore included in both plots. It should again be noted that Specimen 1-NSM.1b was added to the testing program in order to verify the feasibility of applying the FRP strips overhead. A different epoxy was used for this application (see Section 3.6.2).

Table 4.8: NSM Specimen Test Results

Specimen ID	M_{test} (kip-ft)	M_n (kip-ft)		M_{test} / M_n		M_{test} / M_c	Steel Stress, f_s (ksi)	Rupture Stress, $f_{f,max}$ (ksi)	f_{fu}^* (ksi)	Effective Stress, f_{fe} (ksi)	$f_{f,max} / f_{fu}^*$	$f_{f,max} / f_{fe}$	Midspan Deflection at Max Load, Δ (in.)
		$\psi_f = 0.85$	$\psi_f = 1.0$	$\psi_f = 0.85$	$\psi_f = 1.0$								
0-NSM.1	77.11	50.36 ²	53.53 ²	1.53	1.44	1.29	-	-	325	228.1	-	-	1.61
1-NSM.1a	70.81	50.50 ²	53.67 ²	1.40	1.32	1.18	77.79	364.58	325	228.1	1.12	1.60	1.72
1-NSM.1b ¹	58.54	50.68 ²	53.86 ²	1.15	1.09	0.98	72.78	252.72	325	228.1	0.78	1.11	1.10
2-NSM.1	82.87	50.46 ²	53.63 ²	1.64	1.55	1.39	-	-	325	228.1	-	-	1.82
3-NSM.1	68.56	50.59 ²	53.77 ²	1.36	1.28	1.21	76.87	343.02	325	228.1	1.06	1.50	1.62
3-NSM.2	69.25	50.53 ²	53.70 ²	1.37	1.29	1.22	77.17	350.03	325	228.1	1.08	1.53	1.56
3-NSM.3	65.50	50.55 ²	53.72 ²	1.30	1.22	1.15	75.67	315.71	325	228.1	0.97	1.38	1.43

Mean: 1.39 1.31

Minimum: 1.15 1.09

Maximum: 1.64 1.55

¹Epoxy grout and NSM strip applied overhead

²Calculated in accordance with ACI 440.2R-17

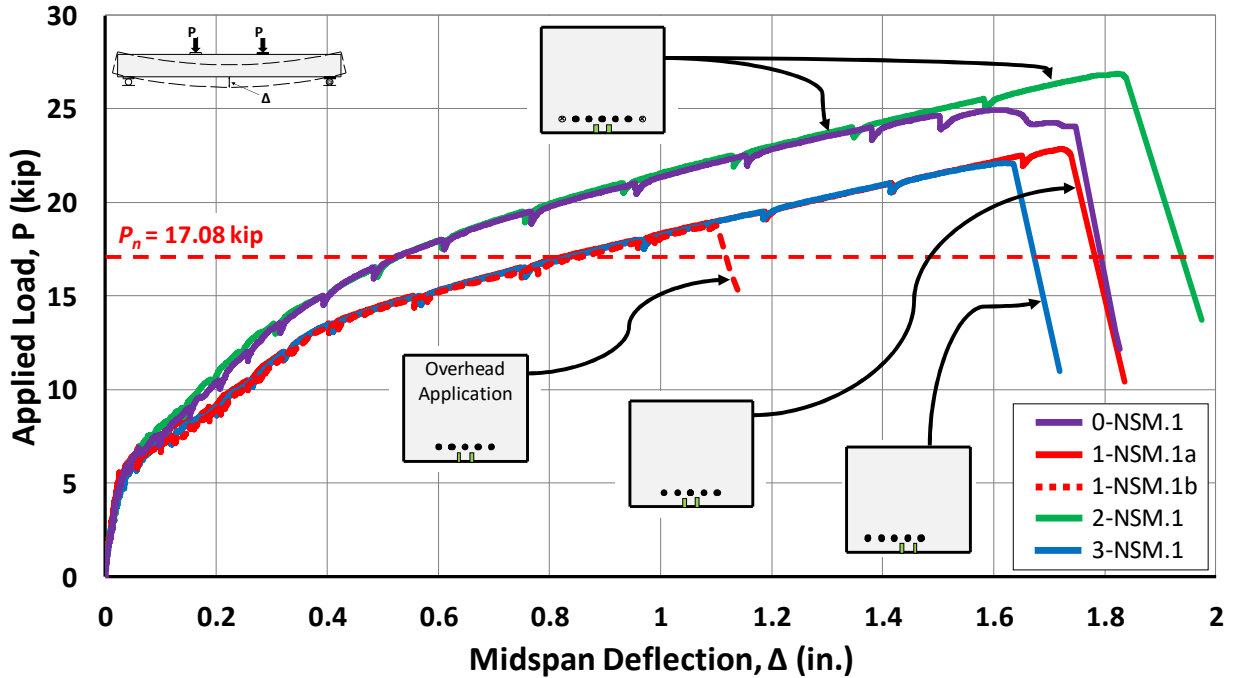


Figure 4.27: Applied Load vs. Midspan Deflection for NSM.1 Specimens

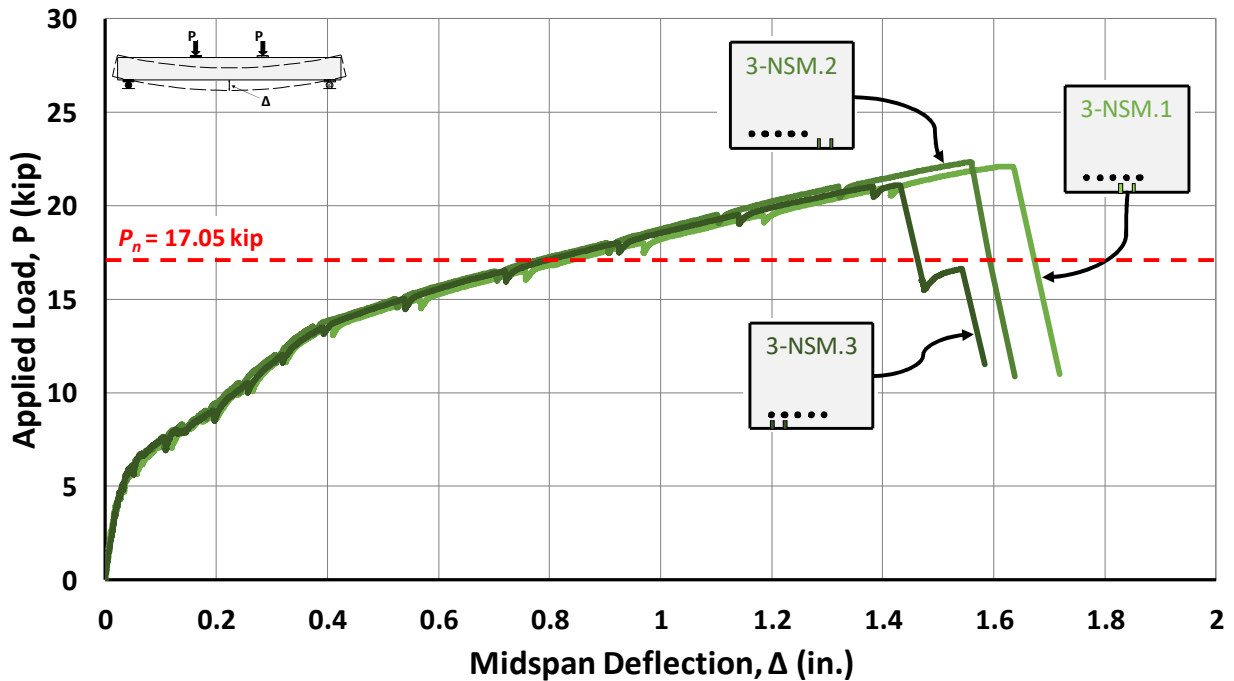


Figure 4.28: Applied Load vs. Midspan Deflection for Group 3 NSM Specimens

Each NSM specimen surpassed its calculated nominal flexural strength, and failed by rupture of the NSM strips. The only specimen that experience some concrete crushing prior to the

rupture of the NSM strips was Specimen 0-NSM.1. The slight loss in load-carrying capacity corresponding to concrete crushing prior to ultimate failure is evident for this specimen in Figure 4.27.

Several key observations are noted from the load-deflection plots. Consistent with the test results previously presented, the two specimens with cut reinforcing bars (Specimens 0-NSM.1 and 2-NSM.1) exhibited a greater post-cracking stiffness compared to all other NSM specimens. Variations in flexural strengths are also evident, with Specimen 2-NSM.1 achieving a failure load notably greater than other specimens. The differences in strength may be at least partially attributed to variations in material properties of the NSM strips or sensitivity to small variations in the installation procedures.

Furthermore, as can be observed from Figure 4.28, the location of the NSM FRP strips in relation to the centroid of the steel reinforcement did not have a significant effect on the response of the specimens. Specimen 3-NSM.3, however, did experience a lower failure load and midspan deflection compared to the other specimens, with the exception of Specimen 1-NSM.1b, discussed later. Although visually unverified due to the nature of the NSM strip rupture within the epoxy grout, the behavior of Specimen 3-NSM.3 near the end of its load-deflection plot (see Figure 4.28) is likely due to the second NSM strip rupturing upon further loading after rupture of the first strip. This behavior, however, cannot be attributed to the location of the NSM without further testing or analysis. As described in Section 3.7, two linear string potentiometers measured the deflection at each edge of the bottom surface of the Group 3 specimens (i.e., all specimens with eccentric steel reinforcement) at midspan and under each of the two load points. No significant differential deflections (i.e., rotation) were measured between the two edges at midspan of the Group 3 specimens with NSM reinforcement (between 0.003 in. and 0.015 in. at the maximum applied load) relative to the differential deflection of the Group 3 control specimen (Specimen 3-C) that had concentric reinforcement (0.024 in. at the maximum applied load). For comparison, the deflections measured at each bottom edge of the Group 3 specimens at midspan and the two load points are included in Appendix C. More tests, possibly with larger eccentricities, should be conducted to confirm that placement of NSM strips relative to corroded steel reinforcement has little to no effect on flexural performance.

Specimen 1-NSM.1b for which the NSM strips were installed overhead proved to be an outlier in the data. Although the process of the overhead application of the NSM strips was a success (see Section 3.6.2) and Specimen 1-NSM.1b reached its nominal flexural strength (with the steel reinforcement expected to have increased slightly beyond the yield stress due to strain hardening), it is apparent that the specimen experienced a premature failure compared to the other NSM specimens. The response curve of Specimen 1-NSM.1b follows the trend of other specimens with excluded reinforcing bars closely until the point of this premature failure. In order to draw a reliable conclusion about the cause of the observed behavior, variations in the material properties of the NSM strips should be investigated further. More tests on specimens with NSM strips installed using the same epoxy as Specimen 1-NSM.1b and additional tests on specimens with strips installed into both overhead and inverted members are also needed.

The rupture of the NSM FRP strips was far less explosive than the externally bonded FRP sheets. When each specimen failed by FRP rupture, the ruptured strips were contained within the epoxy grout. Specimen 1-NSM.1a was destructively investigated to verify that the FRP strips had ruptured as expected. As shown in Figure 4.29, it was found that both FRP strips ruptured at the same location near midspan.



(a) After Failure

(b) After Destructive Inspection

Figure 4.29: FRP Strips of Specimen 1-NSM.1a

As with the specimens with externally bonded FRP sheets, the stress in the NSM strips at failure, f_{f_max} , was estimated and compared to values of f_{fe} and f_{fu}^* for the specimens without cut steel reinforcing bars (see Table 4.8). The calculated strengths of the NSM specimens based on ACI 440.2R-17 were governed by rupture of the FRP strips. The value of f_{fe} is therefore equal to $0.7E_f\varepsilon_{fu}$, where E_f and ε_{fu} are the modulus of elasticity and design rupture strain, respectively, as reported by the manufacturer (see Table 3.3). Considering the specimens in Table 4.8 that did not include cut steel bars, the NSM strips were estimated to have reached a 42% greater stress on average than the calculated value of f_{fe} . As expected, the lowest value of f_{f_max} was calculated for Specimen 1-NSM.1b with strips installed overhead. The value of f_{f_max} still exceeded f_{fe} by 11%. However, the value of f_{f_max} for this specimen was only 78% of f_{fu}^* reported by the manufacturer of the NSM strips.

The theoretical load-deflection curve for the NSM case (f'_c taken as 7030 psi) is plotted in Figure 4.25 with the load-deflection responses of the five NSM specimens without cut steel reinforcing bars. The plot again demonstrates that a relatively simple analysis tool can provide a reasonable representation of the FRP-strengthened members.

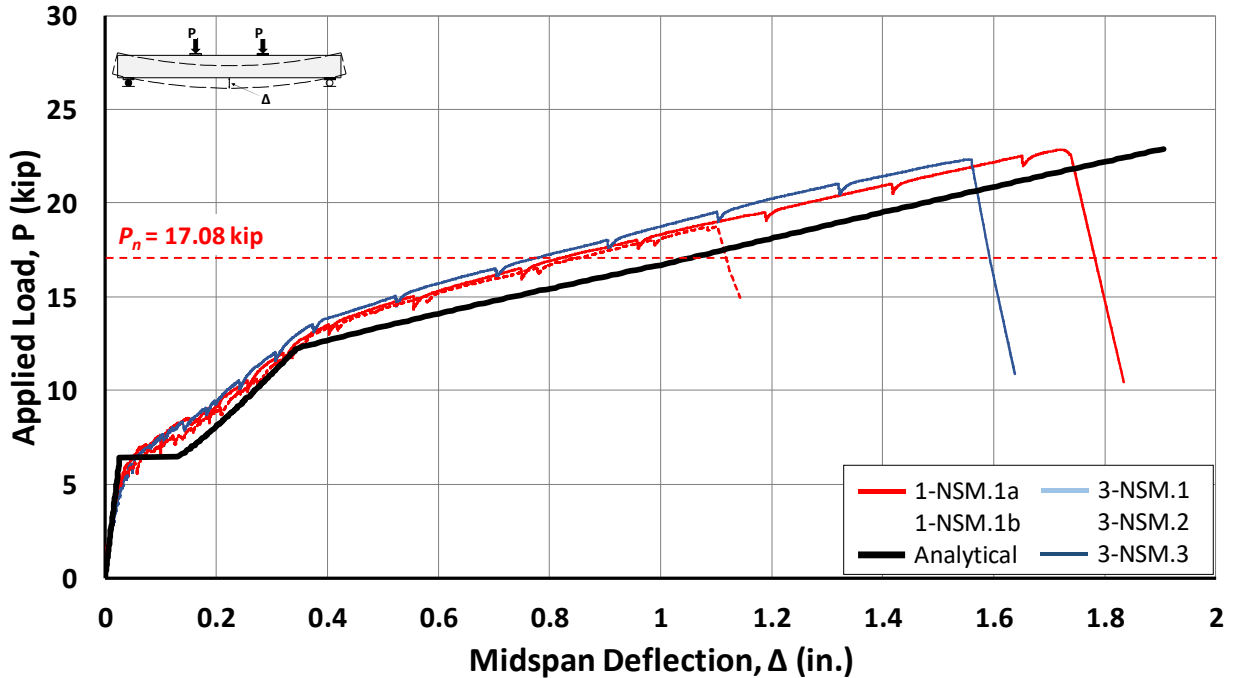


Figure 4.30: Comparison of Theoretical and Experimental Responses for Near-Surface-Mounted Specimens

4.6 Test Results By Group

Comparisons of specimens within each group, excluding Group 0 (see Section 4.4), are presented in this section. Studying the test results by each group allows the effectiveness of the FRP strengthening system in regaining the strength and stiffness of the control specimen to be evaluated. Furthermore, direct comparisons can be made between the FRP systems and anchorage details used for the strengthening of beams with particular cases of artificial deterioration simulated by cut or excluded reinforcing bars.

4.6.1 Group 1

The test results for the Group 1 specimens are provided in Table 4.9, and the corresponding response curves are provided in Figure 4.31. In Table 4.9, the ratios M_{test}/M_C and M_{test}/M_D are listed, where M_C is the experimental flexural capacity of the control specimen (Specimen 1-C) and M_D is the experimental flexural capacity of the artificially deteriorated specimen not strengthened with FRP (Specimen 1-D). It should be noted that the artificial deterioration of the Group 1 specimens was achieved by excluding one reinforcing bar on each side of the member.

Table 4.9: Group 1 Test Results

Specimen ID	M_{test} (kip-ft)	M_n (kip-ft)		M_{test} / M_n		M_{test} / M_c	M_{test} / M_D	Steel Stress, f_s (ksi)	Rupture Stress, $f_{f,max}$ (ksi)	f_{fu}^* (ksi)	Effective Stress, f_{fe} (ksi)	$f_{f,max} / f_{fu}^*$	$f_{f,max} / f_{fe}$	Midspan Deflection at Max Load, Δ (in.)
		$\psi_f = 0.85$	$\psi_f = 1.0$	$\psi_f = 0.85$	$\psi_f = 1.0$									
1-C	59.80	46.11 ²		1.30		1.00	1.34	88.32	-	-	-	-	-	3.23
1-D	44.68	33.88 ²		1.32		0.75	1.00	89.17	-	-	-	-	-	3.63
1-EB.1	54.91	47.33 ³	49.91 ³	1.16	1.10	0.92	1.23	70.60	88.19	105	73.8	0.84	1.19	0.81
1-EB.2	71.71	47.26 ³	49.84 ³	1.52	1.44	1.20	1.60	77.15	148.19	105	73.8	1.41	2.01	1.63
1-NSM.1a	70.81	50.20 ³	53.31 ³	1.41	1.33	1.18	1.58	77.79	364.58	325	228.1	1.12	1.60	1.72
1-NSM.1b ¹	58.54	50.38 ³	53.51 ³	1.16	1.09	0.98	1.31	72.78	252.72	325	228.1	0.78	1.11	1.10

¹Epoxy grout and NSM strip applied overhead

²Calculated in accordance with ACI 318-19

³Calculated in accordance with ACI 440.2R-17

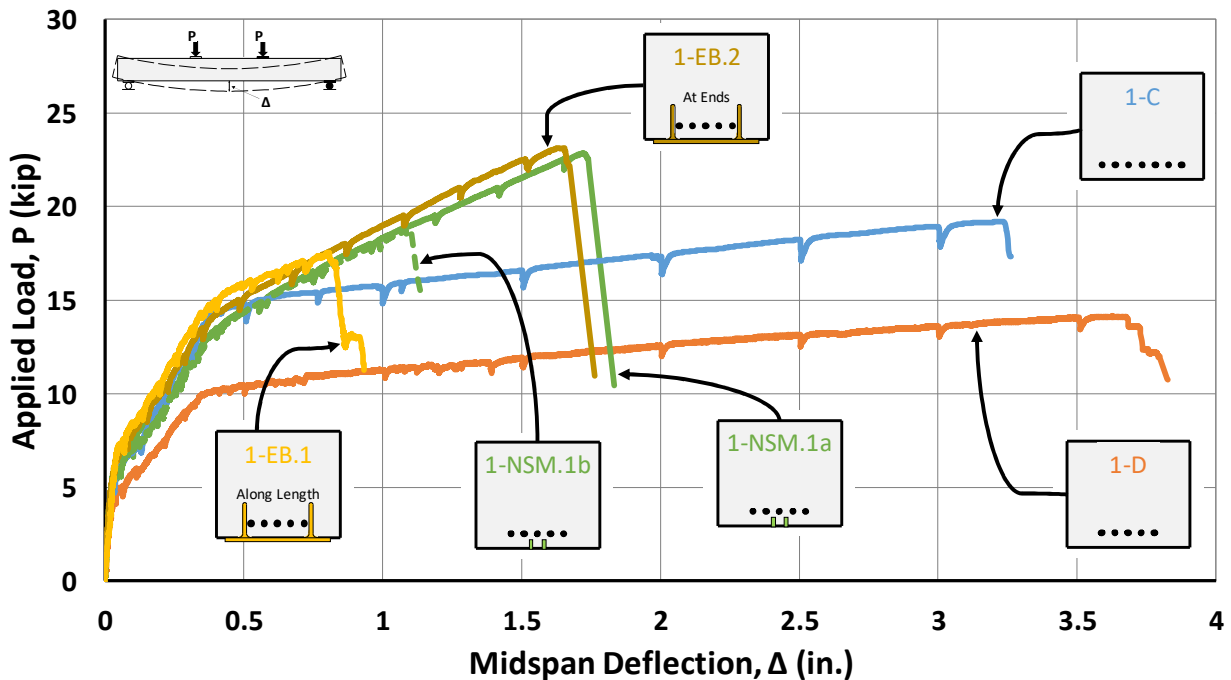


Figure 4.31: Applied Load vs. Midspan Deflection for Group 1 Specimens

As indicated in Table 4.9, the nominal flexural strengths, M_n , for the four specimens strengthened with FRP were relatively similar (average $M_n = 51.64$ kip-ft for $\psi_f = 1.0$). The control specimen had a slightly less nominal flexural capacity of 46.11 kip-ft. Despite similar calculated strengths, the actual capacities of the strengthened beams varied. Specimen 1-EB.1 strengthened with an externally bonded sheet with anchors along its length only reached 92% of the strength of the control specimen and failed at a midspan deflection of only 25% of the deflection achieved by the control specimen. The specimen with NSM strips installed overhead (Specimen 1-NSM.1b)

approached, but did not achieve, the strength of the control specimen ($M_{test}/M_C = 0.98$), and also exhibited poor ductility. Specimen 1-EB.2 (externally bonded sheet anchored at its ends) and Specimen 1-NSM.1a (NSM strips installed on inverted beam) behaved similarly to each other and demonstrated the best performance out of the strengthened specimens of Group 1 with M_{test}/M_C values of 1.20 and 1.18, respectively. Nevertheless, even these specimens only achieved a deflection equal to approximately half of the deflection of the control specimen.

The strengthening systems in Group 1 all succeeded in regaining post-cracking stiffness relative to the damaged specimen. The four strengthened specimens regained or nearly regained the full stiffness of the control specimen between first flexural cracking and yielding of the steel reinforcement. These results are consistent with expectations based on the analysis tool described in Section 4.3. After yielding of the steel reinforcement, all FRP-strengthened specimens had a significant increase in stiffness compared to the control specimen (Specimen 1-C).

4.6.2 Group 2

The test results for the Group 2 specimens are summarized in Table 4.10. The response curves for all specimens in Group 2 are provided in Figure 4.32. The artificial deterioration of the Group 2 specimens was achieved by cutting one reinforcing bar on each side of the member at midspan.

Table 4.10: Group 2 Test Results

Specimen ID	M_{test} (kip-ft)	M_n (kip-ft)		M_{test} / M_n		M_{test} / M_c	M_{test} / M_D	Steel Stress, f_s (ksi)	Rupture Stress, $f_{L,max}$ (ksi)	f_{fu}^* (ksi)	Effective Stress, f_{fe} (ksi)	$f_{L,max} / f_{fu}^*$	$f_{L,max} / f_{fe}$	Midspan Deflection at Max Load, Δ (in.)
		$\psi_j = 0.85$	$\psi_j = 1.0$	$\psi_j = 0.85$	$\psi_j = 1.0$									
2-C	59.41	45.77 ¹		1.30		1.00	1.31	-	-	-	-	-	-	3.45
2-D	45.40	33.67 ¹		1.35		0.76	1.00	-	-	-	-	-	-	1.63
2-EB.1	60.10	47.25 ²	49.82 ²	1.27	1.21	1.01	1.32	-	-	105	73.8	-	-	0.68
2-EB.2	72.79	47.29 ²	49.87 ²	1.54	1.46	1.23	1.60	-	-	105	73.8	-	-	1.25
2-NSM.1	82.87	50.16 ²	53.28 ²	1.65	1.56	1.39	1.83	-	-	325	228.1	-	-	1.82

¹Calculated in accordance with ACI 318-19

²Calculated in accordance with ACI 440.2R-17

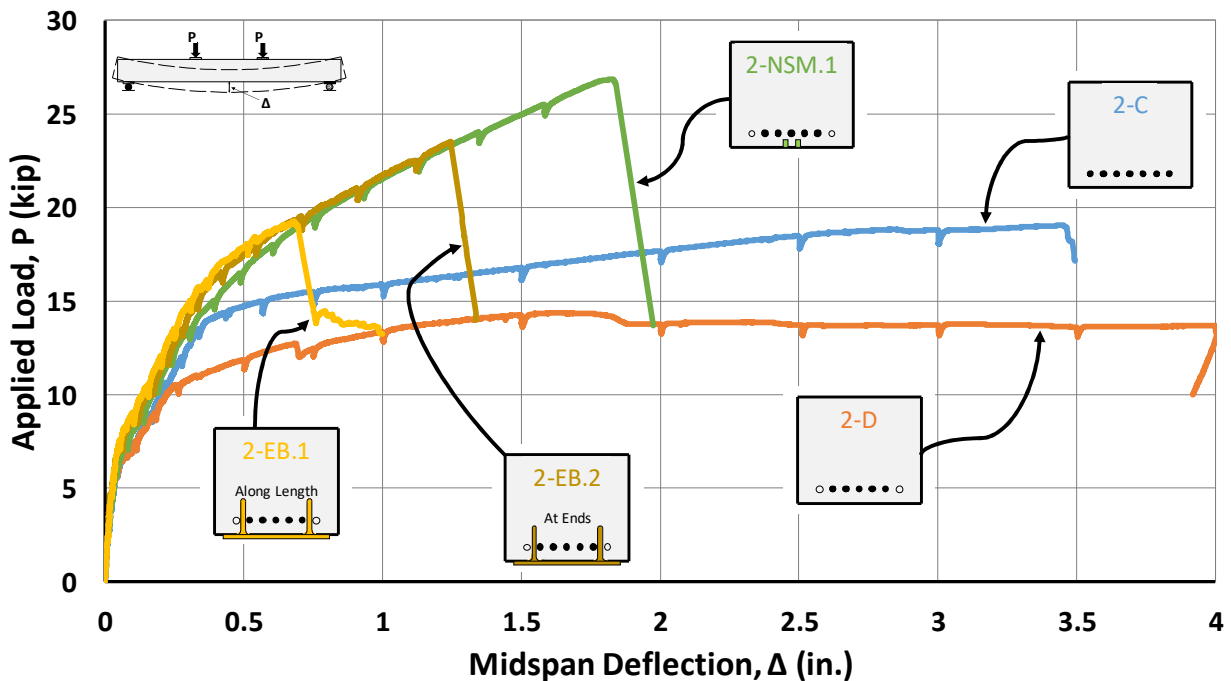


Figure 4.32: Applied Load vs. Midspan Deflection for Group 2 Specimens

Relative to the corresponding control specimens, the load-deflection plots of the strengthened specimens in Group 2 demonstrate similar behaviors, in terms of strength and maximum deflection, as the strengthened specimens in Group 1 (see Figure 4.31). The primary difference is the discrepancy between the load capacities and maximum midspan deflections of Specimens 2-NSM.1 and 2-EB.2. Although expected to have similar capacities as demonstrated by Specimens 1-NSM.1a and 1-EB.2, Specimen 2-EB.2 seems to have experienced a premature failure. Possible causes of the early failure are sensitivity to small variation in the application of

the FRP system and local effects due to concentrated strains at the location of the cut reinforcing bars.

As indicated in Table 4.10, the three FRP-strengthened specimens in Group 2 all exceeded the strength of the control specimen (Specimen 2-C). However, Specimen 2-EB.1 barely exceeded the strength of Specimen 2-C ($M_{test}/M_C = 1.01$), while Specimen 2-NSM.1 achieved a strength 39% greater than the control beam. Similar to Specimen 1-NSM.1a from Group 1, Specimen 2-NSM.1 only reached a deflection equal to approximately half the deflection of the control beam.

As shown in Figure 4.32, the three strengthened specimens adequately regained the stiffness of Specimen 2-C between first flexural cracking and yielding of the steel reinforcement. Furthermore, as expected, the strengthened specimens exhibited a significant increase in stiffness compared to the control specimen after yielding of the steel reinforcement.

4.6.3 Group 3

The test results for the Group 3 specimens are provided in Table 4.11, and the corresponding response curves are plotted in Figure 4.33. The artificial deterioration of the Group 3 specimens was achieved by excluding two reinforcing bars on one side of the member. The eccentricity of the longitudinal reinforcing bars in the artificially deteriorated specimens in Group 3 allowed for three different locations for the NSM strips to be tested. The results of the corresponding specimens are described in Section 4.5.5. To avoid clutter, the only NSM specimen plotted in Figure 4.33 is Specimen 3-NSM.1. The responses of all three NSM specimens in Group 3 are provided in Figure 4.28.

Table 4.11: Group 3 Test Results

Specimen ID	M_{test} (kip-ft)	M_n (kip-ft)		M_{test} / M_n		M_{test} / M_c	M_{test} / M_D	Steel Stress, f_s (ksi)	Rupture Stress, $f_{f,max}$ (ksi)	f_{fu}^* (ksi)	Effective Stress, f_{fe} (ksi)	$f_{f,max} / f_{fu}^*$	$f_{f,max} / f_{fe}$	Midspan Deflection at Max Load, Δ (in.)
		$\psi_j = 0.85$	$\psi_j = 1.0$	$\psi_j = 0.85$	$\psi_j = 1.0$									
3-C	56.83	45.90 ¹		1.24		1.00	1.28	84.07	-	-	-	-	-	2.88
3-D	44.47	33.92 ¹		1.31		0.78	1.00	88.67	-	-	-	-	-	3.63
3-EB.1	58.36	47.42 ²	50.00 ²	1.23	1.17	1.03	1.31	71.97	100.00	105	73.8	0.95	1.36	0.96
3-EB.2	71.62	47.40 ²	49.98 ²	1.51	1.43	1.26	1.61	77.07	147.27	105	73.8	1.40	2.00	1.69
3-NSM.1	68.56	50.29 ²	53.41 ²	1.36	1.28	1.21	1.54	76.87	343.02	325	228.1	1.06	1.50	1.62
3-NSM.2	69.25	50.23 ²	53.35 ²	1.38	1.30	1.22	1.56	77.17	350.03	325	228.1	1.08	1.53	1.56
3-NSM.3	65.50	50.25 ²	53.36 ²	1.30	1.23	1.15	1.47	75.67	315.71	325	228.1	0.97	1.38	1.43

¹Calculated in accordance with ACI 318-19

²Calculated in accordance with ACI 440.2R-17

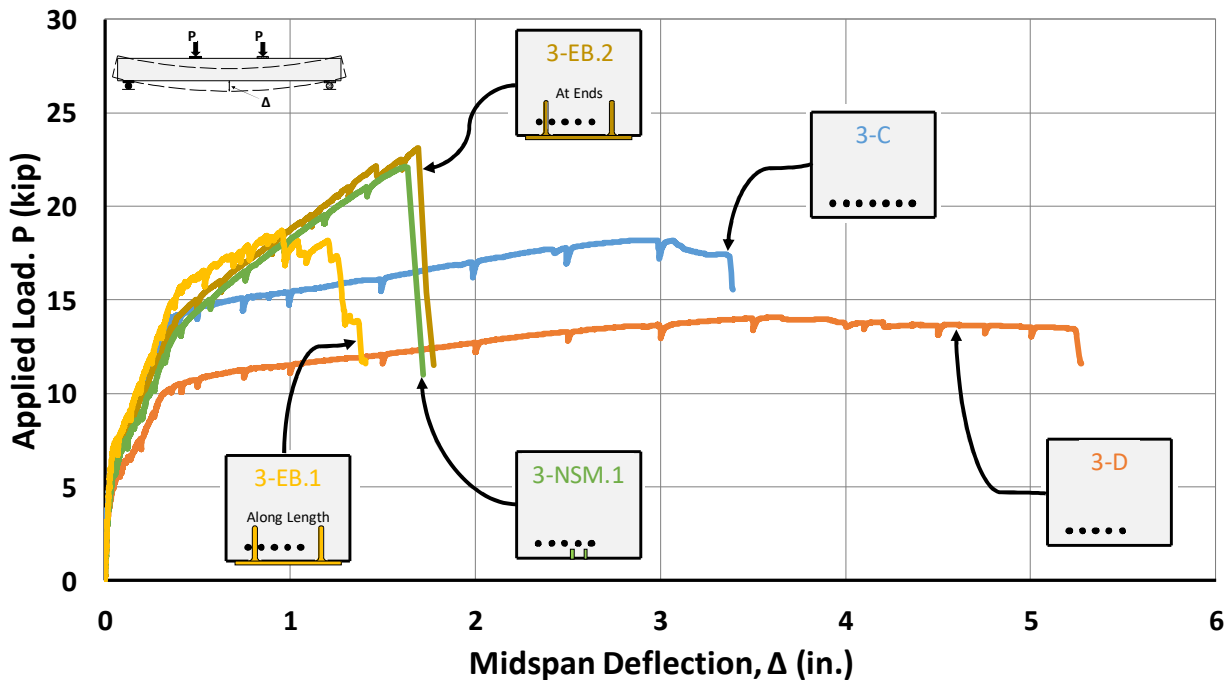


Figure 4.33: Applied Load vs. Midspan Deflection for Group 3 Specimens

Again, relative to the corresponding control specimen, the behavior of the strengthened specimens shown in Figure 4.33, in terms of strength and maximum deflection, are similar to the results of the strengthened specimens in Group 1 (see Figure 4.31). Furthermore, the FRP strengthened specimens regained or nearly regained the stiffness of the control specimens after cracking and prior to yielding of the steel reinforcement.

All FRP-strengthened specimens in Group 3 surpassed the strength of the experimental control specimen (Specimen 3-C). However, the specimen with an externally bonded sheet with anchors along its length again presented a premature failure compared to the other strengthened specimens and only achieved a M_{test}/M_C value of 1.03.

As described in Section 3.7, displacements at midspan and under the load points were measured on both sides of the Group 3 specimens to capture any differential displacements (i.e., rotation) caused by the eccentricity of the reinforcement. As discussed in Section 4.5.5, the differential displacements measured during the tests were insignificant for the NSM specimens in Group 3. Similarly, the differential displacements at the maximum applied load for the other specimens with eccentric steel reinforcing bars in Group 3 (Specimens 3-D, 3-EB.1, and 3-EB.2) were small (between 0.002 in. and 0.053 in.). The deflections measured at each bottom edge of the Group 3 specimens at midspan and the two load points are included in Appendix C.

4.7 Summary

The results and observations from 22 beam tests were described in this chapter. In order to best analyze the results and draw substantive conclusions, the tests were compared both by specimen type (Control - C, Artificial Deterioration - D, Externally Bonded - EB, and Near-Surface-Mounted - NSM) and by group (Groups 1-3). The specimens in each group (except the pilot group) were detailed with the same initial simulated field condition.

Both the externally bonded system and the near-surface-mounted system were designed to result in similar calculated nominal flexural strengths as the control specimen in each group. Because a control (C) specimen and an artificially deteriorated (D) specimen were included in each group, the effectiveness of the FRP strengthening systems were easily evaluated. In general, both FRP strengthening systems were successful in achieving or surpassing the strength of the control specimen. The FRP systems also allowed the strengthened specimens to achieve a flexural stiffness between concrete cracking and yielding of the steel reinforcement that was similar to that of the control specimens. However, the FRP strengthening systems caused a substantial reduction in ductility, which is consistent with the nature of the abrupt failures of FRP materials.

The average moment capacity, M_{test} , of the specimens with externally bonded sheets anchored at the ends of the member (EB.2 specimens) is 28% greater than the average moment capacity of specimens with externally bonded sheets anchored along the length of the member (EB.1 specimens). As noted in Section 4.5.4.3, stress concentrations in the longitudinal FRP sheets near the FRP anchor points likely caused the sheets to be vulnerable to rupture at these locations, leading to premature failure of the EB.1 specimens due to rupture of the sheet near midspan. Although two of the EB.2 specimens (Specimens 0-EB.2 and 1-EB.2) experienced rupture of the FRP sheet near an anchor point, the effect of the stress concentration at the anchors did not affect the strength of the member, likely because the anchor points were located in a region of the beam span experiencing little moment. For the specimens in the experimental program, consistent results led to the conclusion that FRP anchors near the end of the FRP sheet provided sufficient anchorage and that installing additional anchors along the length of the beam can have a negative impact on the capacity of the member.

The eccentricity of the steel reinforcement in the specimens and the relative placement of NSM strips to the steel reinforcing bars did not result in any clear effect on the behavior of the members. For one specimen, the NSM strips were installed overhead using a different epoxy than the other NSM specimens. This beam experienced a premature failure compared to other test specimens. Further study of various epoxies and installation conditions are needed to better understand their effects.

The analysis tool that was developed for the experimental program proved to be helpful in understanding the behavior of the FRP strengthening systems. Values for material properties were input into the tool based on material tests, and the analysis model was calibrated by adjusting the stiffness values of the FRP so that the resulting load-deflection plot displayed a similar post-yielding stiffness as the load-deflection curves from the experiments. The behavior of the specimens with cut bars could not be accurately modeled due to the difficulty in quantifying the contribution of the cut bars. The tool demonstrated that a relatively simple analysis procedure can be used to provide reasonable estimates for the load-deflection behavior of FRP-strengthened beams tested in flexure. However, an accurate estimation of the FRP composite rupture strain is needed to determine when failure will likely occur along the load-deflection curve.

Overall, from the consideration of the results of the experimental program, both externally bonded and NSM FRP strengthening systems are shown to be viable methods for strengthening flexural members if properly designed and installed.

CHAPTER 5. SUMMARY AND CONCLUSIONS

5.1 Summary

An experimental program consisting of tests on 22 reinforced concrete beams was conducted to evaluate the effectiveness of FRP strengthening systems. The specific details of the beam specimens and the FRP systems that received primary focus were selected to specifically evaluate potential flexural strengthening method for deteriorated adjacent box beam bridges in Indiana. Researchers (Frosch et al. 2020a, 2020b) have previously identified common deterioration mechanisms for adjacent box beam bridges in the state, and potential methods for strengthening weakened members was of interest. With this focus, the objectives of this experimental program were as follows:

- Directly compare the effectiveness of two strengthening methods: externally bonded FRP sheets and near-surface-mounted FRP strips
- Assess the ability of the two repair methods to restore the strength and stiffness of artificially weakened laboratory specimens
- Investigate anchorage techniques of externally bonded FRP sheets to the flexural tension side of a member
- Verify FRP application procedures

Before providing the details of the experimental program, an introduction to FRP flexural strengthening systems was first provided. Then, the test program was presented, including the details of the 22 beam specimens, which were divided into three groups in addition to an initial pilot group. The separation of the specimens within the three primary groups was based on a common simulated field condition within each group. While each group contained one full-strength control specimen, Group 1 included specimens with one reinforcing bar excluded at each corner, Group 2 included specimens with one reinforcing bar cut at midspan at each corner, and Group 3 included specimens with two reinforcing bars excluded at one corner. Because the initial, or field simulated, condition was held constant within each group, the FRP strengthening system therefore acted as the independent variable. After the details of the experimental program were described, the test results were analyzed and presented.

5.2 Observations and Conclusions

The key observations and conclusions from the experimental program are presented below. The items listed fulfill the project objectives and provide insights into viable flexural-strengthening methods for box beam bridges as well as other reinforced concrete flexural members.

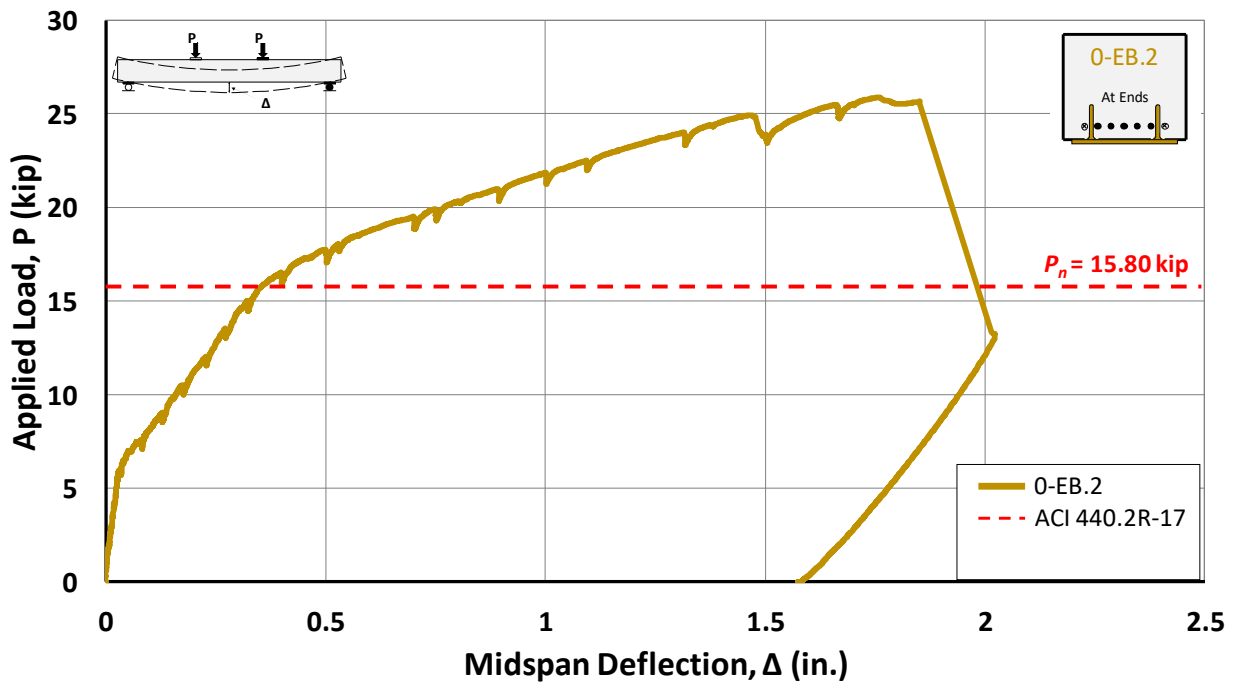
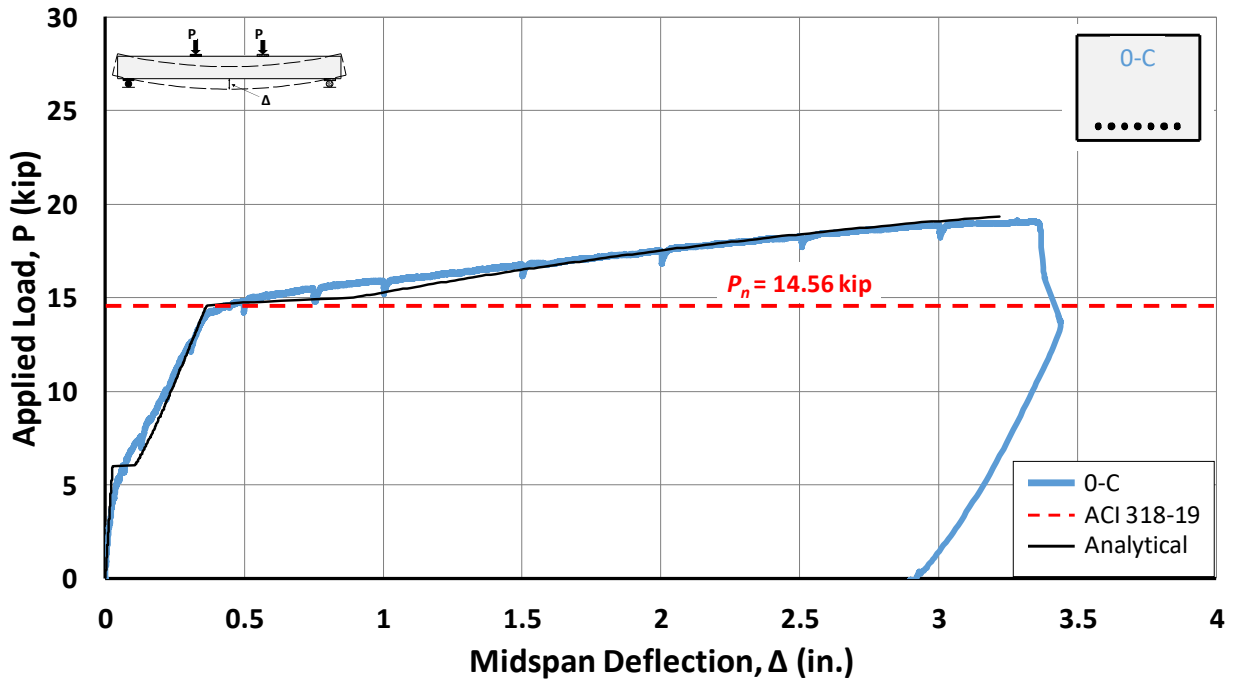
- Both the externally bonded FRP system (if appropriately anchored) and the NSM FRP system proved to be effective techniques for strengthening the flexural members of the test program if properly designed and installed.
- It was determined that the U-wrap anchor configuration that was used during the pilot tests was not the best option in terms of fully developing the primary FRP sheet. It is possible that this anchorage method could be modified (i.e., additional plies at the end or additional single-ply wraps extending into the span of the beam) to better anchor the primary FRP sheet.
- When comparing the experimental results from tests on the EB.1 specimens (FRP anchors along the length of the primary FRP sheet) and EB.2 specimens (FRP anchors at the ends of the primary FRP sheet), it was determined that the EB.2 specimens were able to consistently gain more capacity than the EB.1 specimens. It is thought that the separation and redirection of fibers in the FRP sheet required for the installation of the FRP anchors result in stress concentrations at the anchor locations. The stiffness of the anchors may also contribute to the high concentration of stresses. Although both anchorage methods may lead to these stress concentrations in the primary FRP sheet, the EB.1 specimens were impacted more due to anchors being located in regions of high moment along the length of the beam.
- All FRP-strengthened specimens, other than Specimens 1-EB.1 and 1-NSM.1b, regained the experimental moment capacity of the control specimen in their respective group (see M_{rest}/M_C column in Table 4.1).
- Considering the midspan deflection at the maximum applied load during the experimental tests, all FRP-strengthened specimens experienced reduced ductility compared to the specimens without FRP.
- While the FRP-strengthened specimens achieved post-cracking stiffnesses similar to that of the control specimens, all FRP-strengthened specimens exhibited significantly higher post-yielding stiffnesses relative to the control specimens.

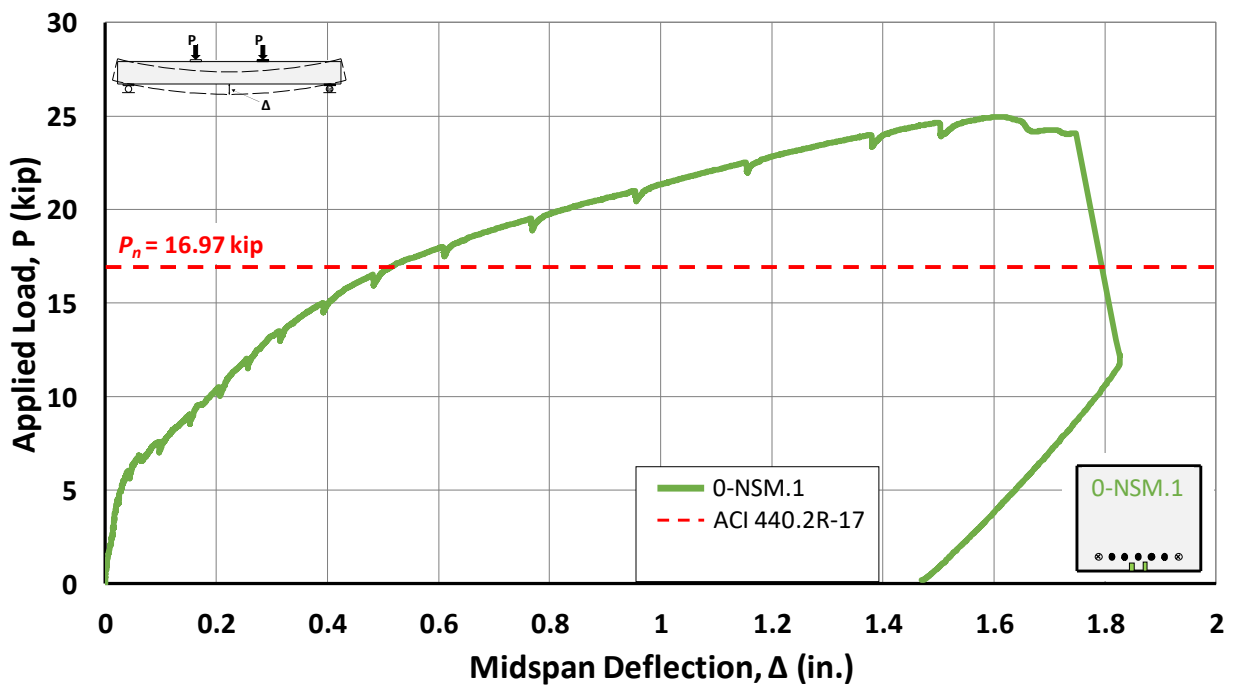
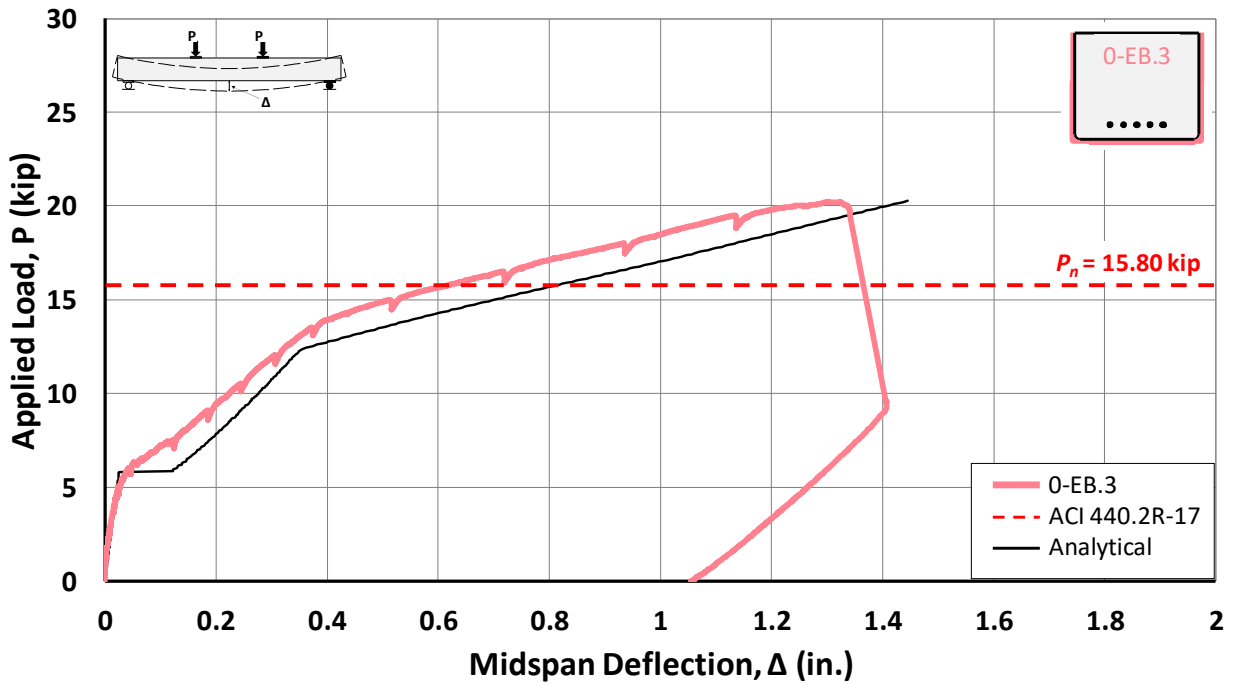
- For the specimens in Group 3 of the experimental program, the eccentricity of the steel reinforcement and the relative placement of the NSM strips did not play a significant role in the effectiveness of the FRP strengthening systems or the overall performance of the members.
- The FRP-strengthened specimens with cut bars (Group 2) exhibited greater post-cracking and post-yielding stiffnesses compared to the FRP-strengthened specimens with excluded bars (Groups 1 and 3). Although the cross sections at midspan were identical, the presence of the cut bars contributed to this increased stiffness. In general, for the specimens with cut bars, cracking was more concentrated at midspan (i.e., where the bars had been cut) relative to the members with excluded bars.
- While the FRP strengthening systems were applied to all other specimens with the member in an inverted position, NSM strips were installed in Specimen 1-NSM.1b from underneath the member as would occur in the field. A different epoxy with a higher viscosity was used for Specimen 1-NSM.1b. The overhead installation was successful, but the specimen failed at a lower moment capacity compared to the other NSM specimens. The cause of the reduction in strength is not known with certainty. More tests are needed to determine the potential impact of various epoxies, variations in material properties, and any potential negative effects of overhead applications.
- In general, the experimental moment capacities of all specimens were greater than the calculated moment capacities (see column M_{test}/M_n in Table 4.1). It should be noted that some of this increase can be attributed to the strain-hardening of the steel reinforcement, which was not accounted for in the calculated moment capacities.
- The analysis tool that was developed to better understand the behavior of the FRP strengthening systems demonstrated that a relatively simple analysis procedure can be used to provide reasonable estimates for the load-deflection behavior of FRP-strengthened beams tested in flexure.
- The FRP strengthening system installation procedures followed during the experimental program, while advantaged by a controlled laboratory setting, were deemed to be successful. Although care was taken to apply each FRP strengthening system in the same manner, small variations may have contributed to some of the differences in behavior observed during the test program.

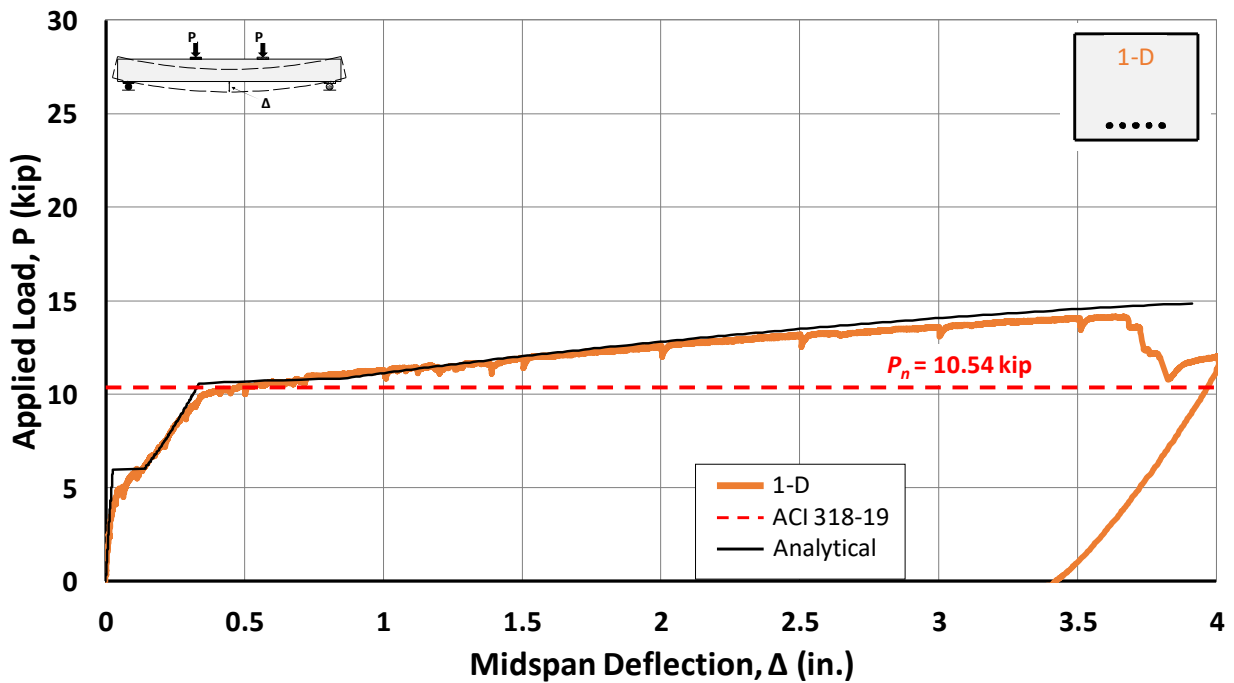
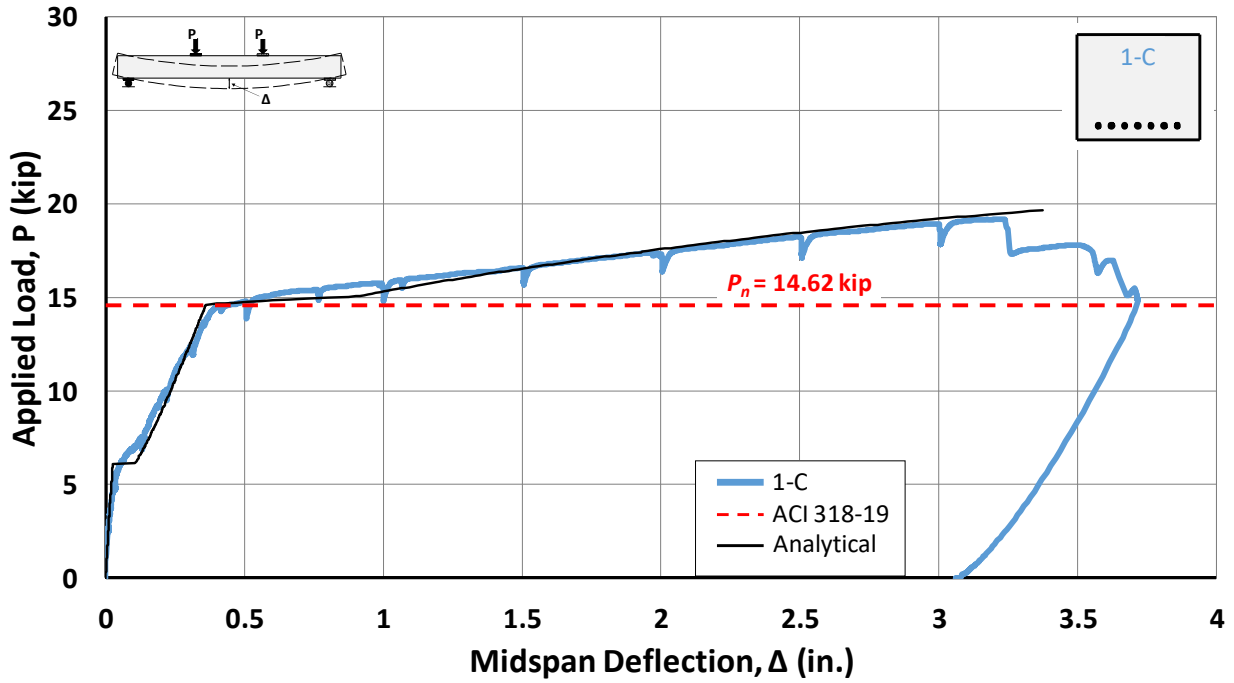
5.3 Concluding Remarks

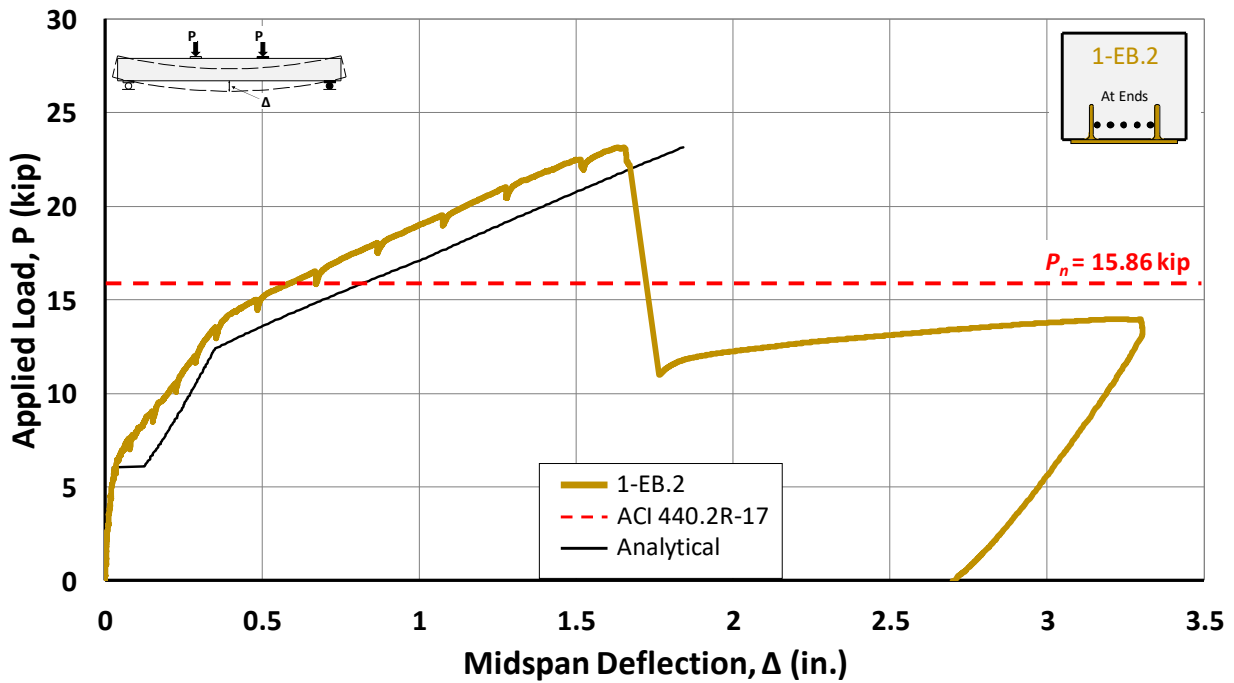
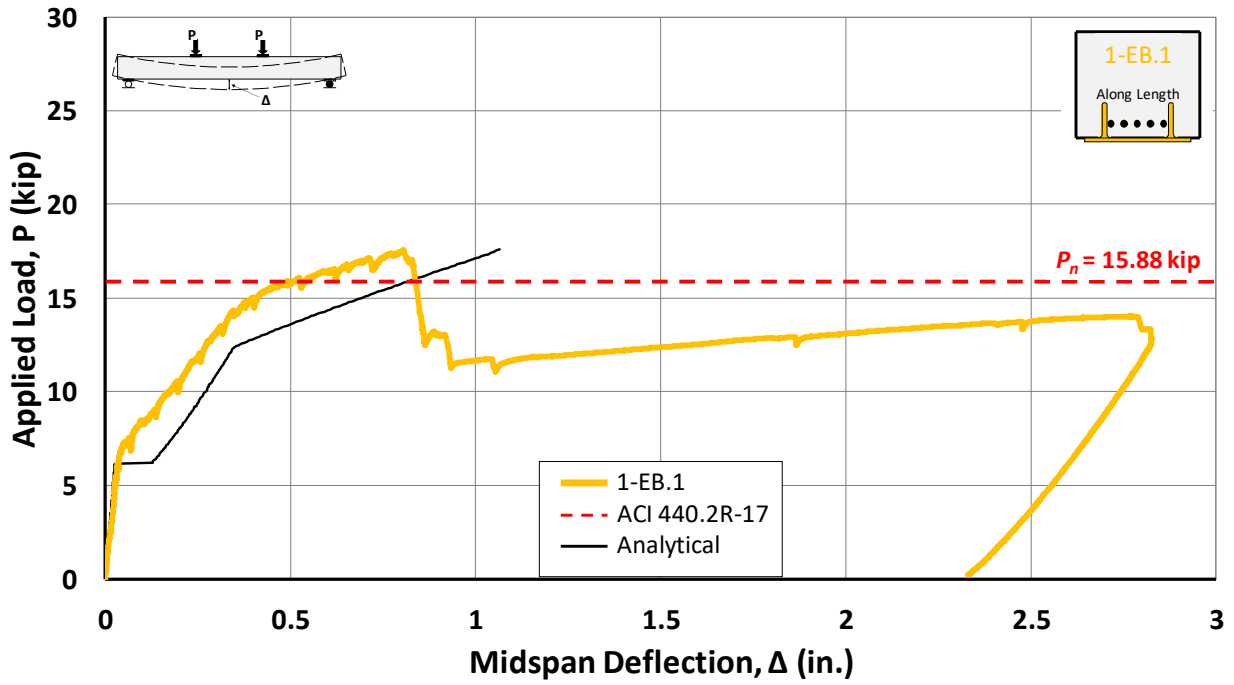
The scope of this research program was to supplement the growing FRP research for structural applications by successfully conducting laboratory tests directed by the objectives listed in Section 5.1. The objectives were considered during the experimental program so that the results and findings would lead toward implementation in the field. The results and carefully-considered observations in this document can be used to inform the design and application of FRP for the strengthening of existing bridge members.

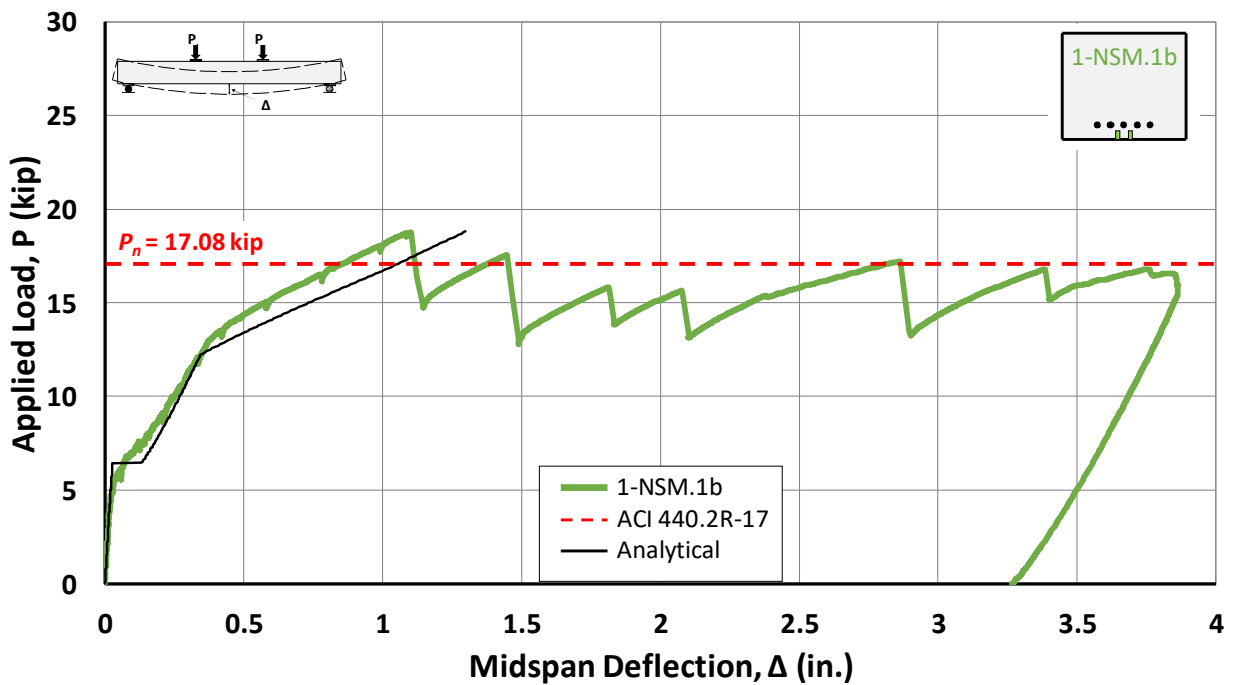
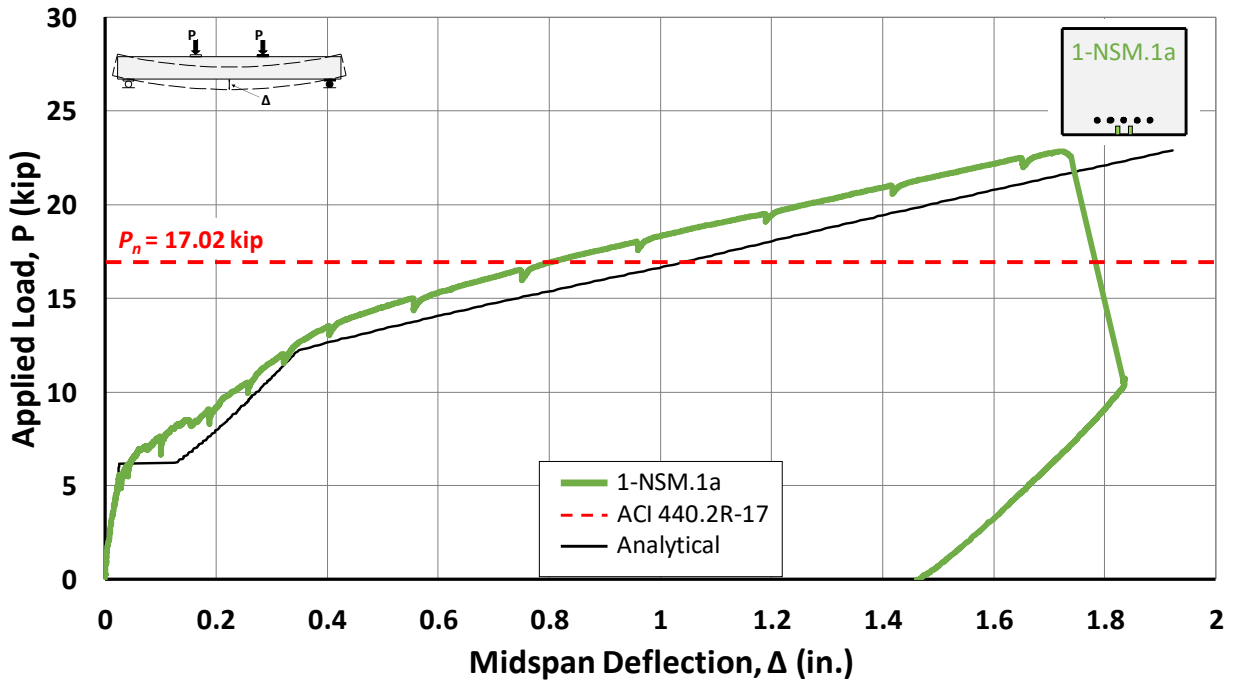
APPENDIX A. LOAD-DEFLECTION PLOTS

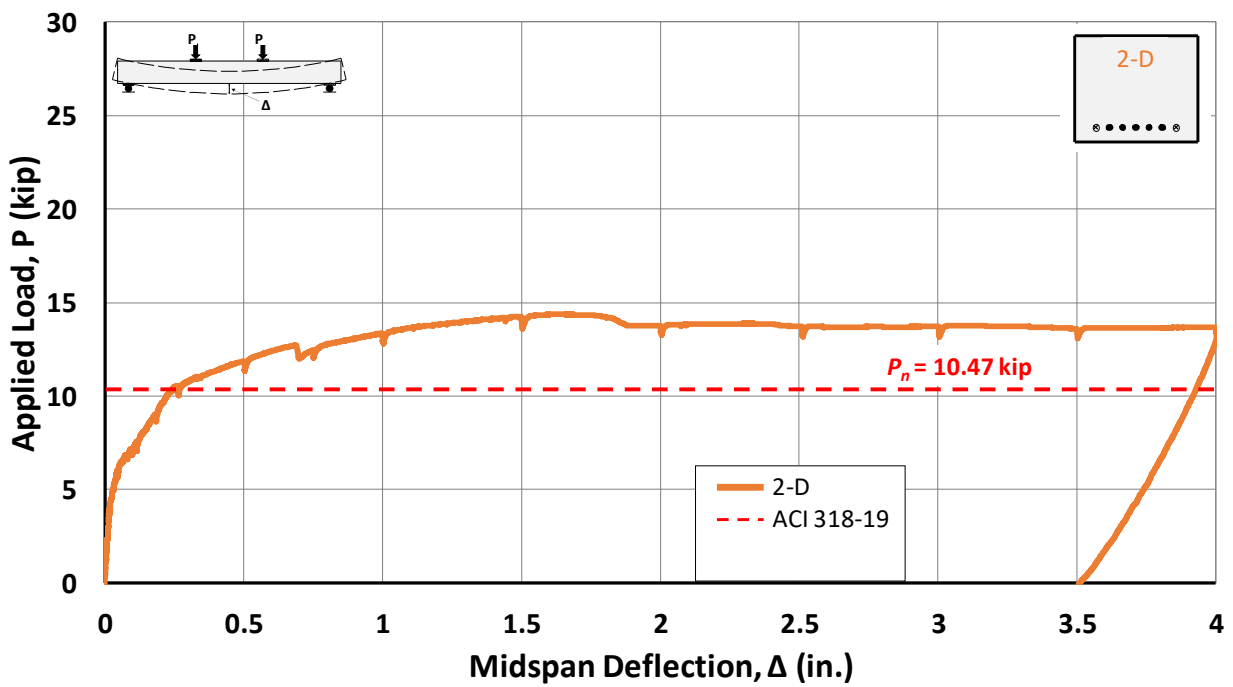
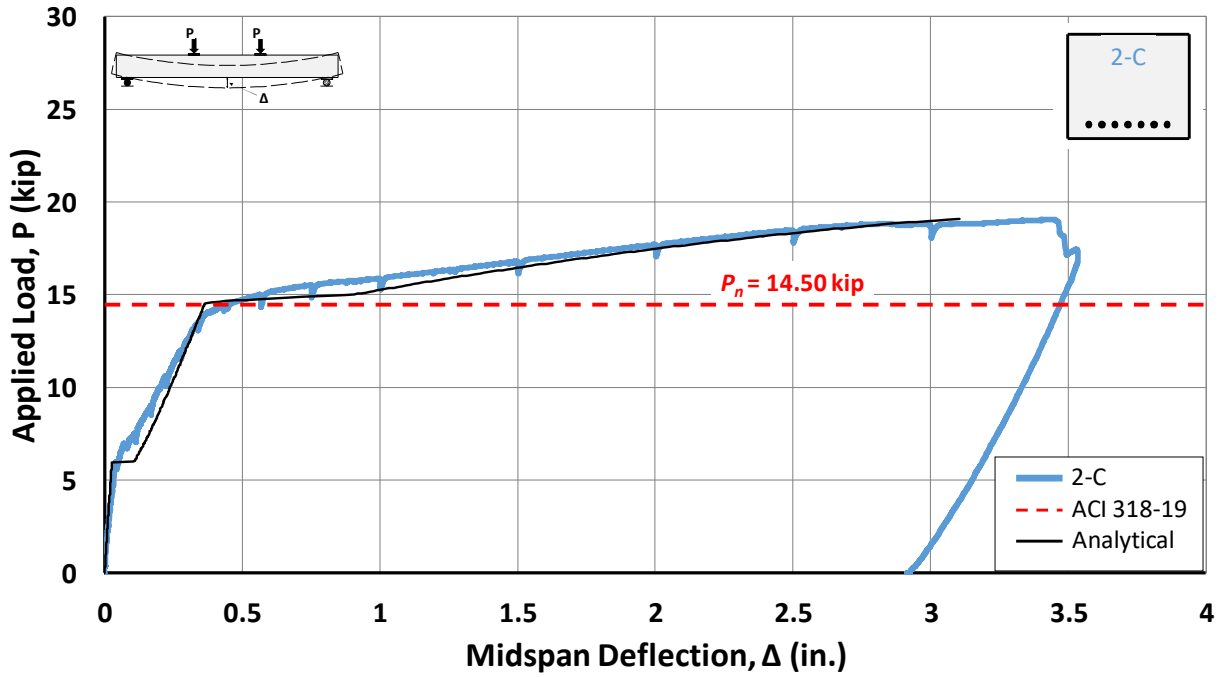


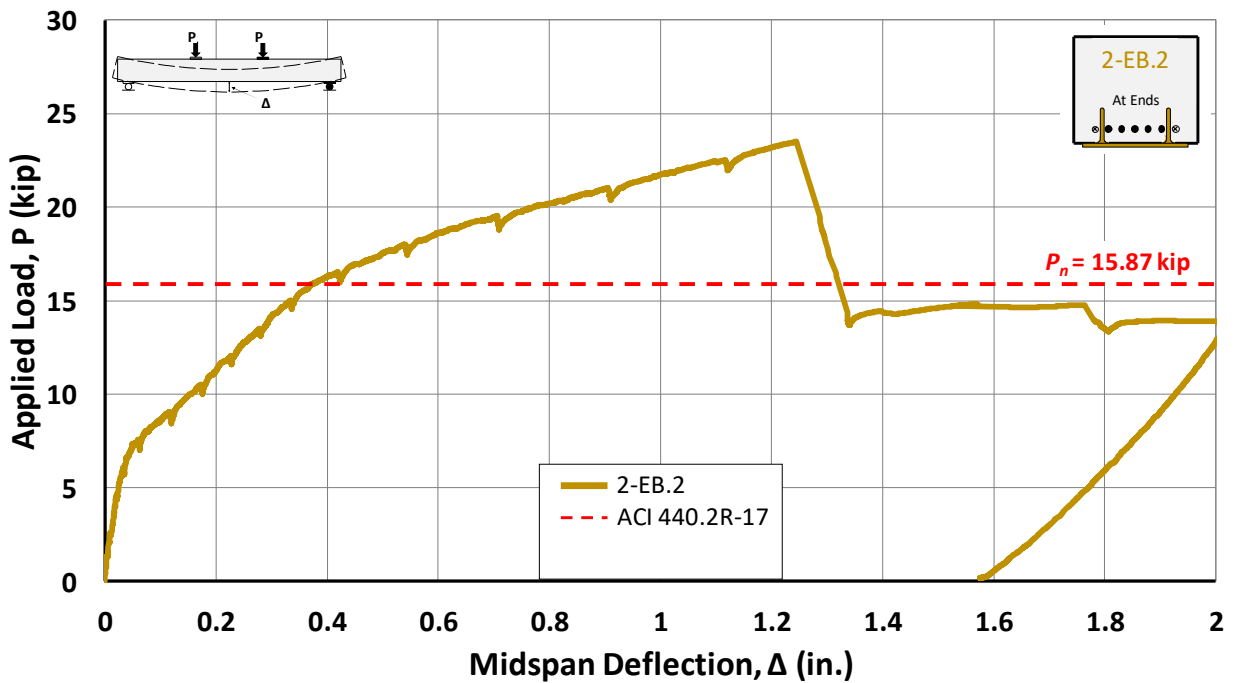
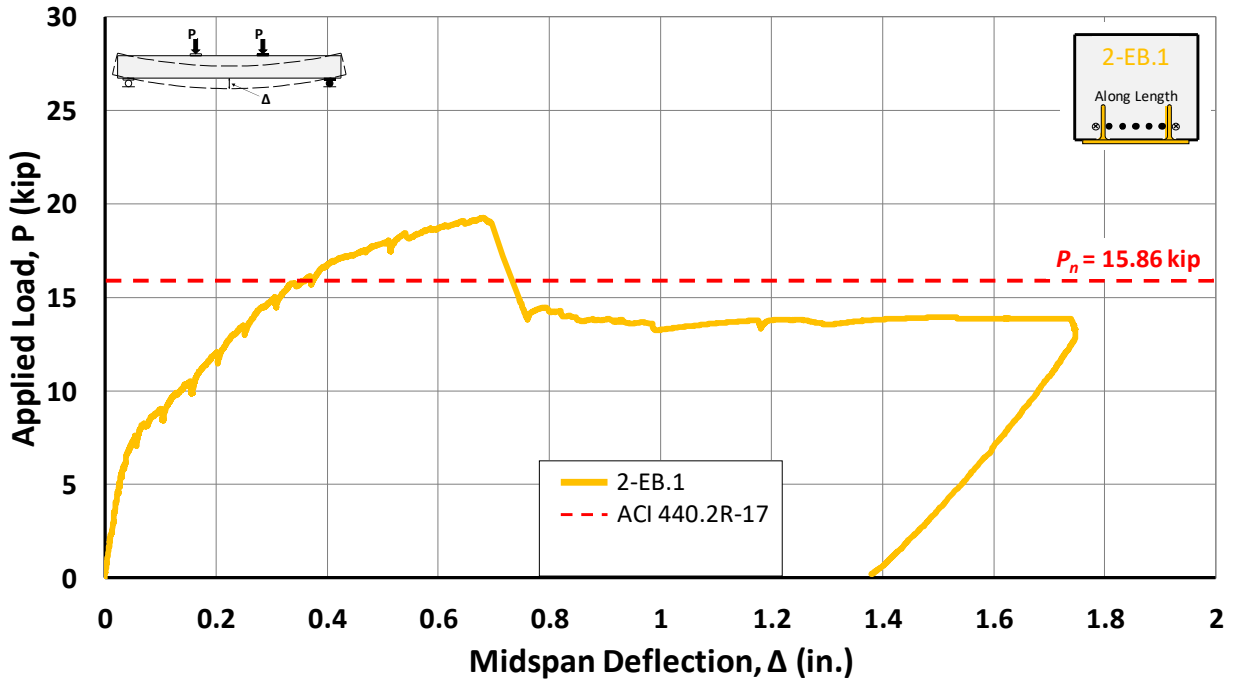


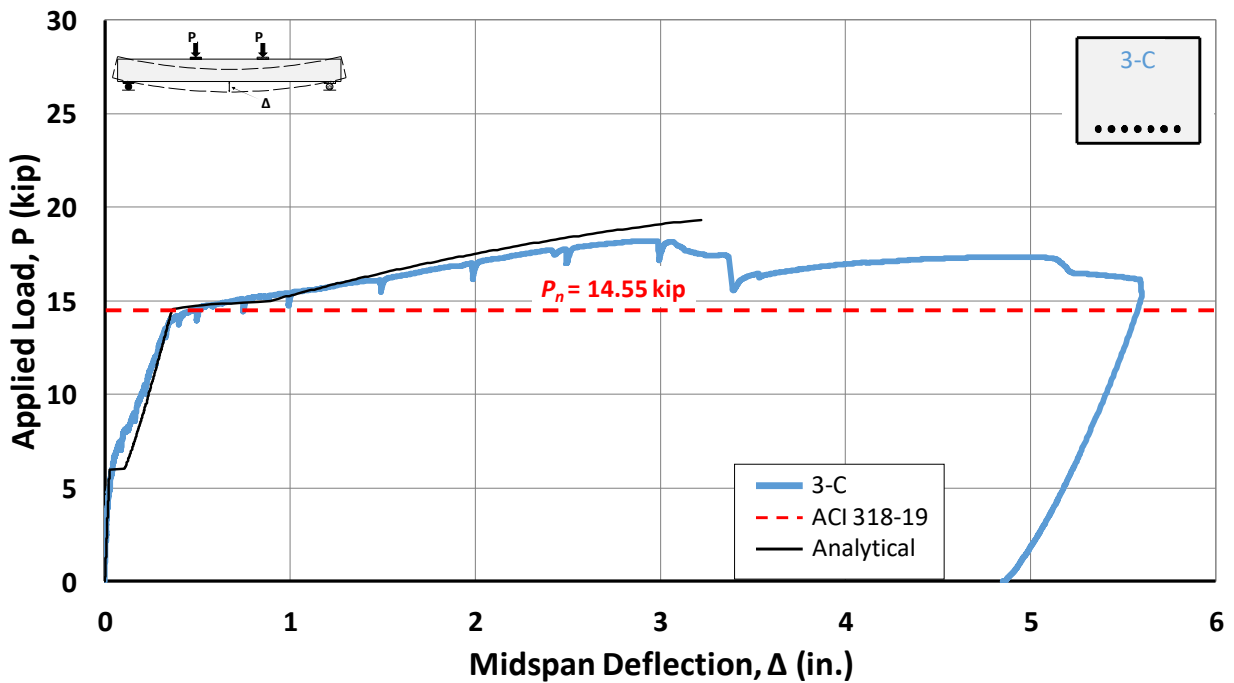
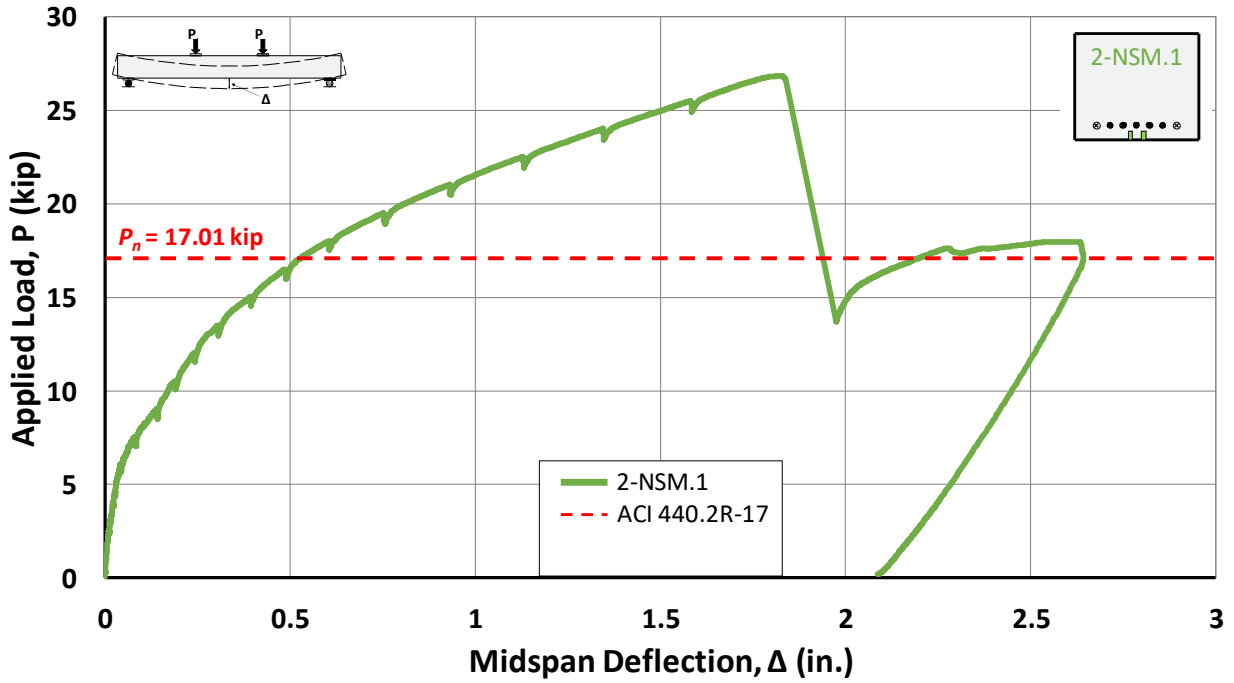


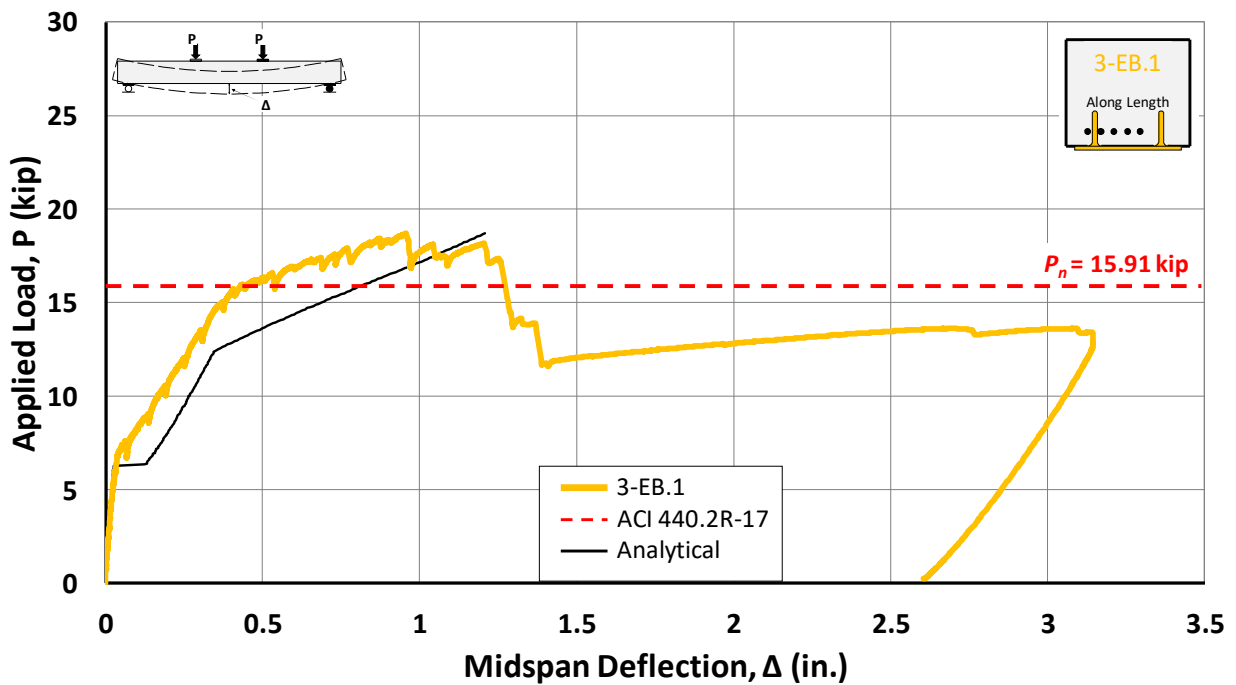
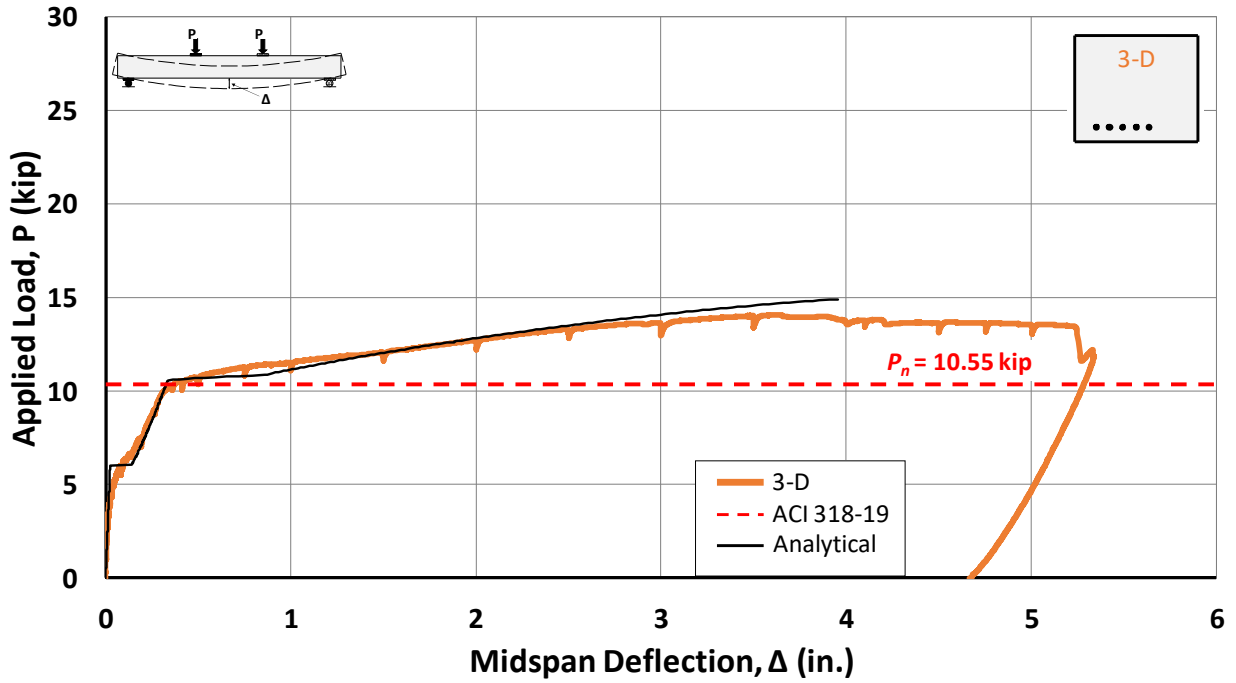


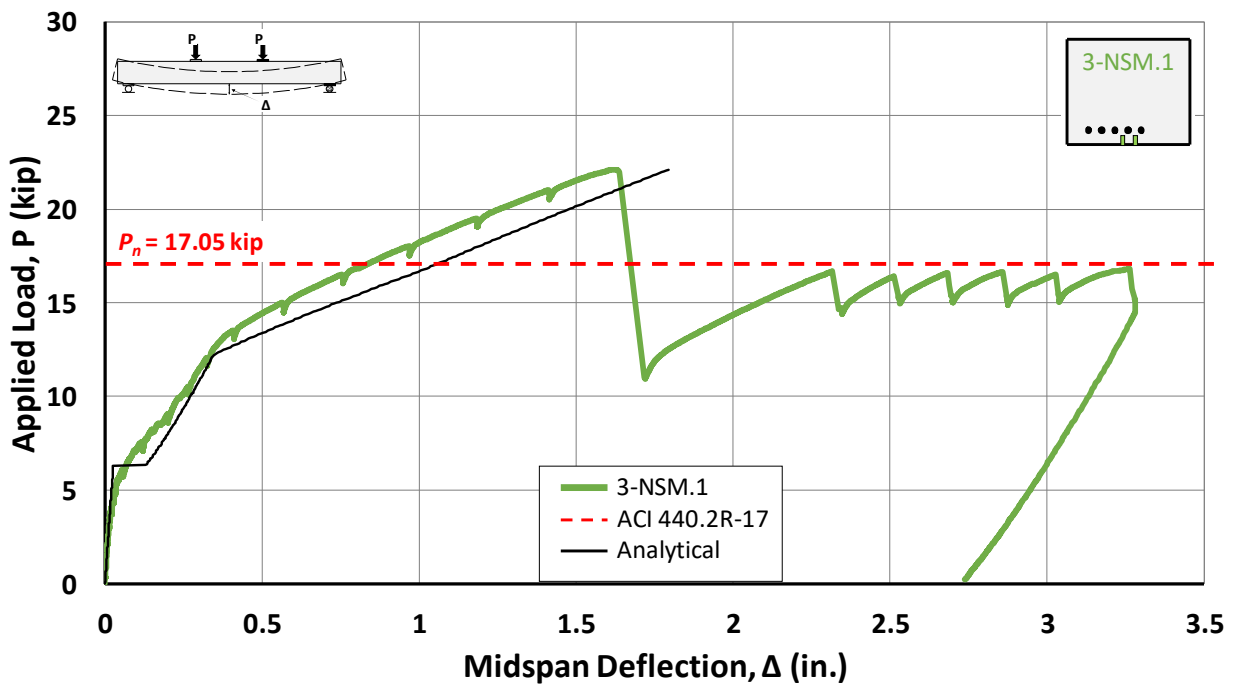
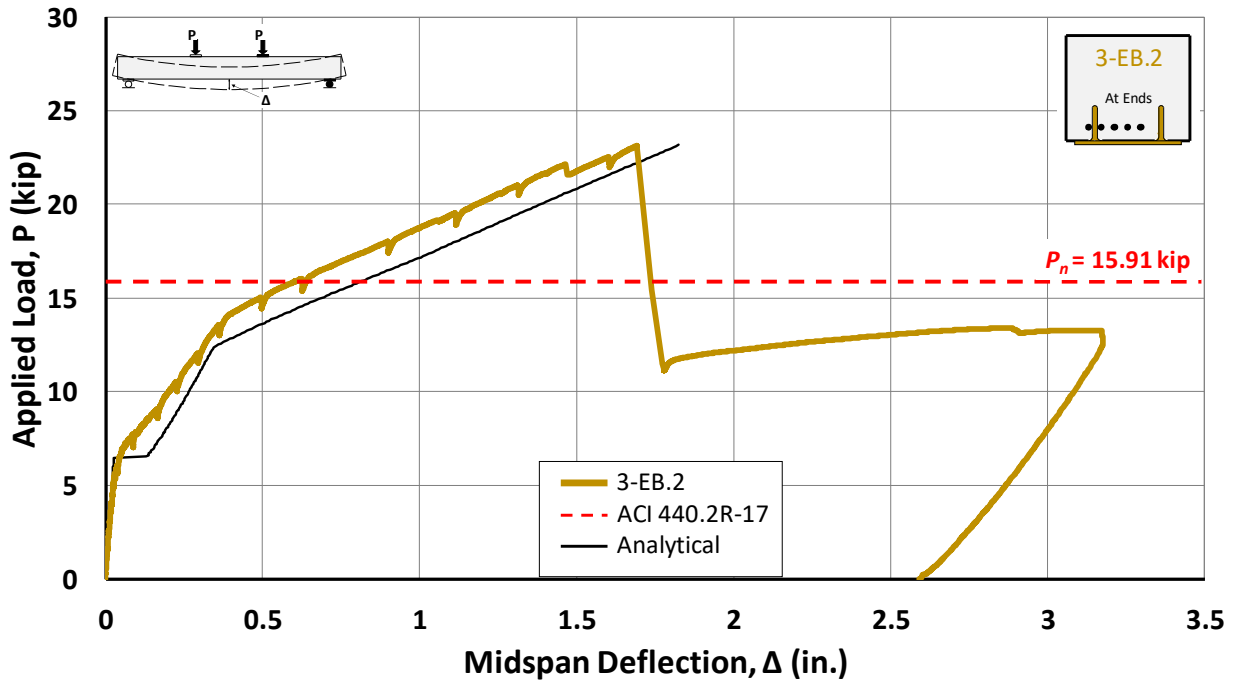


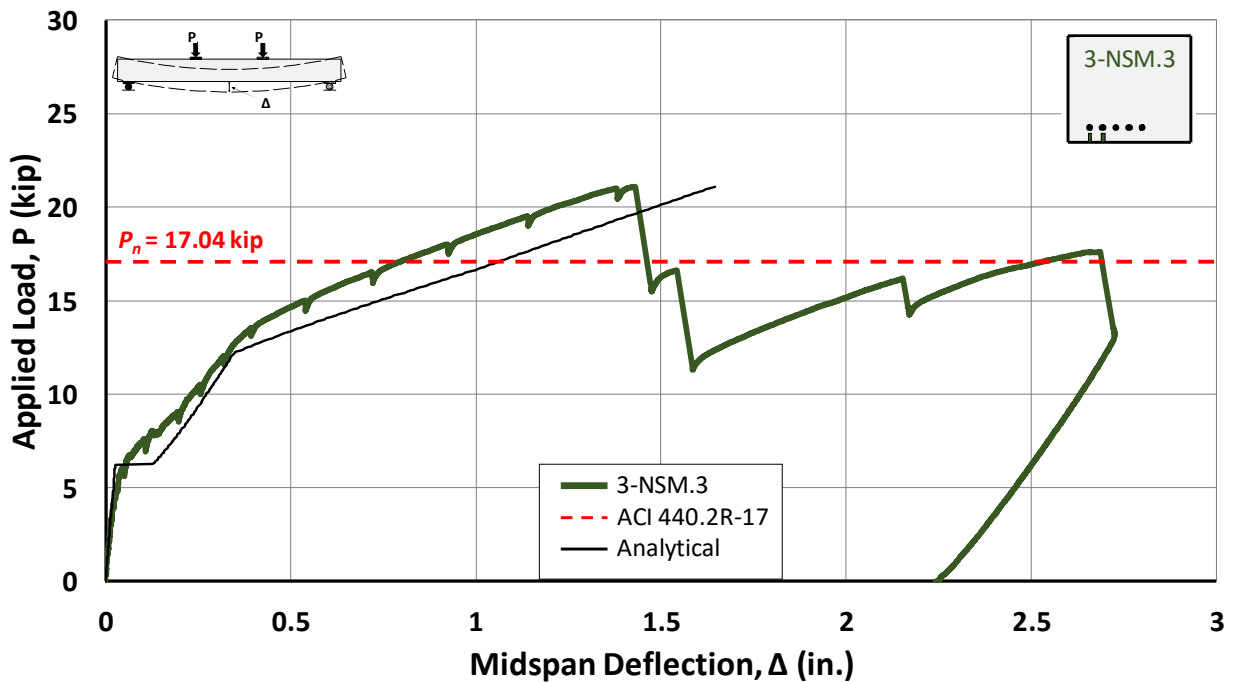
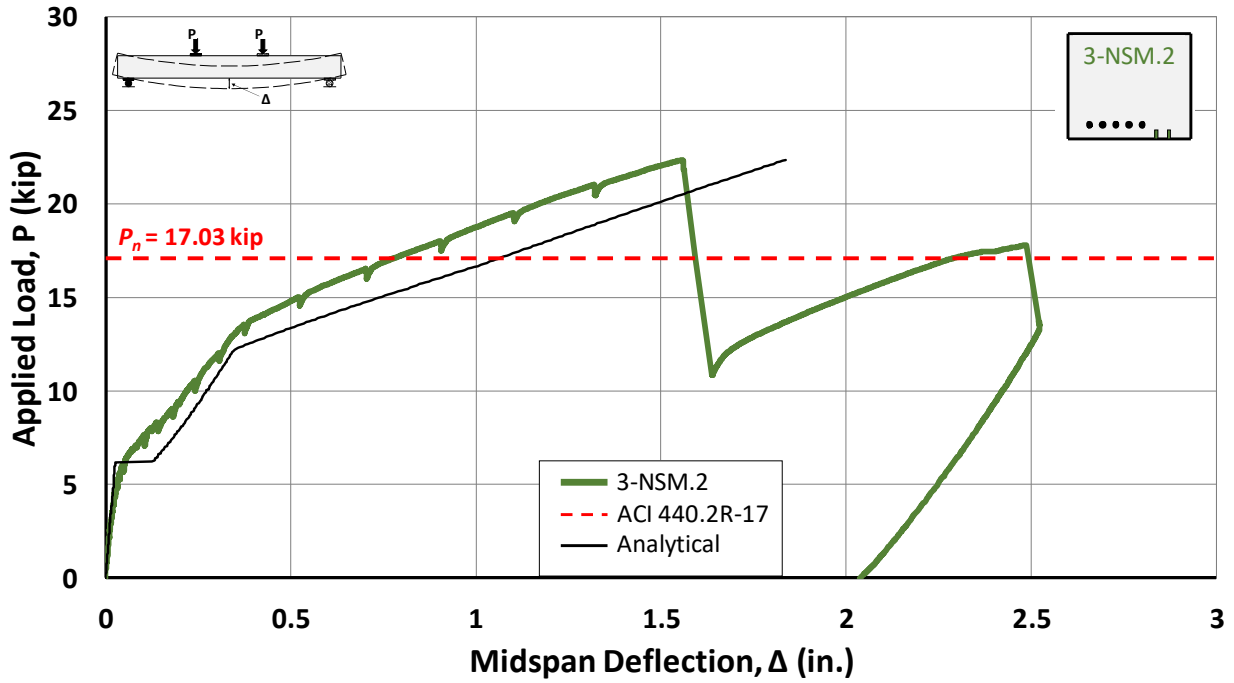












Specimen ID	Corresponding to Maximum Load		Corresponding to Midspan Deflection at Maximum Load		Percent Difference
	Steel Stress, f_s (ksi)	Rupture Stress, f_{f_max} (ksi)	Steel Stress, f_s (ksi)	Rupture Stress, f_{f_max} (ksi)	
0-EB.3	73.88	117.18	72.67	106.32	9.27%
1-EB.1	70.60	88.19	70.20	67.29	23.70%
1-EB.2	77.15	148.19	75.49	132.15	10.82%
1-NSM.1a	77.79	364.58	76.27	329.28	9.68%
1-NSM.1b	72.78	252.72	71.05	217.01	14.13%
3-EB.1	71.97	100.00	70.20	80.31	19.69%
3-EB.2	77.07	147.27	76.03	137.22	6.82%
3-NSM.1	76.87	343.02	75.51	311.99	9.05%
3-NSM.2	77.17	350.03	75.00	300.65	14.11%
3-NSM.3	75.67	315.71	73.93	277.21	12.19%

Averages:

EB.1	71.29	94.10	70.20	73.80	21.69%
EB.2	77.11	147.73	75.76	134.69	8.82%
NSM	76.06	325.21	74.35	287.23	11.83%

APPENDIX C. GROUP 3 MIDSPAN DEFLECTION MEASUREMENTS

Specimen ID	Avg. Midspan Deflection at Max Load, Δ (in.)	West Edge, Δ (in.)	East Edge, Δ (in.)	Difference (in.)
3-C	2.88	2.896	2.872	0.024
3-D	3.63	3.654	3.601	0.053
3-EB.1	0.96	0.958	0.956	0.002
3-EB.2	1.69	1.710	1.675	0.035
3-NSM.1	1.62	1.630	1.615	0.015
3-NSM.2	1.56	1.559	1.556	0.003
3-NSM.3	1.43	1.434	1.427	0.007

APPENDIX D. CONCRETE COMPRESSION TESTS

Group	Specimen ID	Concrete Strength, f_c (psi)
0 (Pilot)	0-C	6370
	0-EB.2	6110*
	0-EB.3	6120*
	0-NSM.1	6140*

*No test day data, grown from 28-day strength gain curve

0-C	Compressive Strength		
	S1	S2	S3
d ₁ (in)	5.929	5.959	5.942
d ₂ (in)	5.932	5.97	5.96
d ₃ (in)	6.09	6.066	6.073
d ₄ (in)	6.102	6.097	6.07
h ₁ (in)	12.196	12.115	12.139
h ₂ (in)	12.198	12.128	12.18
h ₃ (in)	12.156	12.077	12.136
h ₄ (in)	12.232	12.078	12.121
Load (lb)	175970	184112	183147
Stress (psi)	6196	6462	6453
Area (in ²)	28.39935	28.49152	28.38046
Average	6370.51		

Group	Specimen ID	Concrete Strength, f_c (psi)
1	1-C	6820
	1-D	6560
	1-EB.1	6920
	1-EB.2	6680
	1-NSM.1a	6490
	1-NSM.1b	7030*

*No test day data, grown from 28-day strength gain curve

1-C	Compressive Strength		
	S1	S2	S3
d ₁ (in)	5.927	5.975	5.951
d ₂ (in)	5.929	5.931	5.946
d ₃ (in)	6.057	6.053	6.04
d ₄ (in)	6.055	6.081	6.078
h ₁ (in)	12.045	12.093	12.059
h ₂ (in)	12.066	12.111	12.025
h ₃ (in)	12.069	12.066	12.088
h ₄ (in)	12.095	12.056	12.068
Load (lb)	199217	194408	184991
Stress (psi)	7065	6853	6535
Area (in ²)	28.199	28.369	28.310
Average	6817.38		

1-D	Compressive Strength		
	S1	S2	S3
d ₁ (in)	5.958	5.914	5.911
d ₂ (in)	5.929	5.939	5.952
d ₃ (in)	6.04	6.094	6.067
d ₄ (in)	6.021	6.01	6.116
h ₁ (in)	12.13	12.102	12.047
h ₂ (in)	12.114	12.06	12.069
h ₃ (in)	12.034	12.054	12.074
h ₄ (in)	11.984	12.121	12.037
Load (lb)	187306	187065	180980
Stress (psi)	6653	6640	6376
Area (in ²)	28.152	28.173	28.383
Average	6556.54		

1-EB.1	Compressive Strength		
	S1	S2	S3
d ₁ (in)	6.055	6.054	6.055
d ₂ (in)	6.064	6.051	6.068
d ₃ (in)	5.921	5.926	5.92
d ₄ (in)	5.922	5.938	5.922
h ₁ (in)	12.029	11.795	12.029
h ₂ (in)	12.067	11.826	12.061
h ₃ (in)	12.091	11.794	12.062
h ₄ (in)	12.061	11.764	12.026
Load (lb)	190262	200626	194232
Stress (psi)	6751	7114	6890
Area (in ²)	28.185	28.201	28.192
Average	6918.06		

1-EB.2	Compressive Strength		
	S1	S2	S3
d ₁ (in)	6.043	6.077	6.048
d ₂ (in)	6.064	6.036	6.062
d ₃ (in)	5.952	5.935	5.945
d ₄ (in)	5.944	5.938	5.944
h ₁ (in)	11.971	11.93	11.946
h ₂ (in)	12.013	11.949	11.984
h ₃ (in)	12.012	11.91	11.97
h ₄ (in)	11.97	11.89	11.935
Load (lb)	190532	188397	187246
Stress (psi)	6737	6671	6623
Area (in ²)	28.281	28.241	28.272
Average	6677.00		

1-NSM.1a	Compressive Strength		
	S1	S2	S3
d ₁ (in)	5.921	5.926	5.935
d ₂ (in)	5.915	5.925	5.928
d ₃ (in)	6.053	6.071	6.021
d ₄ (in)	6.07	6.032	6.08
h ₁ (in)	12.163	12.056	12.063
h ₂ (in)	12.19	12.04	12.052
h ₃ (in)	12.169	12.072	12.071
h ₄ (in)	12.09	12.07	12.061
Load (lb)	173605	189077	185996
Stress (psi)	6161	6713	6598
Area (in ²)	28.178	28.166	28.190
Average	6490.68		

Group	Specimen ID	Concrete Strength, f_c (psi)
2	2-C	6020
	2-D	6000
	2-EB.1	6630
	2-EB.2	6800
	2-NSM.1	6390

2-C	Compressive Strength		
	S1	S2	S3
d ₁ (in)	6.051	5.933	5.94
d ₂ (in)	6.063	5.933	5.954
d ₃ (in)	5.932	6.056	6.051
d ₄ (in)	5.934	6.055	6.062
h ₁ (in)	12.045	12.116	12.125
h ₂ (in)	11.998	12.097	12.185
h ₃ (in)	12.012	12.1	12.06
h ₄ (in)	12.046	12.102	12.114
Load (lb)	173546	168331	168002
Stress (psi)	6148	5965	5938
Area (in ²)	28.227	28.220	28.291
Average	6017.16		

2-D	Compressive Strength		
	S1	S2	S3
d ₁ (in)	6.03	5.935	5.96
d ₂ (in)	6.07	5.945	5.932
d ₃ (in)	5.947	6.11	6.054
d ₄ (in)	5.939	6.098	6.098
h ₁ (in)	11.926	12.156	12.099
h ₂ (in)	11.948	12.124	12.097
h ₃ (in)	11.929	12.139	12.097
h ₄ (in)	11.918	12.151	12.129
Load (lb)	168553	158750	171286
Stress (psi)	5968	5574	6036
Area (in ²)	28.241	28.482	28.378
Average	6002.08		

2-EB.1	Compressive Strength		
	S1	S2	S3
d ₁ (in)	6.055	6.046	6.068
d ₂ (in)	6.065	6.08	6.051
d ₃ (in)	5.944	5.935	5.934
d ₄ (in)	5.949	5.935	5.94
h ₁ (in)	11.994	11.96	12.035
h ₂ (in)	12.026	11.97	12.071
h ₃ (in)	12.049	11.935	12.045
h ₄ (in)	12.016	11.919	12.005
Load (lb)	187173	190631	184304
Stress (psi)	6613	6744	6522
Area (in ²)	28.305	28.265	28.258
Average	6626.46		

2-EB.2	Compressive Strength		
	S1	S2	S3
d ₁ (in)	6.074	6.058	6.053
d ₂ (in)	6.036	6.059	6.064
d ₃ (in)	5.941	5.953	5.95
d ₄ (in)	5.955	5.942	5.957
h ₁ (in)	11.879	11.943	11.99
h ₂ (in)	11.921	11.99	11.943
h ₃ (in)	11.916	11.943	11.949
h ₄ (in)	11.88	11.905	11.996
Load (lb)	191478	199268	186358
Stress (psi)	6769	7041	6578
Area (in ²)	28.288	28.303	28.331
Average	6795.76		

2-NSM.1	Compressive Strength		
	S1	S2	S3
d ₁ (in)	5.934	5.934	5.93
d ₂ (in)	5.949	5.936	5.933
d ₃ (in)	6.03	6.047	6.075
d ₄ (in)	6.06	6.061	6.056
h ₁ (in)	12.116	12.092	12.1
h ₂ (in)	12.039	12.066	12.101
h ₃ (in)	12.001	12.067	12.112
h ₄ (in)	12.071	12.09	12.09
Load (lb)	167664	186401	186961
Stress (psi)	5943	6605	6616
Area (in ²)	28.211	28.223	28.260
Average	6387.89		

Group	Specimen ID	Concrete Strength, f_c (psi)
3	3-C	6330
	3-D	6680
	3-EB.1	7270
	3-EB.2	7210
	3-NSM.1	6750
	3-NSM.2	6570
	3-NSM.3	6620

3-C	Compressive Strength		
	S1	S2	S3
d ₁ (in)	6.056	6.052	6.048
d ₂ (in)	6.049	6.073	6.054
d ₃ (in)	5.949	5.955	5.966
d ₄ (in)	5.947	5.938	5.943
h ₁ (in)	12.003	12.009	11.919
h ₂ (in)	12.02	12.033	11.968
h ₃ (in)	11.973	11.089	11.965
h ₄ (in)	11.995	11.07	11.922
Load (lb)	180635	177467	159629
Stress (psi)	6388	6267	5641
Area (in ²)	28.277	28.317	28.300
Average	6327.67		

3-D	Compressive Strength		
	S1	S2	S3
d ₁ (in)	5.958	5.994	5.953
d ₂ (in)	5.948	5.952	5.935
d ₃ (in)	6.044	6.051	6.055
d ₄ (in)	6.06	6.067	6.069
h ₁ (in)	11.958	12.082	12.071
h ₂ (in)	11.9	12.035	12.015
h ₃ (in)	11.908	12.007	12.037
h ₄ (in)	11.932	12.068	12.056
Load (lb)	186633	139106	191530
Stress (psi)	6595	4894	6767
Area (in ²)	28.298	28.425	28.303
Average	6681.26		

3-EB.1	Compressive Strength		
	S1	S2	S3
d ₁ (in)	6.036	6.072	6.054
d ₂ (in)	6.074	6.052	6.075
d ₃ (in)	5.934	5.939	5.931
d ₄ (in)	5.946	5.939	5.933
h ₁ (in)	11.986	11.912	11.941
h ₂ (in)	11.96	11.937	11.965
h ₃ (in)	11.983	11.967	11.997
h ₄ (in)	12.014	11.946	11.975
Load (lb)	213264	195054	207755
Stress (psi)	7549	6897	7352
Area (in ²)	28.251	28.279	28.258
Average	7266.18		

3-EB.2	Compressive Strength		
	S1	S2	S3
d ₁ (in)	6.068	6.072	6.037
d ₂ (in)	6.046	6.042	6.078
d ₃ (in)	5.943	5.951	5.93
d ₄ (in)	5.945	5.949	5.93
h ₁ (in)	11.96	11.941	11.962
h ₂ (in)	11.935	11.905	11.947
h ₃ (in)	11.961	11.912	11.914
h ₄ (in)	11.988	11.953	11.931
Load (lb)	206966	203745	201094
Stress (psi)	7319	7198	7127
Area (in ²)	28.279	28.307	28.215
Average	7214.47		

3-NSM.1	Compressive Strength		
	S1	S2	S3
d ₁ (in)	5.985	5.958	5.96
d ₂ (in)	5.996	5.975	5.968
d ₃ (in)	6.067	6.076	6.053
d ₄ (in)	6.06	6.139	6.06
h ₁ (in)	12.227	12.127	12.207
h ₂ (in)	12.15	12.148	12.161
h ₃ (in)	12.168	12.111	12.156
h ₄ (in)	12.169	12.215	12.184
Load (lb)	191635	196706	189057
Stress (psi)	6717	6872	6664
Area (in ²)	28.529	28.624	28.371
Average	6750.96		

3-NSM.2	Compressive Strength		
	S1	S2	S3
d ₁ (in)	5.98	5.976	5.964
d ₂ (in)	5.971	5.967	5.964
d ₃ (in)	6.027	5.989	6.11
d ₄ (in)	6.137	6.102	6.039
h ₁ (in)	12.144	12.122	12.128
h ₂ (in)	12.178	12.205	12.129
h ₃ (in)	12.155	12.226	12.148
h ₄ (in)	12.127	12.125	12.113
Load (lb)	181510	192212	186775
Stress (psi)	6359	6779	6564
Area (in ²)	28.546	28.355	28.456
Average	6567.01		

3-NSM.3	Compressive Strength		
	S1	S2	S3
d ₁ (in)	5.967	5.961	5.959
d ₂ (in)	5.969	5.955	5.959
d ₃ (in)	6.047	6.041	6.018
d ₄ (in)	6.077	6.043	6.055
h ₁ (in)	12.149	12.121	12.094
h ₂ (in)	12.116	12.089	12.111
h ₃ (in)	12.127	12.087	12.076
h ₄ (in)	12.062	12.091	12.093
Load (lb)	181784	191964	188873
Stress (psi)	6397	6789	6685
Area (in ²)	28.416	28.274	28.253
Average	6623.88		

REFERENCES

- ACI Committee 318, 2019, “318-19: Building Code Requirements for Structural Concrete and Commentary.” American Concrete Institute; 2019
- ACI Committee 440, 2015, “440.1R-15: Guide for the Design and Construction of Structural Concrete Reinforced with Fiber-Reinforced Polymer Bars.” American Concrete Institute; 2015
- ACI Committee 440, 2017, “440.2R-17: Guide for the Design and Construction of Externally Bonded FRP Systems for Strengthening Concrete Structures.” American Concrete Institute; 2017
- Sika, 2015, “SikaWrap FX-50 C Product Data Sheet Edition 5.16.2015,” Sika Corporation, 2015.
- Sika, 2016, “SikaWrap Hex 117C Product Data Sheet Edition 5.17.2016,” Sika Corporation, 2016.
- ASTM, 2014, “C469/C469M: Standard Test Method for Static Modulus of Elasticity and Poisson’s Ratio of Concrete in Compression.” ASTM International; 2014
- ASTM, 2017, “C496/C496M: Standard Test Method for Splitting Tensile Strength of Cylindrical Concrete Specimens.” ASTM International; 2017
- ASTM, 2019, “C192/C192M: Standard Practice for Making and Curing Concrete Test Specimens in the Laboratory.” ASTM International; 2019
- ASTM, 2020, “C39/C39M: Standard Test Method for Compressive Strength of Cylindrical Concrete Specimens.” ASTM International; 2020
- ASTM, 2020, “C150/C150M: Standard Specification for Portland Cement.” ASTM International; 2020
- Frosch, R. J., Williams, C. S., Molley, R. T., & Whelchel, R. T. (2020). *Concrete box beam risk assessment and mitigation: Volume 1—Evolution and performance* (Joint Transportation Research Program Publication No. FHWA/IN/JTRP-2020/06). West Lafayette, IN: Purdue University.<https://doi.org/10.5703/1288284317117>
- Frosch, R. J., Williams, C. S., Molley, R. T., & Whelchel, R. T. (2020). *Concrete box beam risk assessment and mitigation: Volume 2—Evaluation and structural behavior* (Joint Transportation Research Program Publication No. FHWA/IN/JTRP-2020/07). West Lafayette, IN: Purdue University.<https://doi.org/10.5703/1288284317118>
- Hassan, T., and Rizkalla, S., 2003, “Investigation of Bond in Concrete Structures Strengthened with Near Surface Mounted Carbon Fiber Reinforced Polymer Strips,” *Journal of Composites for Construction*, V. 7, No. 3, pp. 248-257.

Hibbeler, R.C., 2012, *Structural Analysis, Eighth Edition*, Pearson Prentice Hall, Pearson Education Inc., Upper Saddle River, NJ.

Hognestad, E. 1951, *A Study of Combined Bending and Axial Load in Reinforced Concrete Members*, Bulletin 399, University of Illinois Engineering Experiment Station, Urbana, IL, November, 128 pp.

Hughes Brothers, 2011, "Aslan 500 Carbon Fiber Reinforced Polymer (CFRP) Tape Product Data Sheet," Hughes Brothers, Inc., 2011.

ICRI, 2013, "Guideline No. 310.2R-2013: Selecting and Specifying Concrete Surface Preparation for Sealers, Coatings, Polymer Overlays, and Concrete Repair," International Concrete Repair Institute, 2013.

ICRI, 2016, "Guideline No. 330.2-2016: Guide Specifications for Externally Bonded FRP Fabric Systems for Strengthening Concrete Structures," International Concrete Repair Institute, 2016.

INDOT, 1975, INDOT Bridge Design Manual, 1975.

Molley, R. T., 2017, "Evolution and Performance of Box Beam Bridges in Indiana," Master of Science in Engineering, Purdue University, 2017.

Pevey, J.M., 2018, "A Review of FRP Repair and Strengthening Methods for Application to Indiana Bridges," Master of Science in Engineering, Purdue University, 2018.

Pham, L.T., 2009, "Development of a Quality Control Test for Carbon Fiber Reinforced Polymer Anchors," Master of Science in Engineering, The University of Texas at Austin, 2009.

Quinn, K.T., 2009, "Shear Strengthening of Reinforced Concrete Beams with Carbon Fiber Reinforced Polymer (CFRP) and Improved Anchor Details," Master of Science in Engineering, The University of Texas at Austin, 2009.